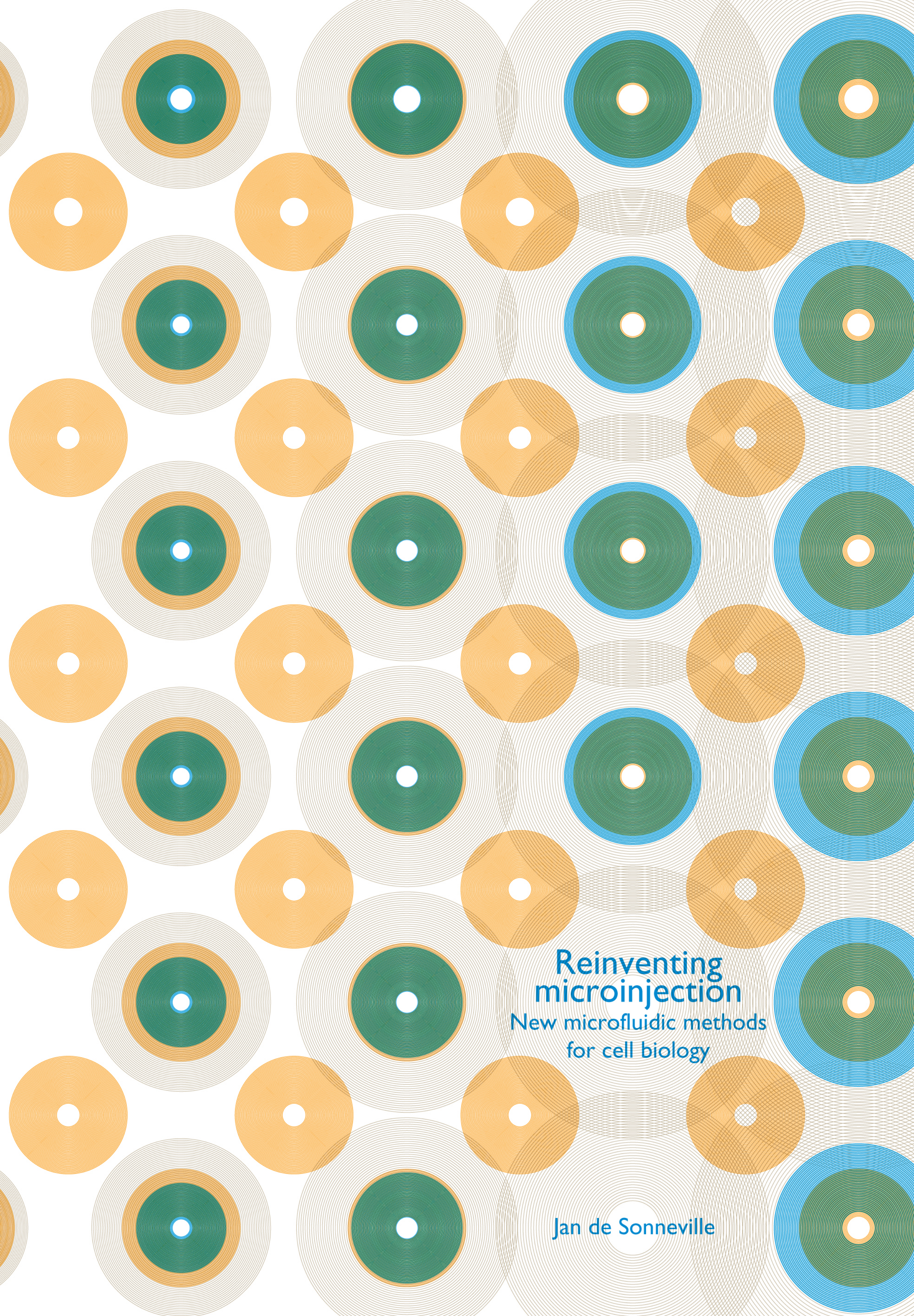

Reinventing microinjection

New microfluidic methods for cell biology

Jan de Sonneville

Reinventing Microinjection

New microfluidic methods for cell biology

Jan de Sonneville

Reinventing Microinjection

New microfluidic methods for cell biology

Proefschrift

ter verkrijging van de graad van Doctor aan

de Universiteit Leiden,

op gezag van Rector Magnificus prof.mr. P.F. van der Heijden,

volgens besluit van het College voor Promoties

te verdedigen op woensdag 16 november 2011

klokke 16.15 uur

door

Jan de Sonneville,

geboren te Amsterdam

in 1980.

Promotiecommissie:

Promotores
Prof. dr. J.P.Abrahams
Prof. dr. M.H.M. Noteborn

Copromotor
dr. M.E. Kuil

Overige Leden
Prof.dr. H.P. Spaink
Prof.dr. J. Brouwer
Prof.dr. T.H. Oosterkamp
Prof.dr. S. Osanto
dr. E.H.J. Danen

© by Jan de Sonneville. All rights reserved.

The publication of this thesis was financially supported by Märzhäuser, ZF-screens, Eppendorf and Life Science Methods.

A digital version of this thesis can be obtained from http://ub.leidenuniv.nl.

Chapter 1 Introduction 1

Chapter 2 A versatile microfluidic flow cell for studying the dynamics of shear-stress induced actin reorganization in renal cells 19

Chapter 3 Determination of the size distribution of blood microparticles directly in plasma using atomic force microscopy and microfluidics 39

Chapter 4 A High-Throughput Screen for Tuberculosis Progression 59

Chapter 5 Automated microinjection of cell-polymer suspensions in 3D ECM scaffolds for high throughput quantitative cancer invasion screens 77

Chapter 6 Appeal for better data management 97

Summary 115

Samenvatting 121

Acknowledgements 127

Curriculum Vitae 131

Publications 133

Chapter 1

Introduction

Abstract

Higher organisms are made of cells that must collaborate for the organism to thrive. In multi-cellular organisms, cells are controlled by regulatory processes. Regulation of a cell is a complex process involving many types of interactions. To study regulatory processes, cells have to be grown and stimulated in a controlled way, because a cellular response to external stimuli depends on the internal state of a cell. The accuracy of the study depends on the ability to mimic the *in-vivo* situation, in which cells are exposed to complex and changing environments. However, cells grown in a more complex and changing environment can display a larger variance in behavior. Therefore high-throughput experimentation is required to gain sufficient statistical power.

In this thesis, four new research methods for investigating cell regulatory processes are presented. The design methodology used to create these methods is introduced at the end of this chapter.

Introduction

Cells form the basis of life as we know it. Although there are many different types of cells, and many different species, the cell's chemical factory is a highly conserved machinery, similar among many different species and types of cells. In an organism, most cells share the same DNA sequence, which encodes the amino acid sequence for all the proteins and RNAs that the organism can make. Regulatory proteins that reside close to the DNA interact specifically with individual coding sequences on the genome. Proteins and DNA folding tightly control the gene expressing in a cell[1]. Cell types can have different genes switched on and off, resulting in cell to cell differences that fulfill specific biological functions[2].

Different regulatory processes affecting cells

Physical and biochemical interactions with the direct environment around a cell can affect its gene expression[3] and have been shown to influence differentiation. Control signals from outside the cell use signal transduction cascades within the cell to reach the DNA. Such regulation pathways depend on all proteins involved in each specific signal transduction pathway. There may be different routes leading to a similar change in the gene expression, or different gene expressions leading to similar cellular behavior. The presence of proteins involved in signal transduction pathways is crucial, hence the efficiency of the pathway also depends on the (previous) state of a cell. The current state of a cell and its history have for this reason a great effect on the cellular response to regulatory stimuli.

It is clear that the micro-environment around cells plays an important role in biological experiments. Zooming in on cells in an organism, we can distinguish many different micro-environments. Some cells are floating in a suspension (e.g. white blood cells), some cells form contact with an extracellular matrix (ECM) or with other cells (e.g. liver or nerve cells). The ECM is a matrix of polysaccharides and fibrous proteins, the exact composition and structure determines its rigidity and regulatory properties. It is a challenge to find and mimic these properties *in vitro*, a detailed comparison study of tissue engineered and native heart valves by K. Schenke-Layland is given as example[4].

Next to the 'passive' micro-environment there are many different specific active biological regulatory signals interacting with cells. Hormones or proteins can bind to membrane associated receptor proteins, causing a conformational change and inducing a signal cascade eventually leading to gene regulation[5]. Similar processes can be induced by direct cell-cell interactions. Cells can also release small vesicles containing proteins and/or RNA[6]. These vesicles can then bind to and be incorporated into the outer membrane of other cells, thereby releasing the content in their cytoplasm. Many types of vesicles were discovered, see **Figure 1.1**, and for many, their exact function is still unknown[7].

Bacteria and viruses use cells and their protein production machinery to spread and proliferate. Organisms have special defense mechanisms to combat such diseases, but fast evolution of the disease agents allow them to quickly adapt. Viruses

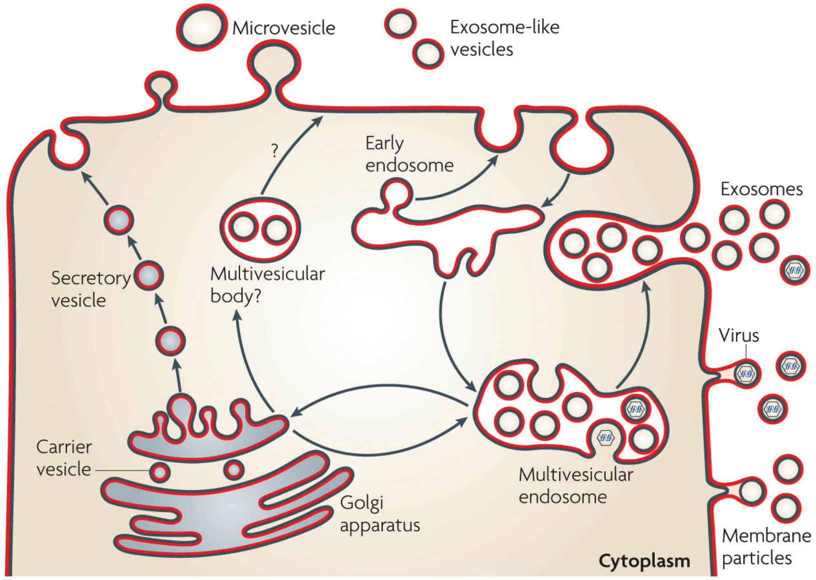
Microvesicle
Exosome-like vesicles
?
Early endosome
Exosomes
Secretory vesicle
Multivesicular body?
Virus
Carrier vesicle
Golgi apparatus
Multivesicular endosome
Cytoplasm
Membrane particles

Figure 1.1 Different processes known to produce micro-vesicles. Based on the origin, vesicles can be characterized on their content and/or membrane composition (shell), based on proteins residing in the shell, or the physical composition, i.e. the number of lipid-layers. The depicted processes of producing vesicles are not yet completely understood.
From Clotilde Théry, Matias Ostrowski and Elodie Segura, Nature Reviews Immunology, 2009 [8]

enter the cells with RNA or DNA and use the cell's own machinery to create new virus particles[9]. Most bacteria do not harm, but for instance help digestion processes, hence the perhaps somewhat surprising observation that a human organism contains more bacteria than cells. However, some bacteria are using human cells to proliferate, divide and spread uncontrollably[10]. Such disease causing bacteria are normally recognized by the defense mechanism of the organism and taken care of by macrophages. Within macrophages the phagocytosis pathway uses special enzymes to break down the bacteria. However, some bacteria, such as those causing tuberculosis, have a defense mechanism against phagocytosis and hijack the macrophages to proliferate at cost of the host organism (**Fig. 1.2**).

In cancer, the mutated cells of the organism itself form a threat to life. Disease can occur when cells are transformed such that the gene regulation limiting cellular growth is altered beyond repair[12]. Normally, such changes would result in cell death, however, in cancer cells also the death regulatory pathways are disrupted,

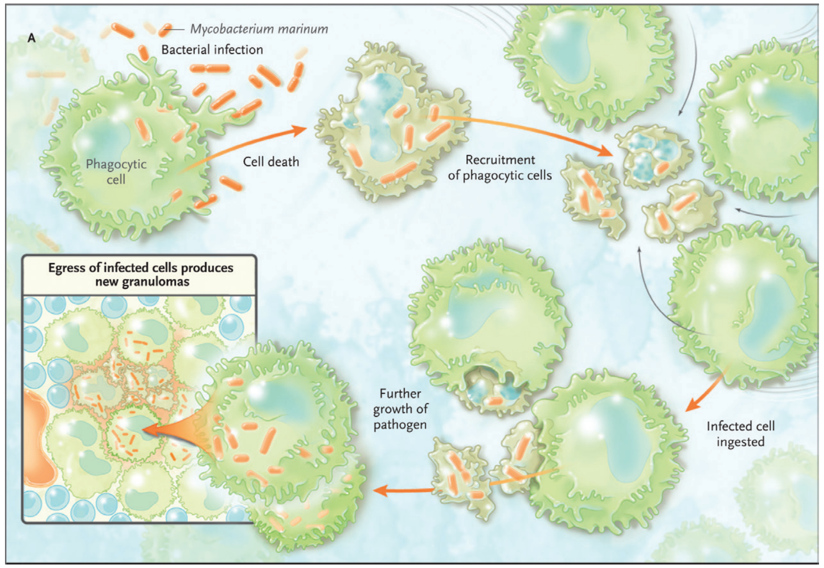
A
Mycobacterium marinum
Bacterial infection
Phagocytic cell
Cell death
Recruitment of phagocytic cells
Egress of infected cells produces new granulomas
Further growth of pathogen
Infected cell ingested

Figure 1.2 Using zebrafish as a model organism. Davis and Ramakrishnan demonstrated that growth of *Mycobacterium marinum* in the phagocyte (the zebrafish equivalent of the human macrophage) eventually leads to cell death. New bacterium niches (granulomas) are formed when infected cells recruit uninfected cells.
From Eric J. Rubin, The new england journal of medicine 2009 [11]

and cells can start to divide and grow uncontrollably[13]. Subsequent activation of other regulatory processes can lead to growth of new blood vessels toward the tumor site, or migration of tumor cells towards new sites. Lack of nutrition causes oxidative stress, by which cells surrounding the tumor (and within the tumor) die. The cellular components can then be recycled by (tumor) cells. Through paracrine (local) cell-cell signaling the surrounding tissue plays an active role in cancer initiation, growth and possible spread[14].

Cancer tumor growth influences therapy strategies. Depending on the cell type, derailed cells form different cancer cell types, which may show different growth, migration and proliferation. It is believed that the micro-environment (**Fig. 1.3**) during tumor growth can initiate further differentiation into multiple different cancer cell types. Some cancer cells may be more involved in migration whereas others may be more involved in proliferation[15].

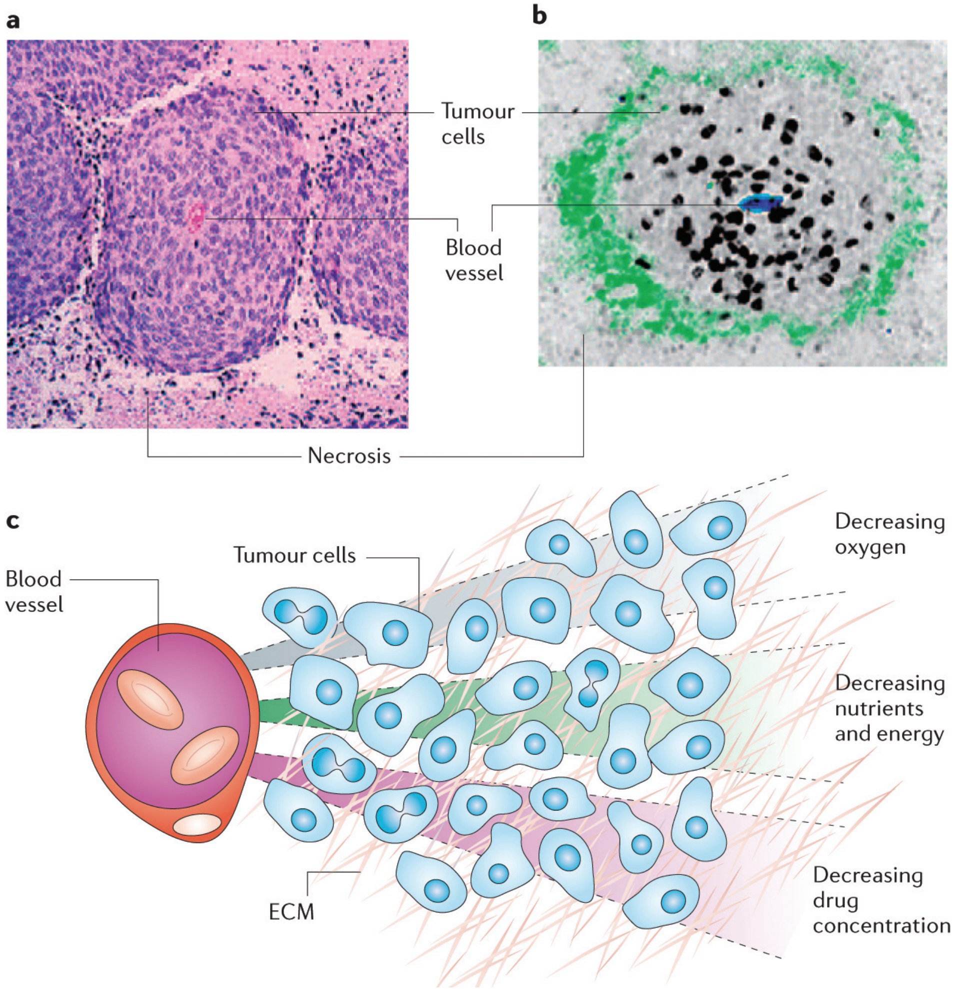

Figure 1.3 The *in-vivo* environment of tumor cells. The blood vessel is the source of nutrients, and of most therapeutics. The nutrient gradient that forms as a result of diffusion is the cause of necrosis of distant cells. However, the gradient of therapeutics may explain the resistance to therapy, as the dose for more distant tumor cells may not reach the required level, or may be less active due to a hypoxic, acidic or nutrient deprived environment. The correlation to the location with respect to the blood vessel can be clearly seen. In (a) cervix cancer around a blood vessel, and in (b) a xenograft of colon cancer around a blood vessel. Black staining shows proliferating tumor cells. Green staining indicates hypoxic regions. Endothelial cells are colored blue. In (c) a schematic overview.

From Andrew I. Minchinton and Ian F. Tannock, Nature Rev. Cancer 2006 [16]

Studying cell regulatory processes

In medicine, during diagnosis, the cellular resolution shown in the above examples is not available without taking biopsies. As a result, from diseases with a cause at the cellular level or smaller, mostly only indirect measurements can be made, which are not always accurate. For example, to measure the recent pandemie fluenza virus infection (2009), the only rapid assays which were available had poor clinical sensitivity (11 to 70%) and could not detect a specific influenza A subtype[17]. Indications of pain, fever or visible abnormalities are results of (disease with) complex regulatory processes, that are difficult to relate directly to cellular disorders. Multiple steps, multiple diagnostic tests and sometimes multiple treatments are used to characterize the cellular origin[18].

Fortunately, many disease interactions with(in) the organism create specific by-products, such as raised protein levels in blood or urine, which sometimes can be measured. Blood tests are more and more focused on the detection of these specific biomarkers[19, 20], known to be associated with specific diseases. To understand and find a specific biomarker, the precise disease mechanisms have to be unraveled. Next to bulk measurements aimed at finding direct correlations (large scale diagnostic testing), this is done using *in-vitro* and *in-vivo* experiments that result in a deeper insight into the complex disease and host mechanisms such that specific biomarkers or possible targets for drug interaction can be found[21].

The interplay between cell migration, cell stress and external forces.

Cancer cells can migrate in an organism, thereby spreading the disease. One of the regulatory pathways in cancer cell migration is the cell adhesion kinetics pathway[22]. Cell adhesion is intensified when forces acts on a cell[23]. *In vitro* this has been shown by stretching a deformable cell support, and by subjecting cells grown in a layer to shearing forces using a fluid flow. Currently, study of this type of cell stress requires dedicated microfluidic systems, that are complex to use[24].

In chapter 2 a simpler system is introduced that could be used to study cell adhesion kinetics in detail using bright-field, phase-contrast, DIC and confocal fluorescence microscopy.

Do blood plasma microparticle numbers associate with disease?

In certain diseases it has been found that the amount of blood plasma microparticles was increased. It could be that these microparticles are actively involved in disease processes or are by-products of other regulatory processes[25]. Currently, there is no convenient method for determining the accurate number, origin and size of microparticles. It has been shown that Atomic Force Microscopy (AFM) can be used to determine size and number of anti body bound microparticles on a mica surface[26]. However, this method involves many treatment and purification steps, which may be affected by systematic errors.

In chapter 3 an improvement in the capture of microparticles on an antibody-coated surface is introduced, which removes the need of ultra-centrifugation, reducing the chance of systematic errors and the time before measurement.

Can we effectively test potential tuberculosis drugs in zebrafish embryos?

In diseases caused by bacterial infections it is difficult to investigate the regulatory processes and spread of the disease as they occur inside the organism. In human imaging, bacteria are too small to see, and therefore small test animals are used to study bacterial infections in detail. Tuberculosis (TB) is a disease caused by *Mycobacterium tuberculosis* in humans[27]. Antibiotics are used to treat the disease, but increased resistance against many antibiotics is cause for global concern[28].

Currently guinea pigs offer the best similar disease symptoms, but are unfortunately also difficult to image and study. Therefore, another similar bacterium is used, *Mycobacterium marinum*, which allows studying the progression in zebrafish embryos. Many of the TB regulatory processes have been unraveled using this zebrafish model, and significant progress can be anticipated when a high throughput system is developed to use zebrafish in faster compound screening to find new drugs.

In chapter 4 a new high throughput system for the infection of zebrafish embryos with (TB) bacteria is introduced which can be used for compound screening. Surprisingly[11], we discovered that zebrafish can also be infected with the human *Mycobacterium tuberculosis* (MTB).

Inhibiting cell migration in 3D

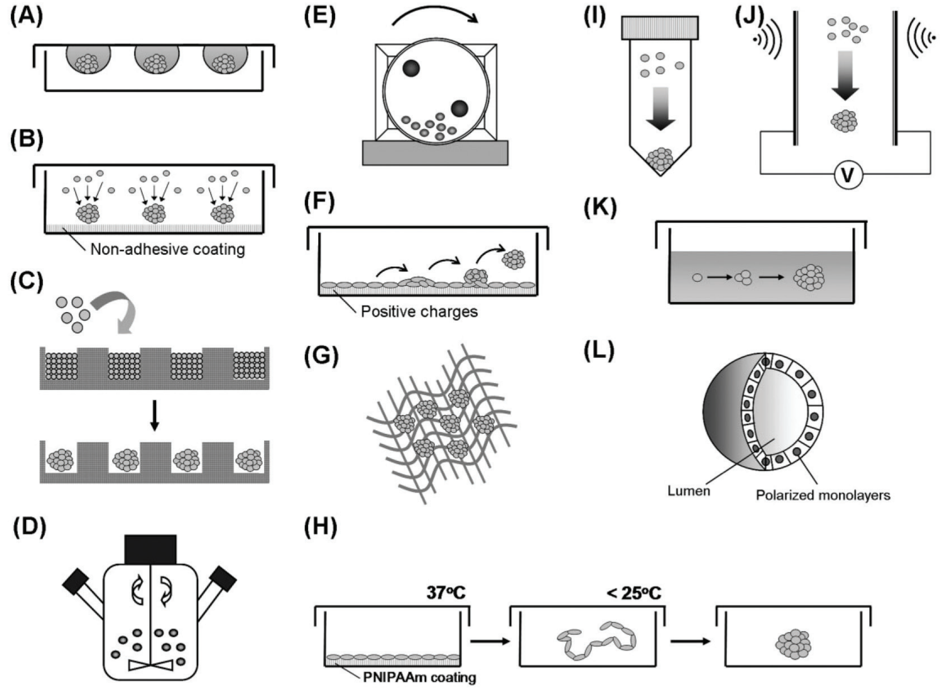

Figure 1.4 Different methods to create multicellular spheroids. In (A) using hanging drops, in (B) using a nonadhesive surface, in (C) using micromolds, in (D) using Spinner flasks, in (E) using Rotary cell culture, in (F) using self assembly of Hepatocytes on Primaria dishes, in (G) using porous 3-D scaffolds, in (H) using PNIPAAm-based cell sheets, in (I) using cell-pellet culture, in (J) using cellular aggregation originating from Electric, magnetic or acoustic forces, in (K) using a mixture of single cells with gel. Epithelial cysts are shown in (L)
From Ruei-Zhen Lin and Hwan-You Chang, Biotechnology Journal, 2008 [29]

Tumor cell migration is often studied *in-vitro* in regular monolayer cell culture. Hanging drop assays (**Fig. 1.4A**) have shown to be valuable in better mimicking the *in-vivo* situation by creating a small tumor of cancer cells in a 3D gel. Confocal imaging and compound testing have shown that cells grown in 3D respond differently to drugs than cells grown on a plate. Hanging drop assays and similar techniques of growing a clump of cells first, followed by embedding in a gel are difficult to perform reproducibly and time consuming. A clump of cells can be formed using many different methods, for an overview, see **Figure 1.4**.

Depending on the cell type it can take up to two weeks for forming a tumor with migrating cells. Cells that do not form cell-cell contacts are not suited for hanging drop assays. In chapter 5 it is shown that injection of a cell suspension into a gel can be used as well to form tumor spheroids similar to those derived from hanging drops. However, the method of injection can be automated and is shown to be usable in high-throughput *in-vitro* tumor migration assays to find new drug compounds. Possibly, this enables personalized treatment based on screen results derived from a patient's own biopsy.

Design aspects of this thesis

This thesis describes novel experimental methods and protocols aimed at studying cells and fragments of cells in a controlled, high throughput fashion. To invent or refine protocols a common design theory was used, introduced in this chapter's supplement. In short, the design theory allows the researcher to extract all elementary operations from a protocol or from methods used in a protocol. In an existing protocol, these elementary operations are performed using a previously chosen solution. To improve the method or protocol, i.e. to enable better, faster or more reliable experimentation, one can look at the performance of each of these solutions. Using the operation criteria of individual solutions one can even look for new/other possible solutions, which might improve the overall performance or the research method. The impact of such an improvement can be predicted and eventually measured during experimentation. For all research projects the improvements with the highest impact are listed below.

Chapter 2. A versatile microfluidic flow cell for studying the dynamics of shear-stress induced actin reorganization in renal cells

Problem: microfluidic chips are complex in use, and require dedicated microscopes or holder systems.

Solution: Using a method of piercing a capillary tube into the side of a PDMS microfluidic chip, a fluid side connection can be established. Such a side connection leaves enough room for all types of optics devices above and below the chip. A microfluidic channel in PDMS fitted with in- and outlet tubes offers a simple and stable platform to study shear stress in adherent cells.

Chapter 3. Determination of the size distribution of blood microparticles directly in plasma using atomic force microscopy and microfluidics

Problem: The concentration of blood plasma microparticles caught on an antibody coated mica surface is too low to measure conveniently using AFM.

Solution: Using a detachable microfluidic channel the same amount of fluid is run over a smaller surface area resulting in a higher number of microparticles attaching to the surface.

Chapter 4. A high-throughput screen for tuberculosis progression

Problem: Manual injecting zebrafish embryos is time consuming and prone to human errors, current automated methods do not scale well.

Solution: A better method of aligning zebrafish eggs has been invented by using a grid of hemispherical holes in agarose gel. The agarose gel allows optimal viewing from below, such that injection can performed vertically, and calibration of the injection depth is achieved by looking at the deformation of the embryo in the plane perpendicular to the optical axis.

Chapter 5. Automated microinjection of cell-polymer suspensions in 3D ECM scaffolds for high throughput quantitative cancer invasion screens

Problem: Current methods to disperse and monitor cells in 3D are slow and difficult to automate.

Solution: Cells are injected into the gel directly, mixing the cells with polymers allows the formation of a compact droplet, in which cell-cell contacts are formed within a day. Automation of injection allows for high-throughput injection and imaging.

References:

1. **Louise Harewood, Frédéric Schütz, Shelagh Boyle, Paul Perry, Mauro Delorenzi et al.** The effect of translocation-induced nuclear reorganization on gene expression. *Genome Res, 2010, 20: 554 - 564.*

2. **Bruce Alberts, Alexander Johnson and Peter Walter**, Molecular Biology of the Cell, 5th Revised edition. *Taylor & Francis Inc; 2007.*

3. **Vikki M. Weake and Jerry L. Workman**, Inducible gene expression: diverse regulatory mechanisms. *Nature Reviews Genetics, 2010, 11: 426 - 437.*

4. **K. Schenke-Layland, I. Riemann, F. Opitz, K. König et al**, Comparative study of cellular and extracellular matrix composition of native and tissue engineered heart valves. *Matrix Biology, 2004, 23: 113 - 125.*

5. **Edwin Cheung and W. Lee Kraus**, Genomic Analyses of Hormone Signaling and Gene Regulation. *Annu Rev Physiol, 2010, 72: 191 - 218.*

6. **Johan Skog, Tom Würdinger, Sjoerd van Rijn, Dimphna H Meijer et al**, Glioblastoma microvesicles transport RNA and proteins that promote tumour growth and provide diagnostic biomarkers. *Nature Cell Biology, 2008, 10: 1470 - 1476.*

7. **Susanne Osanto, Rogier M Bertina, Yuana Yuana, Tjerk H Oosterkamp, Brian A Ashcroft, Maxim E Kuil, Jan de Sonneville**, patent application *WO2010072410.*

8. **Clotilde Théry, Matias Ostrowski and Elodie Segura**, Membrane vesicles as conveyors of immune responses. *Nature Reviews Immunology, 2009, 9: 581 - 593.*

9. **Charles E. Samuel**, Thematic Minireview Series: Toward a Structural Basis for Understanding Influenza Virus-Host Cell Interactions. *J Biol Chem, 2010, 285: 28399 - 28401.*

10. **Matxalen Llosa, Craig Roy and Christoph Dehio**, Bacterial type IV secretion systems in human disease. *Mol Microbiol, 2009, 73: 141 - 151.*

11. **Eric J. Rubin**, The Granuloma in Tuberculosis - Friend or Foe? *N Engl J Med 2009, 360: 471 - 2473.*

12. **Douglas Hanahan and Robert A. Weinberg**, The Hallmarks of Cancer. *Cell, 2000, 100: 57 - 70.*

13. **Kristian Pietras and Arne Östman**, Hallmarks of cancer: Interactions with the tumor stroma. *Experimental Cell Research, 2010, 316: 1324 - 1331.*

14. **D. Hanahan, R.A. Weinberg**, The hallmarks of cancer. *Cell, 2000, 100: 57 - 70.*

15. **Lance A. Liotta and Elise C. Kohn**, The microenvironment of the tumour-host interface. *Nature, 2001, 411: 375 - 379.*

16. **Andrew I. Minchinton and Ian F. Tannock**, Drug penetration in solid tumours. *Nat Rev Cancer, 2006, 6: 583 - 592.*

17. **Writing Committee of the WHO Consultation on Clinical Aspects of Pandemic (H1N1) 2009** Influenza, Clinical Aspects of Pandemic 2009 Influenza A (H1N1) Virus Infection. *N Engl J Med, 2010, 362: 1708 - 1719.*

18. **J. Carl Pallais, Bonnie T. Mackool and Martha Bishop Pitman**, Case 7-2011 - A 52-Year-Old Man with Upper Respiratory Symptoms and Low Oxygen Saturation Levels. *N Engl J Med, 2011, 364: 957 - 966.*

19. **David Cervi, Tai-Tung Yip, Nandita Bhattacharya, Vladimir N. Podust et al.**, Platelet-associated PF-4 as a biomarker of early tumor growth. *Blood, 2008, 111: 1201 - 1207.*

20. **William Whiteley, Mei-Chiun Tseng and Peter Sandercock**, Blood Biomarkers in the Diagnosis of Ischemic Stroke. *Stroke, 2008;39: 2902 - 2909.*

21. **Charles L. Sawyers**, The cancer biomarker problem. *Nature, 2008, 452: 548 - 552.*

22. **J. Thomas Parsons, Alan Rick Horwitz and Martin A. Schwartz**, Cell adhesion: integrating cytoskeletal dynamics and cellular tension. *Nat Rev Mol Cell Biol, 2010, 11: 633 - 643.*

23. **Shawn P. Carey, Jonathan M. Charest and Cynthia A. Reinhart-King**, Forces During Cell Adhesion and Spreading: Implications for Cellular Homeostasis. *Cellular and Biomolecular Mechanics and Mechanobiology 1st Edition., 2011, 29 - 70.*

24. **Amy L. Paguirigan and David J. Beebe**, Microfluidics meet cell biology: bridging the gap by validation and application of microscale techniques for cell biological assays. *BioEssays, 2008, 30: 811 - 821.*

25. **Olivier Rubin, David Crettaz, Jean-Daniel Tissot and Niels Lion**, Microparticles in stored red blood cells: submicron clotting bombs? *Blood Transfus., 2010, 8: s31 - s38.*

26. **Y Yuana, TH Oosterkamp, S Bahatyrova, B Ashcroft et al.**, Atomic force microscopy: a novel approach to the detection of nanosized blood microparticles. *Journal of Thrombosis and Haemostasis, 2010, 8: 315 - 323.*

27. **David N. McMurray**, *Mycobacterium tuberculosis* Complex. *Medical Microbiology. 4th edition, 1996, Chapter 33*, www.ncbi.nlm.nih.gov/books/NBK7627

28. **Mandeep Jassal and William R Bishai**, Extensively drug-resistant tuberculosis. *Lancet Infect Dis, 2009, 9: 19 - 30.*

29. **Ruei-Zhen Lin and Hwan-You Chang**, Recent advances in three-dimensional multicellular spheroid culture for biomedical research. *Biotechnology Journal, 2008, 3: 1172 - 1184.*

Supplement
Functional design theory

Changing protocols, method development

It is known that the change of habitat of cells, taken from a multi-cellular organism, to single cell species culture has a large impact on the cell fate. This effect is significant: some cell types are very difficult to keep alive outside the organism. Studies of cells outside the organism may require the development of new methods that have to be tested and shown to be biologically relevant.

The state of the biological specimen must either be very close to the state in other comparable experiments, or else experiments must be performed to show that the treatment of the specimen does not alter the specimen's state so much that the results have only little predictive value. Next to the fact that there must not be more than a single variable changed between control and wild-type experiments, to be able to address the difference in results to this single variation, the experimental setup itself must also be tested. This is explained in more detail in Chapter 6.

Keeping in mind that biological material is more difficult to control, and often needs inspection using microscopy, the design methodology of new methods and systems for experimentation is similar to methodologies used in standard engineering. The complexity of biological material however, requires discussions between biologists, chemists, physicists and engineers. Literature, experience and other sources of information are used as a source for methods and protocols, which are not always accessible for specialists from other, collaborating fields.

A common design concept and language help to lower the language barriers between people from different fields and guides the design towards system requirements and specifications. In this thesis work standard design principles were used as described in the book "Fundamentals of business engineering and management"[1]. A short introduction of design principles used in this thesis is given below.

Engineering protocols

A cell-biology protocol consists of one or more steps of sample treatment and one or more different measurements. Each of these steps is performed with a specific purpose. Neither purpose of each step is always mentioned in

a protocol, nor the possible outcomes in case errors occur. The new journal "Nature Protocols" offers a good practice of mentioning common pitfalls and control measurements to check if a protocol works as designed.

A key step in engineering (new) methods is to create a list of functions, acting on the sample, in a logical chain, similar to a protocol, where a list of actions is described. Each action is performed using a specific tool or instrument; it is in essence the solution to the function that was required. The tool or instrument to perform the action is chosen based on specific requirements, performance, availability and costs.

When multiple (parts of) protocols can be used resulting in a similar measurement or specimen outcome, there exists one list of functions describing both protocols, here called the golden list of functions (GLF). For example, for the function "separate cells from a suspension", there are two (probably more) lists of possible actions (solutions):

1. pipette cell suspension onto a 1-micron filter, resuspend filtered cells using a pipette
2. fill a tube with the cell suspension, centrifuge at 500 g for 5 minutes, resuspend the cell pellet using a pipette

Each solution can have its own benefits and costs, and required instruments. Clearly in the above example a pipette is a necessity, i.e. when a pipette is not available another solution must be found. The first solution uses (disposable) filters, that can be expensive when a lot of cells have to be separated, while the second requires a centrifuge, which may be cheaper in the long run.

To allow for a fair method comparison the GLF must be found first. Note that this practice is often omitted in review articles, and this correlates strongly with a reduction in the objectivity of the author towards the different methods.

Similarly, when one likes to improve an existing protocol it is wise to construct a list of functions first, as this allows for an overview of all functionalities. Sometimes it might be possible to integrate one or more functions into a new function. This can also help in finding the GLF, which can be explained using the same example as described above, take action list 1, translated to functions:

F1: transfer cell suspension onto filter device results in filtered cells
F2: mix filtered cells with medium

We can ask the question “for what purpose?”, and the answer is as given: “to separate cells from a suspension”. As such the chain of functions is shortened, and one could check if other (parts of) protocols follow the same chain. Even from this simple example it can be seen that the exact answers are not always obvious. Another answer to the question above could be “to increase the cell concentration” or “to remove proteins from the cell suspension”.

To find solutions to given functions, the GLF can be used to generate more - and more detailed - chains of functions. Often it is possible to find many chains of elementary functions that describe a higher function, i.e. a less precise function described at a higher level of abstraction. It’s left for the reader to create a chain of elementary functions of the second list of actions of the above example, to result in two chains of elementary functions that describe “separate cells from a suspension”.

Creating a new protocol or improving an existing protocol is challenging and requires many design decisions. Using the GLF it is easier to see how improvements in one function might influence the performance and or necessity of others. It also allows insight to combine parts of existing protocols, or to search for more solutions for one given function. In this thesis in each article mostly one fundamental function was changed, for example “align zebrafish eggs” in Chapter 4, leading to vast improvements in performance of others.

As an example, a previous solution to align zebrafish eggs was to partly suck the eggs into tiny holes in a plate (**Fig. 1.5**). The article described the successful, advanced method of automatic alignment procedures that were designed to enable fast, automated injections of 25 eggs per run of 2 minutes, using this alignment plate.

From the image in the article, it can already be seen that alignment was not perfect and centered, and therefore required image recognition before each injection. Also it was difficult to scale this design up, as suction of a 1000 eggs on a plate is physically very difficult (eggs rupture because of the required higher suction pressure). As such we choose to search for a better alignment solution (see Chapter 4).

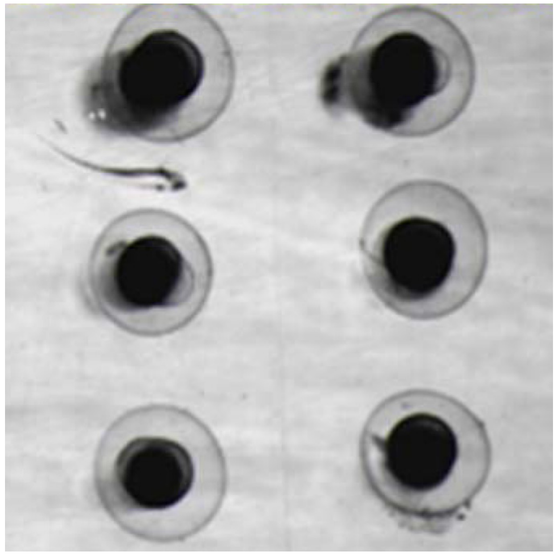

Figure 1.5 Detail from Figure 3, Wenhui Wang, Xinyu Liu, Danielle Gelinas, Brian Ciruna and Yu Sun, PloS ONE, 2007[2]

Discussions with many people, from different disciplines, including mechanical engineers allowed me to find new solutions for specific functions required in existing protocols. Key element in this research was to translate the protocols into the exactly needed functions, and through many discussions find out what requirements of each function are. Within the Cell Observatory many different research groups are located at close proximity, enabling easy communication and discussions. Thus it provided the stimulating, multi-disciplinary environment that is required for the type of work described in this thesis.

References

1. **W. ten Haaf, H. Bikker, D.J. Adriaanse**, Fundamentals of business engineering and management, *Delft University Press, 2002*, http://www.vssd.nl/hlf/b001.htm

2. **Wenhui Wang, Xinyu Liu, Danielle Gelinas, Brian Ciruna and Yu Sun**, A Fully Automated Robotic System for Microinjection of Zebrafish Embryos. *PloS ONE, 2007, 2(9): e862.*

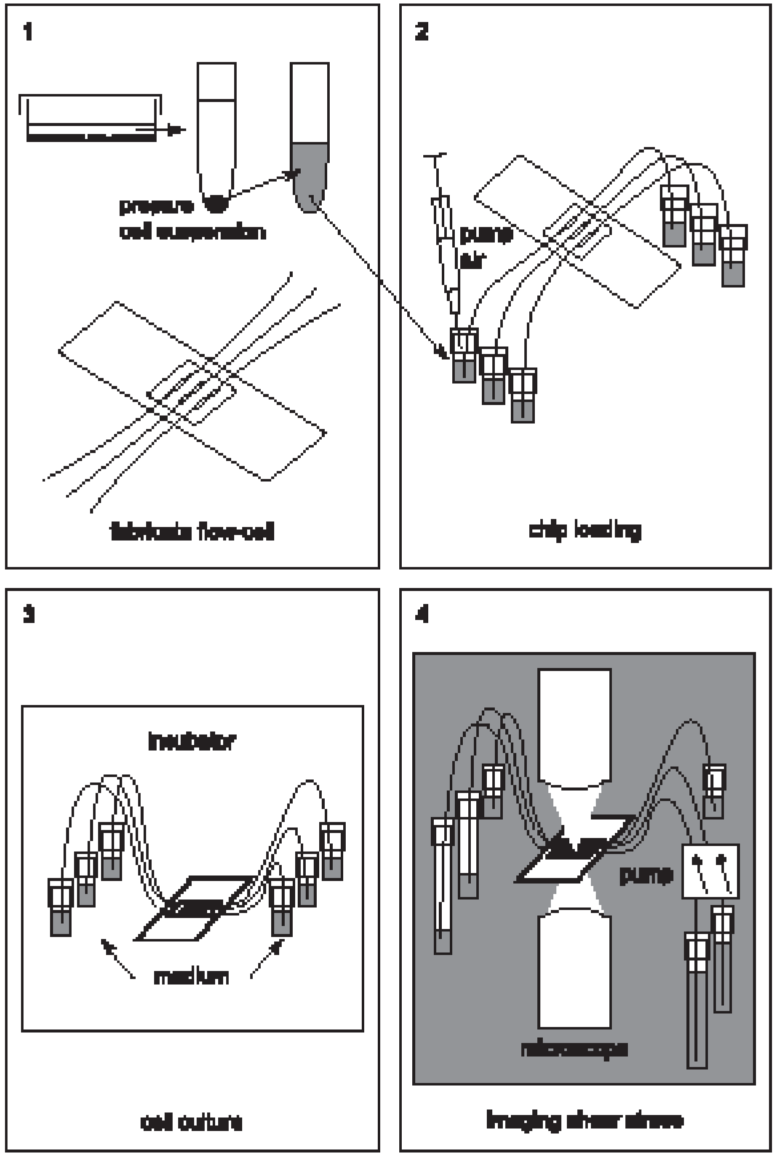
1
pressure
cell suspension
fabricate flow-cell
2
pump
air
chip loading
3
incubator
medium
cell culture
4
pump
microscope
imaging shear stress

Chapter 2

A versatile microfluidic flow cell for studying the dynamics of shear-stress induced actin reorganization in renal cells

Jan de Sonneville[a], Maxim E. Kuil[a],
Esther van Stapele[a], Hans de Bont[b], Henk Verpoorten[c], Mathieu H.M. Noteborn[a], Jan Pieter Abrahams[a], Bob van de Water[b] and
Sylvia E. Le Dévédec[b]

a *Leiden Institute of Chemistry (LIC), Einsteinweg 55, Leiden University, Leiden, the Netherlands*
b *Division of Toxicology, Leiden Amsterdam Center for Drug Research (LACDR), Einsteinweg 55, Leiden University, Leiden, the Netherlands*
c *Department of Fine Mechanics, Leiden University, Leiden, the Netherlands*

Manuscript submitted

Abstract

To resolve spatially and temporally the dynamics of the actin cytoskeleton under shear-stress, we developed a microfluidic flow cell featuring multiple channels. Using novel side connections, the microfluidic device is suitable for various light microscopy techniques in combination with high resolution imaging. In this device, different types of cells can be cultured for weeks without active flow control in a standard cell incubator. We evaluated shear-induced reorganization of the actin cytoskeleton of renal LLC-PK1 cells expressing ectopic GFP-actin. Using this device, we subjected the cells to a laminar flow and quantified in time and space the change in phenotype between control and shear situation. During the time of the experiment, we observed that a laminar flow induces enhanced cell motility associated first with lamellipodia formation, followed by actin stress fibres formation together with a reinforcement of the cortical ring. These results demonstrate the versatility of our newly developed microfluidic flow cell that fits with any standard microscope and indicate that enhanced local tubular flow-mediated shear forces affect the intracellular signalling that drive cytoskeletal reorganization.

Introduction

In the kidney, renal tubular cells are continuously bathed by the tubular fluid. The tubular flow is a main determinant of kidney behaviour in term of transport of water and solutes. Fluid shear stress (FSS) produced by this renal tubular flow is a modulator of salt and water reabsorption. An intact actin cytoskeleton is essential for proximal tubular cells (PTCs) to transmit flow-induced mechanical forces and subsequently modulate transport. The tubular flow rate, relatively stable in physiological conditions, may increase after a substantial reduction of renal mass. As a consequence, one of the hallmarks of renal mass reduction is still the progressive deterioration of the remaining functional nephrons which may be partly caused by flow-induced phenotypic modification of proximal tubular cells (PTCs). This deterioration of renal structures is observed in a large number of renal diseases[1]. In contrast to vascular endothelial cells (Ecs)[2-5] the effect of FSS on cytoskeletal organization of PTCs remains poorly understood[6,7]. Until now, only two studies on PTCs showed that these cells undergo a change in phenotype in response to FSS and that there is a marked redistribution of F-actin[8-11]. Nevertheless, these studies were limited to fixed samples and could not provide spatiotemporal information on FSS-induced renal cell cytoskeletal reorganization.

The best known device to study FSS on adherent cells is a parallel plate chamber[12]. Using such a device, cells are first grown on a coverslip, and then the flow cell is constructed around this coverslip before the flow experiment is performed. This method has several disadvantages. During the construction, prior to the experiment, the cells are subjected to pressure changes and medium flows which are unpredictable and not reproducible. Once assembled, most flow cells, including the parallel plate chamber, are difficult to move, and therefore placed on the microscope for the duration of the experiment. Control experiments, using the same flow cell but without flow or with minimal flow, are for this reason performed at different time-points or locations.

The use of multiple microfluidic channels instead of one large parallel chamber would offer an adapted solution. For this reason we searched for a microfluidic chip platform that does not need to be assembled directly onto the microscope. Furthermore it should be compatible with many types of light microscope setups. Using the gas-permeable properties of polydimethylsiloxane (PDMS), we found that a passive medium flow is sufficient to culture cells for weeks in microfluidic channels, allowing us to create a mobile and flexible usage of the microfluidic cell culture platform. When connected to small medium containing flasks, the microfluidic culture system is compatible with standard cell incubators. Furthermore, a novel side connection to thin glass capillary tubes allowed us to conform to the working distances of both condenser and objective lenses used in high resolution fluorescent light microscopy. In conclusion, we designed a multishear microfluidic device that allows controlled fluidic shear stress on cells in parallel and that is suitable for high resolution light microscopy. This is particularly beneficial for studying the actin cytoskeleton reorganization upon shear stress, as it is demonstrated in this paper.

Following the introduction of the chip, we present the effects of FSS on renal tubular epithelial cells. We exposed LLC-PK1 cells expressing ectopically either GFP-actin or GFP-zyxin to a defined laminar flow in a parallel flow chamber and performed live cell imaging of the actin cytoskeleton re-organization. LLC-PK1 cells express the phenotype of epithelial cells of the proximal tubule and have previously been described to be sensitive to fluid shear stress (FSS)[10]. We have quantified fluid shear stress (FSS)-induced actin cytoskeleton reorganization in time and space. The results show that renal cells respond to FSS with an increase in motility associated with a cytoskeletal reorganization including lamellipodia and cytosolic actin filaments formation together with a reinforcement of the lateral actin network.

Material and Methods

Microfluidic flow cel

To understand in more detail how cells change their phenotype when exposed to laminar flow, we developed a microfluidic flow cell which comprises three channels, allowing for a direct comparison between shear stressand control environment. The PDMS channels are produced using a mould which was fabricated from brass using standard milling techniques.

The flow cell is constructed in a novel way, by injecting bevelled glass capillary tubes from the side into the PDMS chip (**Sup. Mov. 1**). After injecting the glass capillary tube to form in- and outlet, the connections are fixed and the tubes stay attached for the duration of the experiment (**Fig. 2.1(a), 2.1(e)**). With these side-connections the condenser lens has freedom to operate, and can be positioned close to the top of the device. After the flow cell is loaded with cells, it is connected to small reservoirs containing fresh medium (**Fig. 2.1(b)**). The reservoirs are placed slightly above the flow cell, to allow for passive flow of fresh medium to the microfluidic channels, as the medium evaporates slowly through the PDMS. The resulting device is small and stable enough to move easily from incubator to a microscope. Prior to applying shear stress, the cells are grown for a couple of days to the desired confluence.

Preparation of capillaries

Capillary tubes having an outer diameter of 375 micrometer and an inner diameter of 150 micrometer (TSP Fused Silica Tubing, deactivated with DPTMDS, from BGB-shop) are cut using a piece of aluminum oxide to create a slight scratch in the glass, through the polyimide coating. The capillary ends are bevelled using mechanical grinding with a disc containing diamond dust. Before and after the mechanical grinding, the capillaries are rinsed with MilliQ water to remove glass dust.

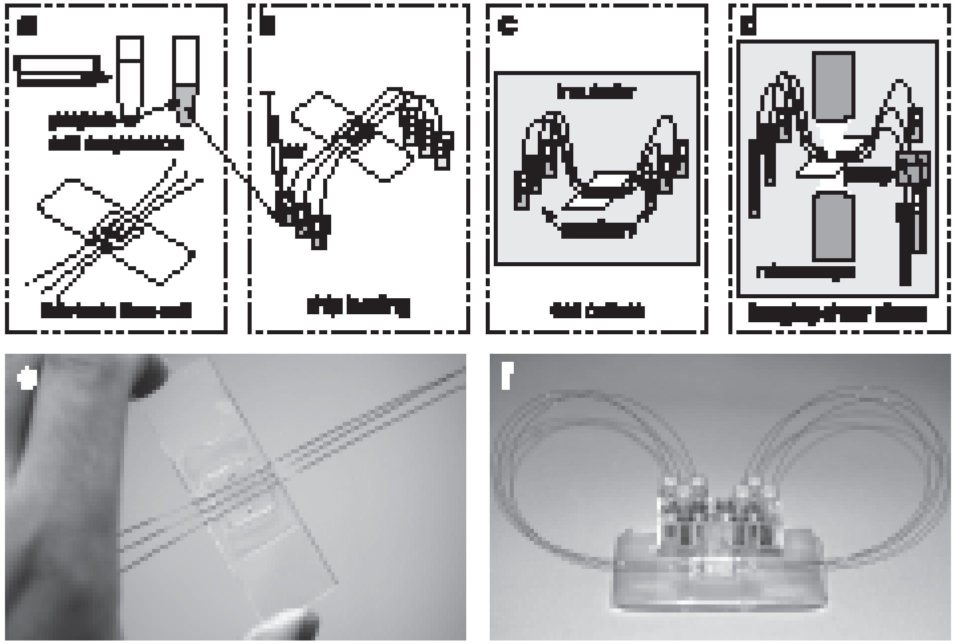

Figure 2.1 Overview of the use of the flow cell for live cell imaging. In a, flow cell is prepared and adherent cells are brough into suspension. In b, using little vials and a syringe to create a pressure, the flow cell is loaded with cells. When cells are loaded, vials containing medium are connected, and the flow cell is placed in the incubator (c) to stimulate cell growth. When cells reach enough confluence, a flow cell is selected and placed in a temperature controlled microscope. One or two channels are connected to the pumping system to apply a shearing force to the cells (d). In (e), a picture of a flow cell, fabricated on a microscope glass. (f) shows a connected flow cell as placed in the incubator.

Mould fabrication

A mould used to create a microfluidic flow cell was fabricated using CNC milling a structure, designed in autocad, out of brass. To be able to create an optically flat surface of the channel, the mould was created in four steps, as illustrated in **Fig. 2.2 (a-d).** First the structure of the circuit is milled out of brass(a), and at the edges of the structure at the same level as the top of the dykes in the structure sacrificial material was maintained. The sacrificial material was used to support the polishing tool, to be able to polish (b) the surface of the top of the dykes. After polishing this sacrificial material was removed. Then, from the bottom little holes are drilled towards the end of the channels, the location of the receiving chambers (c). Finally pins with a diameter of 0.5

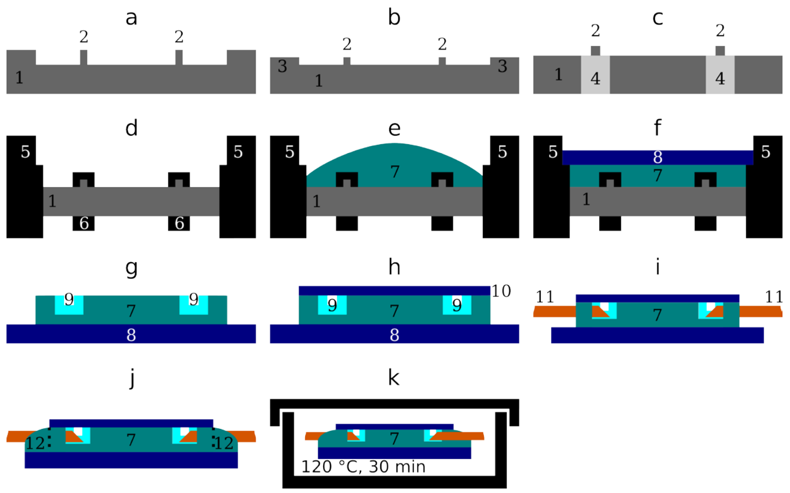

Figure 2.2 Schematic overview of the mould fabrication process. First the channel structure is milled in brass (1; a), followed by polishing of the channels (2; b). After, the polishing support (3) is removed using milling, and holes are drilled (4) through the mould at the place of the connection chambers (c). Rods are placed in the holes (6), and mounted to the desired height (d). A ring(5) is used to support the glass (8) during polymerization of the PDMS (7; e, f). After, the flow cell is removed, cut to the desired size, and placed onto a microscope glass (8; g). Using an oxygen plasma treatment, a coverslip (10) is covalently bound to the PDMS (h). Then the closed flow cell is injected using beveled glass capillary tubes(11) until the connection chambers (9) are reached (i). Finally, extra PDMS is poured over the glass slide and the capillary tubes, to secure the connection (12; j). Before use, the flow cell is sterilized using an autoclave (k).

mm are inserted in these holes and mounted at a height of preferably half the height of the flow cell plus half the diameter of the tubes used to connect the flow cell, these pins will form the receiving chambers (d).

The mould is filled with a mixture of degassed PDMS (Dow Corning Sylgard 184, mixed in a 10:1 ratio), see **Fig. 2.2(e)**. A vacuum is applied to degas the PDMS mixture until all entrapped air is released (takes about 30-60 min). The filled mould is carefully covered (to reduce the chance of reintroducing air bubbles) with a glass plate to create an optically flat surface (f). Curing is performed at 70 degrees Celsius for one hour. The brass mould is removed (g) and an oxygen plasma treatment (Femto, Diener Electronic) is used to covalently bind a cover slide onto the freshly cured polymer flow cell to form the bottom of the microfluidic device (h). For this the glass cover slide is first placed in the oxygen plasma (standard air, 0.1 mbar) for 10 min, after the PDMS part is placed under the same

oxygen plasma for 30 seconds. Then within a couple of minutes both parts are pressed and held together and placed in an oven at 70 degrees Celsius for one hour. On the top side of the PDMS a standard microscope glass is adhered to ease transport and to place the flow cell in a standard microscope setup. After connection (i), an extra layer of PDMS is applied (j). This extra layer provides a stronger bond between the bottom glass plate and the PDMS. Before or after connecting the flow cell, depending on the experiment, the flow cell and capillaries are sterilized using an autoclave at 120 degrees Celsius for 30 minutes (k).

Fluid manipulation in the microfluidic flow cell

Autoclaved flow cells were connected to little septum capped vials (1.5 mL, Grace Alltech) and filled through capillary tubing. After the inlet and outlet of the flow cells were each connected to a vial, a slight overpressure was generated by injecting a syringe needle into a closed vial and injecting clean air. This pressure generates a flow of liquid from the vial through the submerged entry capillary connected to the flow cell and the exit capillaries to the exit (waste) vial. This method was used to rinse, prepare and fill the microfluidic flow cell.

Medium Flow

Using One-Piece Fittings from LabSmith (http://www.labsmith.com) the inlet capillaries were connected to micro-angular gear pumps (mzr2521 and mzr-controller, HNP Mikrosysteme GmbH, Germany) and the outlets of the channels were let to a waste reservoir. The pump was operated at 60 percent of the max speed, and used to pump at a flow rate of 1 mL/hour, through a channel (w/h=300µm/100µm) resulting in a mild shear stress of approx 6 dyn/cm^2 . Formula (1) is used to calculate shear stress assuming parallel plate geometry[13].

$$\tau = \frac{6Q\mu}{bh^2}$$

Formula (1)

Q = flow rate in cm^3/s ($3\cdot10^{-4}$ cm^3/s), µ = viscosity (ca. 0.01 dyn s/cm^2), h = channel height (0.01 cm), b = channel width (0.03 cm), τ = wall shear stress (dyn/cm^2), calculated to be ~6 dyn/cm^2 ($6\cdot10^{-5}$ N/cm^2).

Cell culture

The porcine renal epithelial cell line (LLC-PK1) cells were maintained in DMEM supplemented with 10% (v/v) fetal calf serum and penicillin/streptomycin at 37°C in a humidified atmosphere of 95% air and 5% carbon dioxide. For preparation of stable GFP-actin expressing cell lines, LLC-PK1 cells were transfected with 0.8 µg of DNA of pEGFP-actin[14] (Clontech, Mountain View, CA) and GFP-Zyxin using Lipofectamine-Plus reagent according to the manufacturer's procedures (Invitrogen). Stable transfectants were selected using 800 µg/mL G418. Individual clones were picked and maintained in complete medium containing 100 µg/mL G418. Clones were analysed for expression of GFP-actin and GFP-zyxin using immunofluorescence.

Flow cell preparation and cell loading

After the microfluidic flow cell was perfused first with a collagen solution (30µg/mL) for an hour at room temperature and secondly with the medium for 10 minutes, after a cell suspension of 3 million cells per mL was introduced into the channels. When the channel was fully loaded with cells the cell suspension vial was replaced by a vial of fresh medium such that inlet and outlet of the microfluidic channel have a medium reservoir. The microfluidic flow cell was then placed in the incubator at 37°C for 1 hour to allow the cells to adhere. Three to five days elapsed until the cells had grown at about 80% confluence. During incubation of the cells in the incubator the vials with medium are placed higher than the flow cell such that the channels experience a slight hydrostatic pressure of medium. As PDMS is permeable to air, the medium in the channel slowly evaporated but was refilled with medium from the flasks.

Live cell imaging

Bright field, fase contrast imaging

During cell culture incubation, cell confluence was monitored daily using a standard fase contrast transmission Nikon TMS microscope using a 20X plan apo NA 0.75 lens objective.

Fluorescence confocal imaging

During shear stress experiments cells were visualized during 24 hours with a confocal Nikon TE 2000-E microscope equipped with perfect focus system in a humid climate of 37°C and 5% CO_2. A z-scan was done through the cells to be able to visualize both F-actin stress fibres and cell-cell contact (8 scans every 1,5 µm so in total 12 µm). Movie frames were captured every 10 minutes using a 20x objective for 12 hours.

Nomarski (DIC) imaging, TIRF imaging

The TIRF and DIC pictures were captured on a Nikon TIRF microscope system (Eclipse Ti-2000, Nikon with automated stage) using a 60x plan apo TIRF NA 1.49 lens objective and controlled by NIS-elements AR software (Nikon).

Differential interference contrast (DIC or Nomarski) imaging uses polarized light and selectively captures polarization changes after a second polarization filter used to remove the input light. These polarization changes provide detailed information about the cellular shapes and structure.

Image analysis

Manual cell tracking and image processing and some analysis were done using Image-Pro Plus (version 7.1, Media Cybernetics Inc., Silver Spring, MD) while others were done using the free software ImageJ (NIH). For the analysis of the confocal movies, we used the extended depth of focus. This method combines a Z-stack and results in a single composite best-focus image. For this, the Z-stack was combined with the maximum through depth contrast. Then, the mean value of the pixels from each plane at the current location is calculated. Finally, the pixel from the plane with the largest variance from the mean is selected.

Results

To test the compatibility of the microfluidic device for cell culture, we used three different cell types including human tumor HeLa cells, keratinocytes (data not shown) and renal epithelial LLC-PK1 cells (**Fig. 2.3**).

The PK1 cells were cultured inside the channels for up to three weeks and showed a multilayer structure as is the case as well in a basic culture flask (**Fig. 2.3(a)**). After two days of incubation in a channel, a group of cells is im-

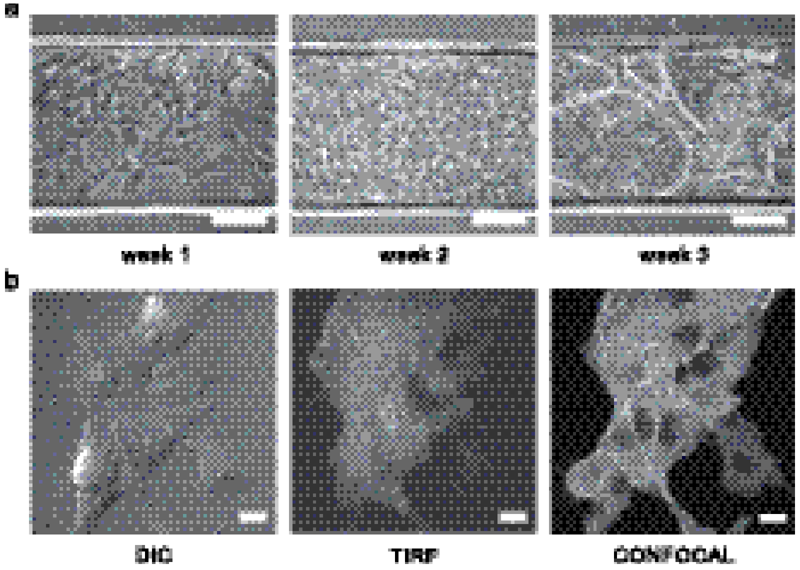

Figure 2.3 Cell culture in a microfluidic channel of the flow cell. In (a), phase contrast microscope images of cells growing in a flow cell during three weeks, scale bar is 100 μm. In (b), the same group of cells is imaged using different microscope live cell imaging techniques, scale bar is 20 μm.

aged using various microscope techniques. The advantages of each technique for studying the actin cytoskeleton in LLC-PK1 cells expressing ectopically GFP-actin are visible in **Fig. 2.3(b)**. Differential Interference Contrast (DIC) microscopy image allows for detailed studies of membrane structures, such as the outer cell-membrane and nucleus. Using Total Internal Reflection Fluorescence (TIRF) microscopy, the actin cytoskeleton can be imaged up to the first 100 nm above the bottom of the microfluidic channel. It shows the focal adhesions as separate bright spots. Confocal microscopy allows studying fluorescently labeled actin, close to the surface, but including structures such as fibres which are invisible to TIRF microscopy. One single plane of a 3-D stack of confocal images is visible in **Fig. 2.3(CONFOCAL)**.

Shear-stress results in enhanced motility in renal epithelial cells

Having established a platform which can be used for stable cell culture in microfluidic channels, and allows for high resolution dynamic live cell imaging, we were interested in analysing differences between fluid shear-stimulated and non-stimulated cells. Previous studies have shown that fluid shear stress induces changes in phenotype in renal cell, based on imaging results of fixed

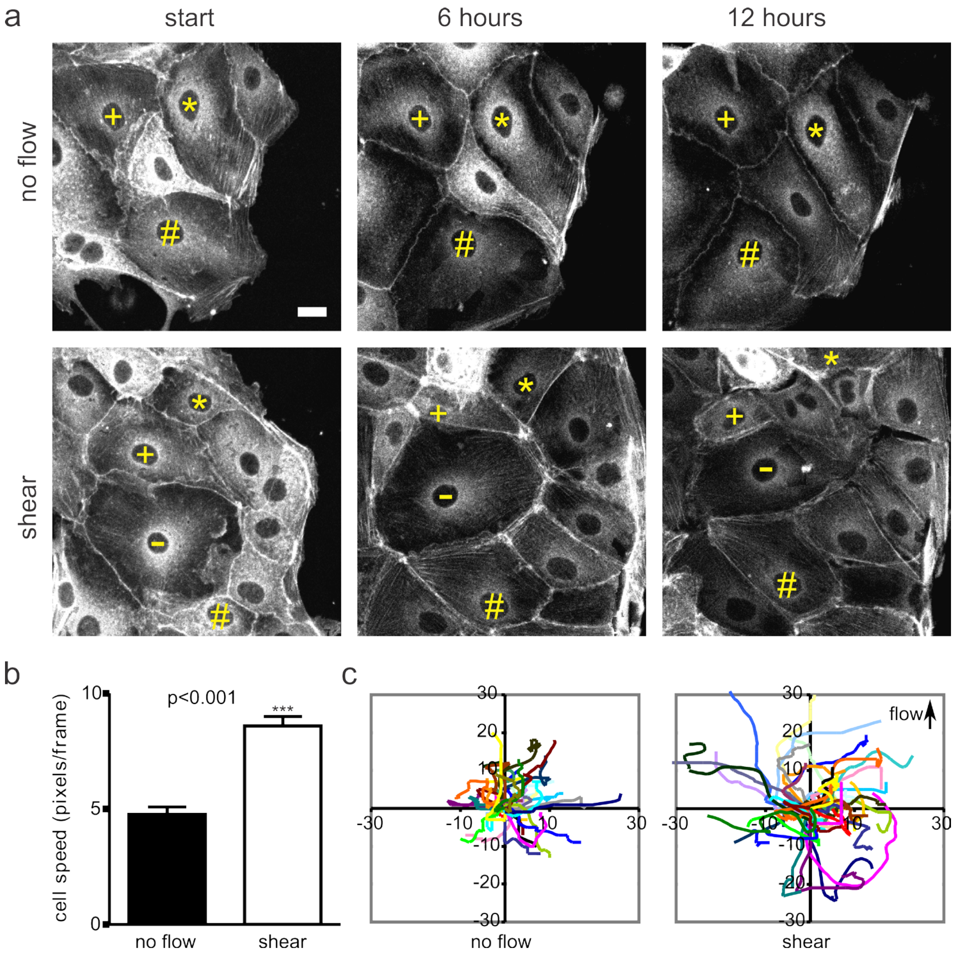

Figure 2.4 Cell tracking analysis of confocal time lapse series of LLC-PK1 cells expressing ectopically GFP-actin. Cell nuclei were manually tracked in sheared and control cells, scale bar is 20 μm (a). Quantification shows a significant increase in cell motility of sheared cells (b). Tracked trajectories show that cells subjected to a flow are more motile, but not in a preferred direction (c).

specimen[8-11]. Here, we quantify the changes in phenotype of renal proximal tubule cells using live confocal microscopy. The FSS within the renal tubular system is estimated in the range of 0.2-20 dyn/cm^2 which is about 10% of that of the endothelial cells[15]. In our study, we chose to apply a FSS of 6 dyn/cm^2 which may be relevant for understanding FSS induced renal disease progression. Subconfluent LLC-PK1 cells were cultured for 3 days and then exposed to either ~0 or ~6 dyn/cm^2 for 12 hours (**Fig. 2.4(a) and Sup. Mov. 2.2**).

During exposure, the cells were imaged by confocal microscopy to monitor the change in phenotype upon FSS. Manual cell tracking of cells grown to subconfluence upon mild shear stress of 6 dyn/cm^2 shows significant increased movement (**Fig. 2.4(b)**), but not in a preferred direction (**Fig. 2.4(c)**) with respect to the fluid flow as it is the case for endothelial cells. These results indicate that renal epithelial cells are FSS sensitive and show increased motility upon fluid shear stress.

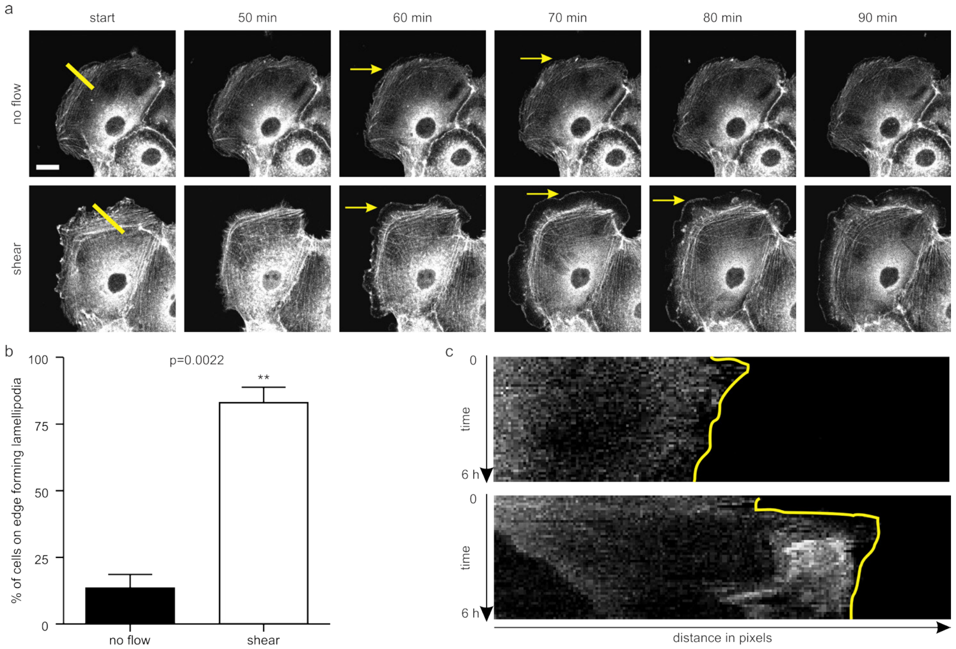

Figure 2.5 Lamellipodia formation in LLC-PK1 cells subjected to FSS. Shear stress induces lamellipodia formation (see arrows indicating newly formed lamellipodia (a). Quantification of cells showing high membrane ruffling activity, scale bar is 20 µm (b). A kymograph of a cell boundary shows the lamellipodia formation in more detail (c)

FSS induces rapid lamellipodia formation

Since confocal time lapse image sequences of the actin cytoskeleton were acquired at 10 min intervals for 12 hours we could quantify the change in phenotype of the renal cells. Within the first hour of shear stress application, lamellipodial protrusion was induced at cell periphery (**Fig. 2.5(a,b) and Sup. Mov. 2.3**). Cells not exposed to the laminar flow showed little rearrangement in their actin meshwork, or only random formation of small ruffles at the cell border. In contrast, the creation of a laminar flow resulted in a strong reorganization of the actin cytoskeletal network with the formation of large lamellipodia in most of the cells located on the edge of an island and active membrane ruffling at cell-cell contacts. The change in membrane dynamics could be quantified by making a kymograph of the lamellar region of the control and sheared cells (**Fig. 2.5(c)**).

FSS induces actin stress fibres and cortical ring formation

Next to the active membrane ruffling, we observed a change in F-actin distribution over the time of the experiment. In the no-flow treated cells, GFP-actin localized preferentially at cell-cell contacts in a relatively thin disorganized actin network. Exposure of the cells to FSS caused formation of arranged thin bundles of actin throughout the cells. In addition, cells became more motile and strengthened their junction by forming a continuous and organized cortical actin network. Imaging of cells expressing the mechanosensitive protein zyxin[16] shows that upon FSS zyxin disappeared from the focal adhesions bound to actin filaments to localize to the junction between cells. Thus, LLC-PK1 cells exposed to FSS induced a significant reinforcement of intercellular junctions. Unlike previously described for epithelial cells, the actin cytoskeleton of unsheared PK1 cells demonstrated few and weak cytosolic actin stress fibres (**Figure 2.6(a)**). Laminar flow (1 mL/min, 6 dyn/cm^2) for 12 h induced a formation of cytosolic actin stress fibres and a reinforcement of the lateral actin network (**Figure 2.6(b)**). This was also confirmed with the live cell imaging of LLC-PK1 cells expressing GFP-zyxin: upon shear stress, zyxin containing matrix adhesions redistribute from the ventral side to the periphery of the cells (**Sup. Fig. 2.1 and Sup. Mov. 2.4**), which correlates with the formation of strong tight junctions.

In conclusion, we demonstrated that our microfluidic device is adapted for studying in details the dynamics of the cytoskeleton in cells upon shear stress.

Discussion

Using our novel device to apply shear stress to LLC-PK1 cells confirmed previously published results and also provided more detailed information on the cytoskeletal reorganization upon FSS in time and space. FSS induced higher

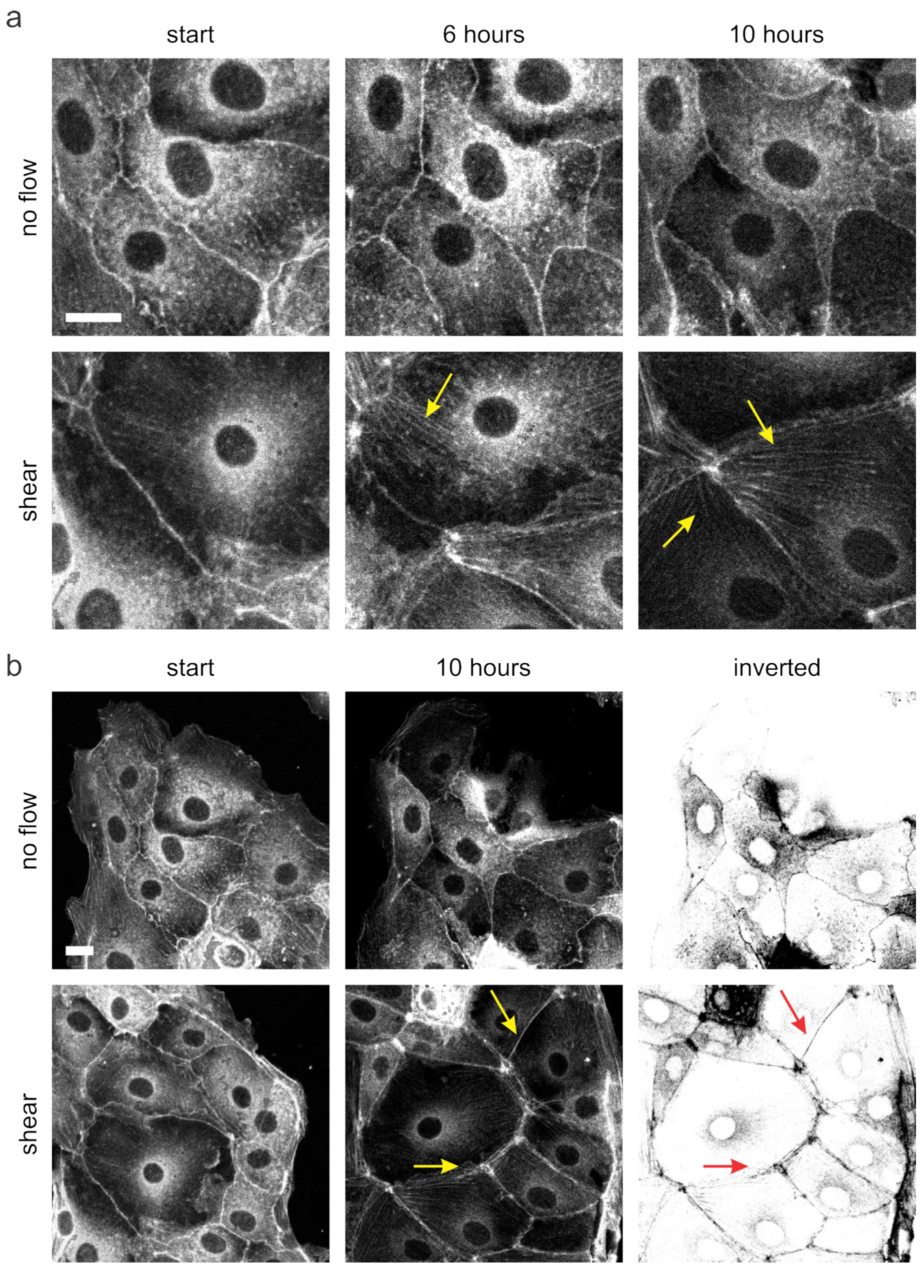

Figure 2.6 Stress fibres formation and actin network reinforcement. Shear stress induces actin fibres formation (see arrows indicating newly formed stress fibres), scale bar is 20 µm (a). In addition, FSS results in the reinforcement of the actin network at the cell-cell contact, scale bar is 20 µm (b). In conclusion, we demonstrated that our microfluidic device is adapted for studying in details the dynamics of the cytoskeleton in cells upon shear stress.

motility of the LLC-PK1 cells which was associated with increased activity of the membranes ruffles. During the course of the experiments with a FSS of 6 dyn/cm^2, the actin cytoskeleton reorganizes in a cortical ring together with stress fibres. Cell-cell junctions become stronger and zyxin, a mechanosensitive protein disappear from the focal adhesions to localize at the cell-cell contacts. Those observations are opposite to those made for endothelial cells but fit partially with observations made on proximal tubular cells[8-11]. The reorganization of cytoskeleton observed in epithelial cells is not identical to that observed in endothelial cells where the actin stress fibres strengthen and align along the flow direction[14]. In contrast, tubular epithelial cells do not align to the direction of the flow, show high motility and reinforce the apical and lateral domains of actin filaments. The polymerisation of new actin filaments is necessary for the cell motility and is probably weak in the no-flow chamber since the cells are cultured for a long period of time. High cell motility was quantified using time-lapse microscopy where LLC-PK1 cells appeared to switch to a motile phenotype within minutes after the onset of the laminar flow. At the same time, within an hour after the start of the experiments, massive membrane ruffling occurred as it was previously observed in podocytes[17]. Renal cells loss in the flow chamber occurred rarely. In response to shear stress, the renal cells may adopt an intermediate adhesiveness (zyxin re-localization), which enables the cells to be more motile but also contributes to increased detachment upon force application. Renal cells seem to weaken their adhesions, rearrange their actin cytoskeleton to be able to migrate. Indeed, cell migration requires persistent lamellipodial protrusion and actin filament polymerisation which was indeed observed in our study. The induction of a migratory, intermediate adhesive phenotype and the reorganization of the actin cytoskeleton in a nonpolarized fashion would fit with the *in-vivo* situation e.g. remodelling after substantial renal mass reduction. This specificity of cytoskeleton reorganization induced by flow depends on the function of the cell.

The microfluidic flow cell is very user friendly. It fits together with the medium reservoirs in a standard incubator, is quite robust in use, can be steam autoclaved, and fits in a standard microscope-glass holder. The passive configuration allows to culture cells in many chips in parallel. During transport the chip is closed, thus sterile, and including the small vials it's a small package which fits in one hand. It is compatible with inverted/upright and transmission microscopes, bright-field, DIC fluorescence, confocal and TIRF microscopy. We used small angular gear pumps for the flow experiments, which also fit inside a standard microscope incubator setup. Gear pumps provide almost constant pressure and can be used continuously. The fluid connection, based upon injection of a bevelled glass capillary into a closed (sealed) flow cell is shown to be reproducible, and reliable.

In our application integrated connection chambers are present as in- and outlet of the microfluidic channel(s). The connection chambers can be of the same size or slightly larger than the connecting capillary tube. Due to the high aspect ratio required, we choose to fabricate our mould using CNC milling that allows us to manufacture moulds with high precision (< 1µm) while the overall height differences can be much larger (in our case up to 2-3 millimetre). The microfluidic channels are machined in a single run and therefore the manufacturing precision of the mould is very high. To allow for high resolution imaging the channels are polished after milling. The connection and liquid injection into our microfluidic flow cell can be performed under a variable angle, although orthogonal connections are most often used (e.g. horizontal (side) or vertical connections). For applications requiring high resolution optical inspection, connecting from the side of the flow cell is a preferred choice. A (manual) side connection was used to enable high resolution fluorescence microscopy of FSS induced actin reorganization in LLC-PK1 cells expressing ectopically green fluorescent actin.

A connection which appears to be quite similar is discussed in a recent paper[18]. Ronalee Lo used a standard syringe needle injected through a septum area that is embedded in a chip. The septum area shown was quite large, requiring the needle to travel a long distance in the chip. Even so the connections were leaky sometimes, and no follow-up study has been published to our knowledge. We tried to use standard syringe needles with our chip design too, and similarly, but more dramatically, the connections were always leaking. A possible explanation is that syringe needles are designed to make a cut. We believe that the cut is torn towards a larger slit in the PDMS when the needle is inserted. This then creates a leaky connection especially when the septum thickness is chosen to be very thin, as in our chip where the wall thickness is about 1-2 mm. Additionally, we tested automated connection and filling, as shown in the supplemented movie. Also reconnection was possible, and tested up to 50 times without visible wear (data not shown). Disconnected chips are 'closed' and thus sterile, therefore this is an interesting option to further explore in the future, to enable high-throughput use of microfluidic chips for cell culture and other applications.

Acknowledgements

The authors have been supported by the department of Fine Mechanics (FMD). We want to thank Heiko van der Linden for use of the clean-room and the oxygen plasma chamber. This research was supported by funding by the Dutch Cancer Society (grant UL 2007-3860), the EU FP7 Systems Microscopy project (HEALTH.2010.2.1.2.2) and Cyttron, in the Besluit Subsidies Investeringen Kennisinfrastructuur program, which in turn is financially supported by the Nederlandse Organisatie voor Wetenschappelijk Onderzoek.

Conclusions

We have developed a versatile easy to handle microfluidic flow cell adapted for live cell high resolution imaging, by using a newly designed side-connection for tubing. Biological testing revealed that different cell types grow normally in this new type of microfluidic circuit. Furthermore, using live cell imaging together with confocal microscopy, we were able to show the dynamics change of renal cells under FSS conditions. When shear stress was applied, we observed enhanced cell migration coupled to ruffle formation and actin rearrangements (e.g. shortening and thickening).

Our described methodology can be systematically applied on different cell-types and imaging technologies. In future applications the system could be used for high content imaging of various biological assays including FSS, chemotaxis or on-chip flow cell differentiation[19].

References

1. **Hostetter TH, Olson JL, Rennke HG, Venkatachalam MA, Brenner BM.** Hyperfiltration in remnant nephrons: a potentially adverse response to renal ablation. *Am J Physiol., 1981, 241: F85 - F93.*

2. **Li S, Butler P, Wang Y et al.** The role of the dynamics of focal adhesion kinase in the mechanotaxis of endothelial cells. *Proc Natl Acad Sci U S A, 2002, 99: 3546 - 3551.*

3. **Mott RE, Helmke BP.** Mapping the dynamics of shear stress-induced structural changes in endothelial cells. *Am J Physiol Cell Physiol., 2007, 293: C1616 - C1626.*

4. **Osborn EA, Rabodzey A, Dewey CF, Jr., Hartwig JH.** Endothelial actin cytoskeleton remodeling during mechanostimulation with fluid shear stress. *Am J Physiol Cell Physiol., 2006, 290: C444 - C452.*

5. **van der Meer AD, Poot AA, Feijen J, Vermes I.** Analyzing shear stress-induced alignment of actin filaments in endothelial cells with a microfluidic assay. *Biomicrofluidics, 2010, 4: 11103 - 11107*

6. **Essig M, Friedlander G.** Tubular shear stress and phenotype of renal proximal tubular cells. *J Am Soc.Nephrol., 2003, 14: S33 - S35.*

7. **Essig M, Friedlander G.** Shear-stress-responsive signal transduction mechanisms in renal proximal tubule cells. *Curr Opin Nephrol. Hypertens., 2003, 12: 31 - 34.*

8. **Duan Y, Gotoh N, Yan Q et al.** Shear-induced reorganization of renal proximal tubule cell actin cytoskeleton and apical junctional complexes. *Proc Natl Acad Sci USA, 2008, 105: 11418 - 11423.*

9. **Duan Y, Weinstein AM, Weinbaum S, Wang T.** Shear stress-induced changes of membrane transporter localization and expression in mouse proximal tubule cells. *Proc Natl Acad Sci USA, 2010, 107: 21860 - 21865*

10. **Essig M, Terzi F, Burtin M, Friedlander G.** Mechanical strains induced by tubular flow affect the phenotype of proximal tubular cells. *Am J Physiol Renal Physiol., 2001, 281: F751 - F762.*

11. **Jang KJ, Cho HS, Kang dH et al.** Fluid-shear-stress-induced translocation of aquaporin-2 and reorganization of actin cytoskeleton in renal tubular epithelial cells. *Integr.Biol (Camb.), 2011, 3: 134 - 141.*

12. **Ives CL, Eskin SG, McIntire LV, DeBakey ME.** The importance of cell origin and substrate in the kinetics of endothelial cell alignment in response to steady flow. *Trans Am Soc Art Int Org., 1983, 29: 269 - 274.*

13. **JA Frangos, LV McIntire, SG Eskin.** *Biotechnol Bioeng., 1988, 32: 1053 - 1060.*

14. **de Graauw M, Tijdens I, Cramer R et al.** Heat shock protein 27 is the major differentially phosphorylated protein involved in renal epithelial cellular stress response and controls focal adhesion organization and apoptosis. *J.Biol.Chem., 2005, 280: 29885 - 29898.*

15. **Cai,Z., Xin, J., Pollock, D.M., and Pollock, J.S.** Shear stress-mediated nitric oxide production in inner medullary collecting duct cells. *Am. J. Physiol., 2000, 279: F270 - F274.*

16. **Yoshigi M, Hoffman LM, Jensen CC, Yost HJ, Beckerle MC.** Mechanical force mobilizes zyxin from focal adhesions to actin filaments and regulates cytoskeletal reinforcement. *J Cell Biol., 2005, 171: 209 - 215.*

17. **Friedrich C, Endlich N, Kriz W, Endlich K.** Podocytes are sensitive to fluid shear stress *in vitro*. *Am J Physiol Renal Physiol., 2006, 291: F856 - F865.*

18. **Ronalee Lo, Ellis Meng.** Integrated and reusable in-plane microfluidic interconnects. *Sensors and Actuators B, 2008, 132: 531 - 539.*

19. **Chau L, Doran M, Cooper-White J.** A novel multishear microdevice for studying cell mechanics. *Lab Chip., 2009, 9: 1897 - 1902.*

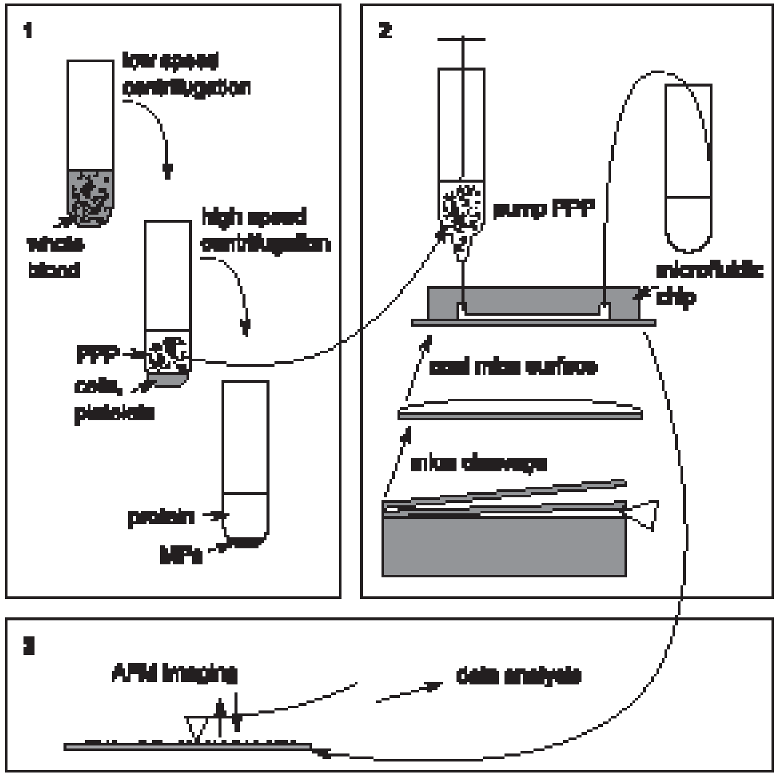
1
low speed centrifugation
whole blood
high speed centrifugation
PFP
cells, platelets
protein
MPs
2
pump PFP
microfluidic chip
coat mica surface
mica cleavage
3
AFM imaging
data analysis

Chapter 3

Determination of the size distribution of blood microparticles directly in plasma using atomic force microscopy and microfluidics

B.A. Ashcroft[a*], J. de Sonneville[b*],
Y. Yuana[c*], S. Osanto[c], R. Bertina[d],
M.E. Kuil[b], T.H. Oosterkamp[a]

* These authors contributed equally to this work.
a *Leiden Institute of Physics, Niels Bohrweg 2, 2333 CA Leiden, the Netherlands*
b *Leiden Institute of Chemistry, Einsteinweg 55, 2333 CC Leiden, the Netherlands*
c *Department of Clinical Oncology, Leiden University Medical Centre, Albinusdreef 2, 2333 ZA Leiden, the Netherlands*
d *Einthoven Laboratory for Experimental Vascular Medicine and Department of Thrombosis and Haemostasis, Leiden University Medical Centre, Albinusdreef 2, 2333 ZA Leiden, the Netherlands*

Manuscript submitted

Abstract

Microparticles, also known as microvesicles, found in blood plasma, urine, and most other body fluids, may serve as valuable biomarkers of diseases such as cardiovascular diseases, systemic inflammatory disease, thrombosis, and cancer. Unfortunately, the detection and quantification of microparticles are hampered by the microscopic size of these particles and their relatively low abundance in blood plasma.

The use of a combination of microfluidics and atomic force microscopy to detect microparticles in blood plasma circumvents both problems. In this study, capture of a specific subset of microparticles directly from blood plasma on antibody-coated mica surface is demonstrated. The described method excludes isolation and washing steps to prepare microparticles, improves the detection sensitivity, and yields the size distribution of the captured particles. The majority of the captured particles have a size ranging from 30 to 90 nm, which is in good agreement with prior results obtained with microparticles immediately isolated from fresh plasma. Furthermore, the qualitative shape of the size distribution of microparticles is shown not to be affected by high-speed centrifugation or the use of the microfluidic circuit, demonstrating the relative stable nature of microparticles *ex vivo*.

Introduction

Blood microparticles (MPs), also known as microvesicles, are small particles shed from the surface of many cells upon stimulation or apoptosis[1]. For a long time they were considered as platelet dust[2], but now they have been recognized to participate in important biological processes[3]. Examples of such processes are surface-membrane traffic and the horizontal transfer of protein and RNAs among neighboring cells, which are necessary for rapid phenotype adjustments in a variety of conditions[3]. In addition, blood MPs have important physiological and pathological roles in blood coagulation, inflammation and tumor progression[4].

Flow cytometry (FCM) and capture-based assays are commonly used methods to measure the number of MPs, define their origin based on membrane antigen expression, and asses their procoagulant features[6,7,8]. However, these methods have their drawbacks. FCM employs laser light which excites at 488

nm, while MPs may have sizes far below this wavelength[9]. Yuana et al.[10] reported the presence of MPs bearing CD41 antigen in plasma with sizes ranging between 10-475 nm using atomic force microscopy (AFM). They also found that the MP numbers detected by AFM are 1,000-fold higher than those detected by FCM. Although capture-based assays using annexin V or MP-specific antibodies allow high throughput assessment of procoagulant features of MPs[11,12,13], these assays give no information on the size and total number of MPs in plasma.

Electron microscopy (EM) has been used for detection of MPs[14,15,16], but this method only provides semi-quantitative information on MPs. Furthermore, sample dehydration and vacuum procedures required in EM might affect the characteristics of MPs. Recently, a promising method, nanoparticle tracking analysis (NTA), has been applied to count MPs in plasma[17]. This method uses a CCD camera system that allows simultaneous tracking of multiple particles. In the future NTA may be able to detect, count, and size antibody-labeled MPs efficiently, thus allowing the detection of subsets of MPs.

Not only is the analytical measurement of MPs a challenge, but also there is no golden standard yet to prepare MPs[18]. Many studies have isolated MPs from platelet free or platelet poor plasma by applying high speed centrifugation or even ultracentrifugation[19,20]. To prevent loss and phenotypic changes of MPs during the isolation procedure, using blood plasma directly for MP measurement would be preferable[21]. Furthermore, the time between blood withdrawal and the actual MP test should be as short as possible to avoid activation of cells and coagulation processes which may affect MP numbers and characteristics.

We propose a method to detect MPs directly in blood plasma by using a microfluidic flow cell and performing subsequent analysis using AFM in liquid-tapping mode. Laminar flow patterns within the flow cell ensure complete fluid turnover in a controlled manner. The flow cell allows experimentation with very small sample volumes. In this study, a detachable flow cell was developed to enable direct contact between the fluid in the microfluidic channel and the surface. Diluted plasma was flown through the microfluidic channel with a controlled pressure driven laminar flow and made to be directly in contact with anti-CD41 antibody-coated mica. MPs exposing CD41 antigen were captured on this surface and subsequently imaged by AFM. We employed the AFM method for MP detection previously used in the study of Yuana et al.[10].

Clotting of the plasma and clogging of the microfluidic channel pose a potential problem within such small volumes and with such a sensitive detection method as AFM. These problems have been solved by diluting plasma with either citrate or EDTA-enriched Hepes buffer and coating the microfluidics channels and the tubing of the microfluidics system. We demonstrated that this method increases the sensitivity of detecting specific MPs in a sample 100 to 1,000-fold. In conclusion, the application of a flow cell allows the AFM measurement of a specific subset of MPs directly in blood plasma.

Materials and Methods

Blood collection and plasma preparation

After giving their informed consent, venous blood of three healthy volunteers is collected by using a 21-gauge needle (BD Vacutainer, San Jose, CA) with minimal stasis. Except for the first four mL, the blood is collected either in 1/10 volume of sodium citrate (3.2%, 0.105 M) or in K2 EDTA (3.6 mg) using 4.5 mL BD Vacutainer tubes (Becton Dickinson, San Jose, CA). Within 10-15 min after withdrawal, the collected blood is centrifuged at 2,000g for 10 min at 20°C, without brake. The supernatant plasma is carefully collected and centrifuged again at 2,000g for 10 min, 20°C, without brake, to obtain platelet poor plasma (PPP). PPP was aliquotted in 250 µL portions, snap frozen in liquid N2, and stored at -80°C until used. Before use, PPP is quickly frozen-thawed at 37°C. Unless stated otherwise PPP is used in the experiments.

Microparticles isolation

For MP isolation, 750 µL of frozen-thawed citrate PPP is centrifuged at 18,890g and 20°C for 30 min, with minimum brake. The supernatant is removed carefully, except for 25 µL containing the MP pellet. This pellet is resuspended in 1 mL of Hepes buffer [10 mM Hepes (Merck, Darmstad, Germany), 137 mM NaCl (Merck), 4 mM KCl (Merck), 0.1 mM Pefabloc SC (Fluka, Munich, Germany), pH 7.4], vortexed, and centrifuged as before. The supernatant is removed, leaving a volume of 25 µL containing the MP pellet. Subsequently, this 25 µL is carefully diluted in 725 µL of Hepes buffer to reconstitute to the original plasma volume (750 µL) before use in the experiment.

Flow cell: mold fabrication

A flow cell mold is fabricated from brass. This brass is milled so that ridges with dimensions of 10 mm x 300 µm x 100 µm are created that shape the liquid channels during polymerization. The top surface of the ridges is polished to allow viewing through the channel from bottom to top after molding. At the end of the ridges, small holes are drilled and small pins are inserted with a diameter of 1 mm and a height of about 1 mm.

Flow cell: fabrication

Polydimethylsiloxane (PDMS) flow cells are fabricated using a Sylgard 184 kit (Dow Corning, UK). Silicone primer and catalyst are mixed in a 10:1 ratio by weight and this mixture is placed in a vacuum chamber for 1 h to remove air bubbles trapped during mixing. Next, the mixture is slowly poured into the mold and then the mold is carefully closed with a glass plate. The mold containing the polymer solution is placed in an oven at 70°C for 1 h. Afterwards, the glass slide with the PDMS flow cell is released from the mold and covered with a clean glass slide to keep the chip channel area dust-free. The polymerized flow cell is shown in **Figure 3.1a**.

Flow cell: setup

The complete microfluidic setup is shown in **Figure 3.1b**. To prepare the flow cell setup, a mica surface (1) is placed on a metal support disc (2). The metal support disc is placed onto the bottom plate of the holder device (4), in a small cavity that closely fits the metal disc. The PDMS flow cell (3) is placed onto the top plate with the open microfluidic channels facing down. Two pins, situated in the holder top plate (5) align the flow cell (see the two holes next to the channels in **Figure 3.1a**) with respect to the mica surface and the holes for the glass capillaries (7) (TSP Fused Silica Tubing, ID/OD 150/375 micrometer, deactivated with DPTMDS, from BGB Analytik Vertrieb, Germany). Then the top and bottom plate are pressed onto each other with four screws (6). Using microscopic inspection the screw pressure is carefully adjusted. The glass capillary tubes are beveled to 45 degrees before use, using a mechanical grinder (Michael Deckel S0) with a disc containing diamond dust. After careful rinsing with water, to remove remaining grinding dust, the glass capillary tubes are gently forced into the PDMS flow cell, and guided through alignment holes situated in the holder top plate.

Mica Surface preparation for attachment of anti-human CD41 monoclonal antibody

The surface of mica (Electron Microscopy Sciences, Washington) for MP at-

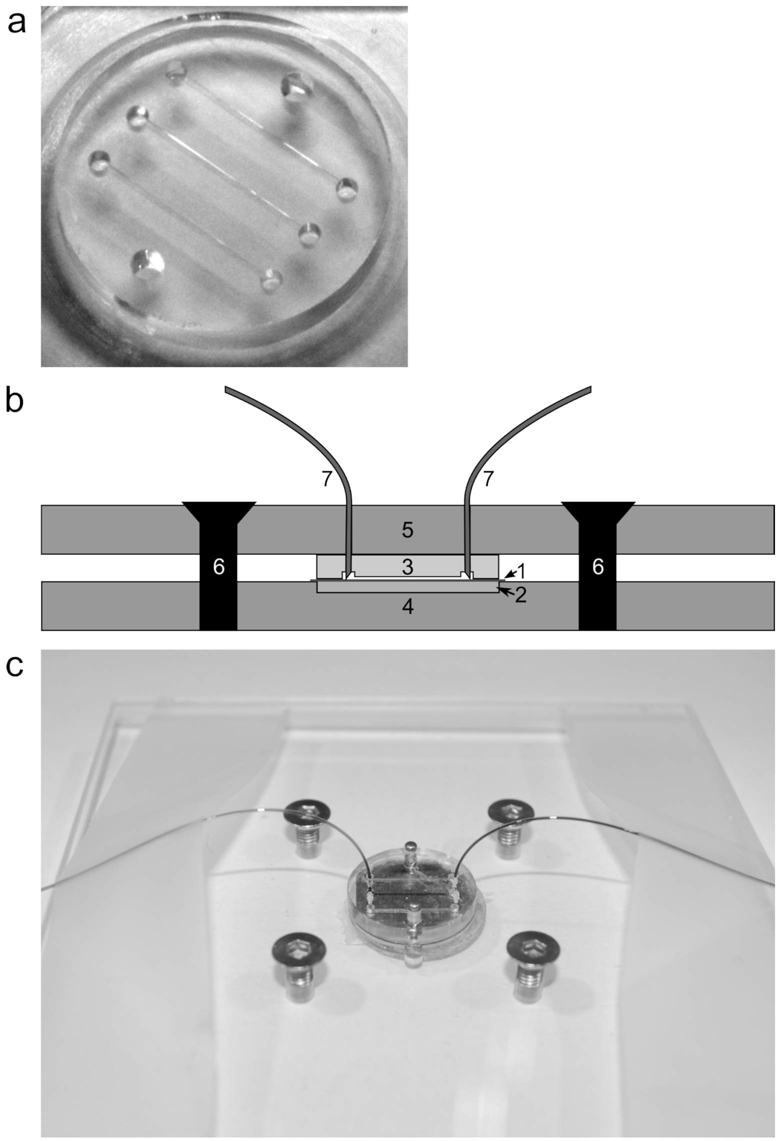

Figure 3.1 Flow cell setup (a) Open PDMS flow cell. (b) Microfluidic flow cell setup with schematic side view. The holder system (4,5,6) is used to press the PDMS chip (3) onto the mica surface (1). The glass capillary tubes (7) are guided through holes in the holder top plate (5) to reach the connection chambers in the chip (3). The metal disc (2) is used as a support for the mica surface. In the photo (c), the middle channel is connected and filled with a dark blue solution; the glass capillary tubes are bent towards the side using scotch tape. The dark solution and scotch tape are for illustration purposes and are not used in experiments.

tachment is prepared as described before[10] with a slight modification. Freshly cleaved mica disks (diameter 12 mm) are overnight immersed in DMSO containing 55% (w/v) ethanolamine at 70° C. Subsequently, the mica surfaces are rinsed twice with dry DMSO at 70°C and then with HPLC grade ethanol to remove the DMSO. Next, the mica surfaces are put for 10 min into 30 mL phosphate buffered potassium (PBK) (10.2 g KCl, 0.97 g K2H2PO4 and 5.71 g K2HPO4 per L) (pH 7.4) previously saturated with EGTA by adding 100 mg EGTA. The surfaces are then rinsed with Hepes buffer, before 20 µL of 0.05 mg/mL (in Hepes buffer) mouse anti-human CD41 antibody clone P2 (Beckman Coulter, Fullerton, CA) is applied to the surface and incubated for 3 h. Excess anti-CD41 is removed by washing with Hepes buffer. Anti-CD41 antibody coated-mica surfaces are stored in Hepes buffer until used. As a negative control, mouse IgG1 pure clone X40 (Becton Dickinson, San Jose, CA) is used (0.05 mg/mL in Hepes buffer). The IgG1 isotype control antibody is allowed to incubate for 3 h on the functionalized mica surfaces. All chemicals are purchased from Sigma Aldrich (Munich, Germany) unless otherwise indicated.

Prior to the attachment of MPs antibody-coated mica surfaces were inspected by using AFM to ensure that the number of false spots and holes in the antibody coating was minimized.

Attachment of microparticles without using microfluidics

PPP (100 µL EDTA plasma) is dropped onto the mica surface coated with IgG1 isotype control and anti-CD41 antibody ("drop method"). To check the saturation of MPs on the anti-CD41-coated surface, PPP is incubated on the surfaces for 2, 30, and 60 min. Similar to what was found by Yuana et al[10], 30 min incubation seemed to be sufficient. On anti-IgG1-coated surface PPP was incubated for 60 min to match the long exposure time on the anti-CD41 surface. The surfaces are carefully rinsed with Hepes buffer and then scanned by AFM to determine the number of MPs captured on CD41- and IgG1 isotype control- coated mica surfaces.

Attachment of microparticles using microfluidic flow cell

The open microfluidic flow cell (PDMS) is attached to a mica surface as described above. A 1 mL-syringe (Becton Dickinson, San Jose, CA, USA) is connected to a Harvard Apparatus PicoPlus (Harvard apparatus, Holliston, MA, USA) syringe pump and set at a constant flow speed of 0.01 mL/min. The syringe is connected to the glass capillary tubes using Luer-Lock Adapters and One-Piece Fittings from LabSmith (Livermore, CA, USA). The glass capillary tubes are gently forced into the microfluidic chip using the beveled end.

The channels of the cell are rinsed with 50 µL EGTA-enriched Hepes buffer (5 mM EGTA, 10 mM Hepes, 137 mM NaCl, 4 mM KCl, 0.1 mM Pefabloc® SC, pH 7.4) buffer for about 5 min. Hundred fifty µL of either EDTA plasma diluted with EDTA-enriched Hepes buffer (20 mM EDTA (Sigma Aldrich), 10mM Hepes, 137 mM NaCl, 4 mM KCl, 0.1 mM Pefabloc® SC, pH 7.4) or isolated MPs diluted with Hepes buffer is allowed to flow through the channel in the flow cell for about 15 min total flow time. The channel is then rinsed with 50 µL Hepes buffer (~5 min flow time). Before removal from the flow cell, the back of the mica is carefully marked to indicate the location of the channel in the AFM. Subsequently, the flow cell is removed and the coated surface with the attached MPs is rinsed with Hepes buffer and stored in Hepes buffer until imaged by AFM. All steps are performed at room temperature (RT).

AFM imaging

AFM imaging is performed with a Digital Instruments Multi-mode AFM (Veeco, New York, NY, USA) using the E scanner. Olympus cantilevers (Olympus, Tokyo, Japan) with force constant of 2 N/m and a resonant frequency of 70 kHz are used. The liquid cell tip holder (Veeco) is rinsed with ethanol and milli-Q water between each sample to prevent contamination. Each image was scanned at 10 x 10 µm and 10 images are taken at a variety of locations on the surface. For each particle, the sum of pixel heights multiplied by the pixel area is used to estimate a volume and subsequently to calculate its (spherical) diameter.

Results

Generally, glass, polymer or similar materials are used with microfluidics. However, the AFM cantilever must have physical access to the top of the sample and AFM requires an atomically flat background to give the best image of the sample. Mica is preferred surface material because it has distinct atomically flat layers that can be easily separated for cleaning and functionalization. As PDMS binds strongly to mica, the mica surface can be pealed away when the PDMS is removed, ruining the sample. In our study, the mica surface is functionalized with antibodies to produce a hydrophilic mica surface that cannot bind to the PDMS flow cell. Anti human-CD41 antibody was used to coat the functionalized mica to capture platelet MPs (PMPs) bearing CD41 surface antigen. PMPs constitute 80-95% of blood MPs detected by FCM[22,23]. The IgG1 isotype control is used as a control for nonspecific binding of MPs on anti-CD41-coated surface. A schematic overview of the experiment is given in **Figure 3.2**. The microfluidic setup used in **Figure 3.2b** is constructed from a PDMS flowcell (**Figure 3.1b**), attached to the mica surface by a removable holder system (**Figure 3.1b,c**) so that the flow cell can be removed from the surface of the sample without damaging either the attached MPs or the mica.

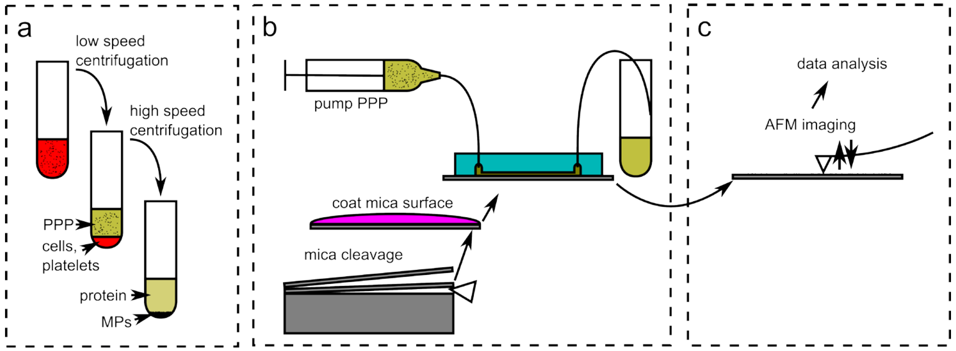

Figure 3.2 Schematic overview of experiments Collected blood plasma is centrifuged twice to acquire PPP. In some experiments blood plasma proteins are removed by use of high-speed centrifugation (a). Using an antibody coated mica surface, a fresh PDMS chip and a holder system a microfluidic setup is build, and the PPP is run over a small surface area (b). Finally, mica surface is removed and imaged using AFM, followed by automated image analysis (c).

Application of microfluidic system to count MPs in plasma

With microfluidics many more MPs in the plasma sample will have a chance to interact with the antibody-coated mica surface by flowing an equal volume of plasma over a very small active surface area in the confined volume of the microfluidic channel. To examine this we applied the microfluidic system and compared it with the drop method to count MPs in plasma obtained from two healthy donors. For the microfluidic system two samples were prepared: the first sample consists of MPs isolated from citrate PPP, reconstituted to the original plasma volume, and subsequently diluted 5 times with Hepes buffer; the second sample is EDTA PPP diluted 5 times with EDTA-enriched Hepes buffer. For the drop method undiluted EDTA plasma is used.

	Number of particles attached on anti-CD41-coated mica	
Samples	Mean	SEM
Reconstituted isolated-MPs D1	218	51
Reconstituted isolated-MPs D2	276	50
EDTA plasma D1	203	80
EDTA plasma D2	240	40
EDTA plasma drop D1	0.15	0.09
EDTA plasma drop D2	3	1.5

Table 3.1 Comparison of microfluidic method and drop method to count CD41-positive MPs For the microfluidic method MPs isolated from citrate PPP and diluted EDTA PPP of two healthy donors, D1 and D2, were used. Isolated MPs were reconstituted to the original plasma volume and subsequently five-fold diluted in Hepes buffer (Reconstituted isolated-MPs D1/D2). EDTA PPP was diluted five-fold with EDTA-enriched Hepes buffer (EDTA plasma D1/D2). For the drop method undiluted EDTA PPP from the same healthy donors was used (EDTA plasma drop D1/D2).

In all samples processed by the microfluidic system, the AFM detected MPs attached on anti-CD41-coated mica surface (**Table 3.1**). The attachment of these MPs was specific because there were at least two times less particles found attached on the IgG1-coated surface compared to those on the anti-CD41-coated surface (**Table 3.1**). This also confirms that these MPs bear CD41 surface antigen (CD41-positive MPs). Using image quantification software we found in the samples processed by microfluidic system that there is no significant difference in the number of MPs attached on anti-CD41-coated surface (218, 276, 203, and 240 MPs/100 μm^2). Strikingly, there were hardly any MPs captured on anti-CD41 coated-surface by using the drop method, even after one hour incubation of plasma on the surface (3 MPs/100 μm^2 anti-CD41-coated surface and 3 MPs/100 μm^2 IgG1-coated surface, **Table 3.1**).

It has been reported in the literature[24,25] that when EDTA is used as anticoagulant for blood collection, the CD41/CD61 complex on the plasma membrane of platelets may loose their affinity for anti-CD41 and CD61 antibodies. To check this we have used FCM to measure the binding of anti-CD61 and anti-CD41 antibodies to platelet MPs in citrate- and EDTA-anticoagulated blood plasma. We found that the numbers of CD41/CD61-positive MPs in citrate and EDTA plasma are not significantly different (see **Figure 3.S1** in the supplementary information).

Despite the fact that macroscopic clotting could be prevented by diluting EDTA PPP with EDTA-enriched Hepes buffer, we noticed in preliminary experiments that there still was some clotting in the small confinements of the microfluidic channel. In some studies it has been shown that unmodified PDMS is not compatible with some of the blood/plasma components and may initiate activation of the clotting system[26,27]. Platelets adhere more strongly to the surface of unmodified PDMS than to the modified PDMS[28]. Moreover, unmodified PDMS is hydrophobic and this might induce clotting when plasma is introduced in the microfluidic channel[29,30]. To prevent this clotting in the microfluidic channels, a solution of EGTA-enriched Hepes buffer was flowed through the channel before application of the plasma. EGTA is also known as a strong chelator of calcium ions, but it is not known to the authors whether the EGTA also can physically be adsorbed on the PDMS, acting to prevent clotting on the surface of the channel, or if EGTA performs its anti-clotting action in some other way.

Analysis of AFM images

The AFM images provide a unique challenge for image processing. As images are generated by scanning line after line, each neighboring line scan can have a different offset, slope or parabolic background (**Figure 3.3a,e**). This background must be dealt with for the accurate determination of neighboring scan lines to calculate the heights and volumes of the MPs correctly. The most commonly used techniques involve performing linear regression on the fast scan line and then subtracting the background estimate from each line. This technique is frequently foiled by small, high features on the surface, such as MPs. To overcome this difficulty, a special technique is developed in our lab. First, a standard linear regression subtraction is performed (**Figure 3.3b,f**). Second, Labview IMAQ is used to find all the particles (**Figure 3.3c,g**). Third, the regions containing the particles are then removed from the background subtraction input and the linear regression subtraction is performed again to provide a much flatter surface (**Figure 3.3d,h**). While this is a computationally expensive task, it provides the high precision background subtraction for the needed accurate determination of the particle volumes.

Particle counting is performed by using the Labview IMAQ library to determine the location of the particles. The Count Objects 2 VI is first used to filter and obtain a list of possible particles. This software uses a threshold to make a binary

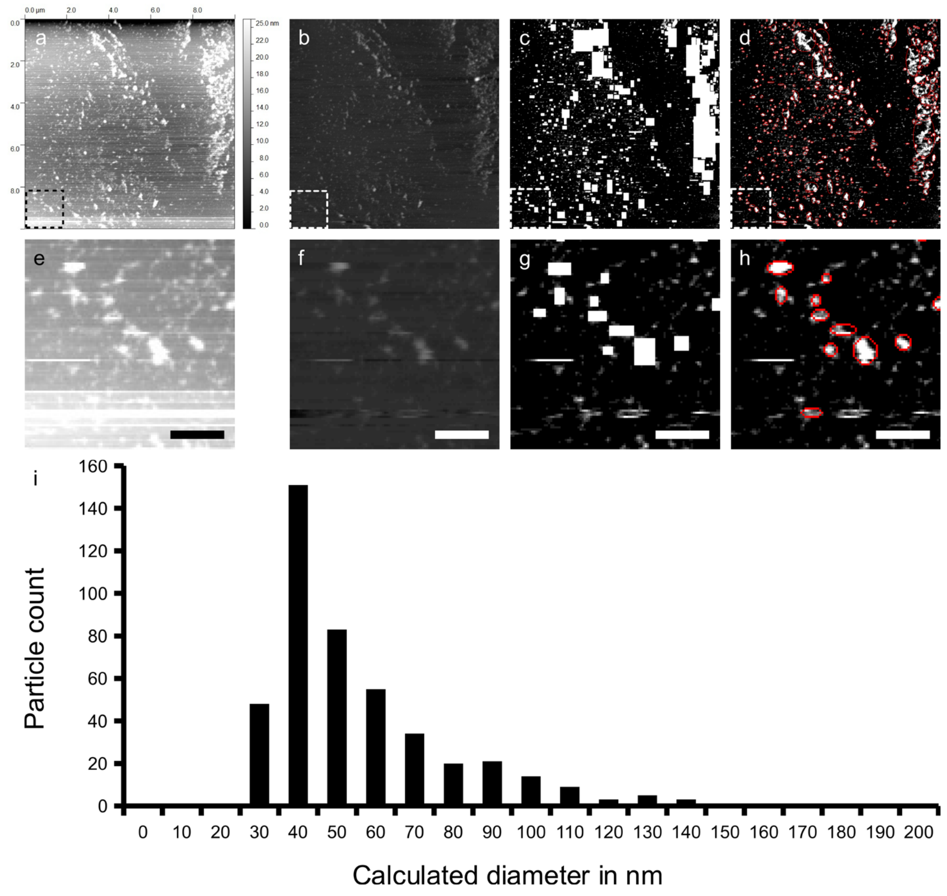

Figure 3.3 AFM image quantification Original AFM image, intensity represent height, see scale bar on the right side (a). This image is flattened using the standard linear regression background subtraction (b). White squares show all the particles that are found on the image from image A (c). The background is subtracted, corrected for the shadowed regions, and the particles are correctly sized (d). The bottom row (e,f,g,h) shows an enlarged region of (a,b,c,d) respectively, scale is 500 nm. The measured particles are indicated with red ellipses (d,h). The size distribution graph of particles detected from this image (100 µm^2) is depicted (i).

image, and then uses the watershed method to count the particles. Particles that touch the boundaries will not be counted. Additionally, all holes within the particles are automatically filled. The lower limit of height, width, and breadth of the particles is set to separate them from the background. For counting, the particle must at least 3 nm high and occupies at least 3 pixels. The particle must be larger than 1 pixel in width or breadth. By setting this limit constant selection rules can be applied throughout a large dataset of AFM images.

As can be deduced from **Figure 3.3** the height is smaller than the width in detected MP profiles, the MPs appear disc shaped after binding to the surface. Using the disc radius and height, the particle volume is estimated and converted into an effective diameter assuming that MP have a spherical shape in solution[10]. This procedure ignores the effects of tip flattening. It seems that this does not have a major effect on the final calculated volume of the particles (results not shown), and only a small systematic error exists in the volume calculations from the tip broadening effect. The size distribution of the example image is shown in **Figure 3.3i**.

Size distribution graphs are made to further analyze possible differences between MPs captured from diluted isolated MPs and from diluted EDTA plasma, to see if high-speed centrifugation has an effect on the particle size. No significant differences in the number and size distribution of CD41-positive MPs was observed before and after high-speed centrifugation (supplementary **Table 3.S1**, supplementary **Figure 3.S2**). As mentioned before, we do not need to concentrate particles using high-speed centrifugation, however the clotting probability is strongly reduced by removal of blood plasma proteins. Therefore we use purified MPs, reconstituted to the original volume for all further experiments.

Relationship between MP concentration and number of MPs captured on anti-CD41-coated surface

Prior to measuring the concentration of MPs in a sample, the dynamic range should first be established. Therefore we used MPs isolated from frozen-thawed citrate PPP of a healthy volunteer. Isolated MPs are first reconstituted with Hepes buffer to reach the original plasma volume before isolation (100%) and subsequently diluted 2 to 40-fold. These diluted MP fractions are run through the microfluidics system to measure the number of captured CD41-positive MPs. **Figure 3.4a** shows that only at sufficiently low concentrations (<10%) there is a linear relationship between the MP concentration and the number of particles attached on the anti-CD41-coated surface. Probably because of unspecified binding in the microfluidics circuit the line does not cross the origin (0,0). At higher concentrations (>10%) the number of MPs captured to the anti-CD41-coated surface reaches a maximum of ~250 particles/100 µm^2. This number of captured MPs is very similar to those reported in **Table 3.1** for the reconstituted isolated MP fraction and EDTA plasma which are diluted 5 times before processing with the microfluidic system.

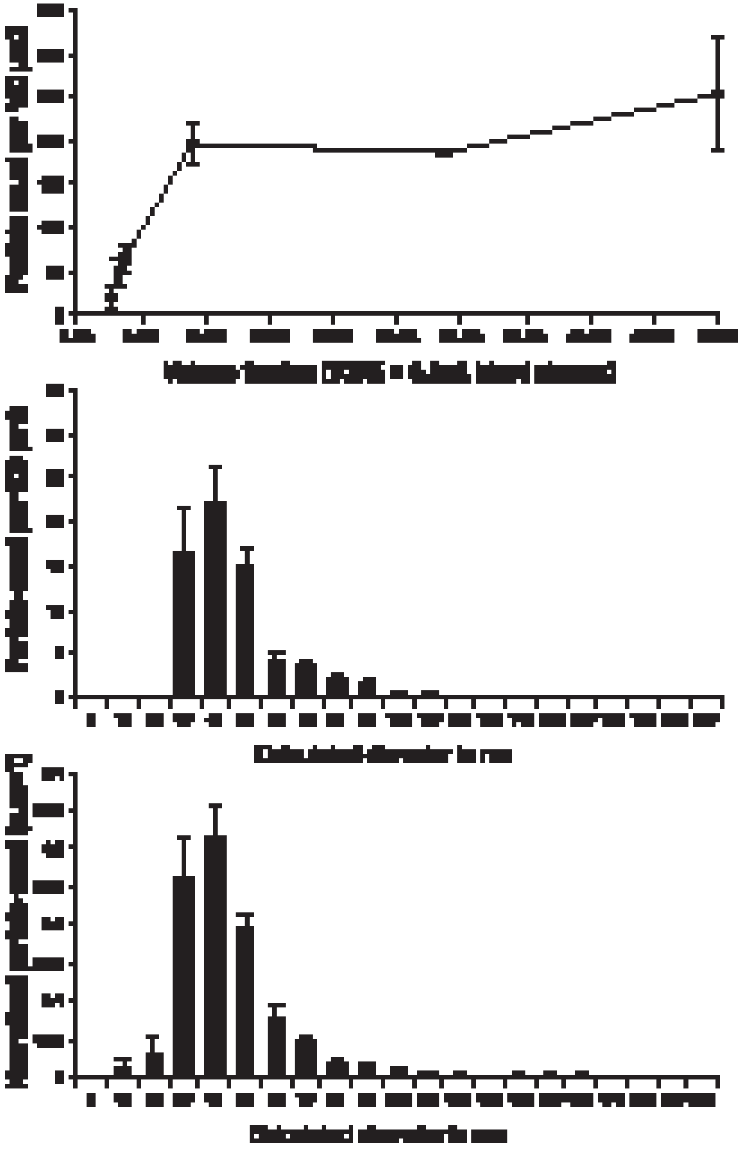

Figure 3.4 Relationship between the MP concentration in the sample and the number of CD41-positive MPs detected by AFM MPs isolated from frozen-thawed citrate PPP are diluted from 50% to 2.5% (100% is undiluted reconstituted-isolated MPs) in Hepes buffer and run through the microfluidics device (a). These experiments were done on two different days using the same plasma pool of one healthy volunteer. The size distribution from a single dilution (3.8%) is based on three images (b). A normalized size distribution of all dilutions averages is weighted equally (c). Scale bars represent the standard error of the mean.

Percent Reconstituted MPs	2.6%	3.2%	3.8%	9.1%	29%	50%	80%
Dilution	75	60	50	20	5	2	1
Number of processed images	5	7	3	9	1	5	5
Number of particles	98	339	196	1766	186	1270	373
Mean*	30	49	46	54	50	45	51
Median*	29	42	42	46	46	40	41
Standard deviation*	12	27	15	28	20	17	34
Range*	68	192	87	301	152	160	283
Min*	8	26	27	26	26	25	23
Max*	76	218	114	327	177	185	306

*Values based on calculated particle diameter in nanometer

Supplementary Table 3.2 Statistics obtained from the dilution experiment of Figure 5

The AFM images show that, typically, the particles are not uniformly distributed on the surface (**Figure 3.3a**). As a result, the standard error of the mean is quite large (**Figure 3.4a**). The linear range is rather small, and it may be difficult to find a suitable working range when samples differ as strongly in particle counts as mentioned before[10]. Interestingly, it is found that the size distribution does not differ significantly between different images (**Figure 3.4b**), and different dilutions (**Figure 3.4c, Supplementary Table 3.2**) of the same sample, with the exception of the highest dilution. This sets microfluidic capture combined with AFM imaging as the first method able to measure the size distribution of a specific subset of MPs directly in PPP.

Discussion

We report on a novel method to identify and characterize a specific subset of MPs directly in plasma. To enable the measurement of MPs directly in plasma, we have developed a method that combines a microfluidic system and AFM detection. Microfluidic channels allow blood plasma to flow over a small surface of antibody coated mica, resulting in a high enough surface concentration of specifically bound MPs to detect and quantify using AFM. A much higher number of MPs is captured from (diluted) plasma on antibody-coated mica than without, using this microfluidic method (plasma drop system). Further optimization of the method is required for high-throughput measurements.

For the first time it is demonstrated that the size distribution of CD41-positive MPs is robust against high-speed centrifugation and dilution. However, to prevent clotting to occur, the use of MPs isolated by means of high-speed centrifugation is advised.

Yuana et al[10] have shown that MPs isolated from fresh citrate PPP have calculated, spherical like diameters (dsph) of ~50 nm (range 10-475 nm). Using microfluidics we found that MPs isolated from frozen-thawed citrate PPP and frozen-thawed EDTA PPP have a similar calculated diameter (dsph) of ~45 nm. Software has been developed to automate the measurement and counting of MPs. This results in much more consistent results and provides faster data analysis. By comparing the results from previous experiments by Yuana et al[10] to the new automated quantification of the same dataset we observed that the size distribution was similar to those reported earlier (data not shown).

There are advantages and disadvantages in using the microfluidic system and AFM to measure MPs. In this study we found that about 10 µL of plasma is enough to count significant number of MPs and determine their size distribution. Furthermore, the microfluidic system allows the measurement of MPs directly in plasma thus reducing time between venepuncture and MP measurement and also preventing MP loss because of washing steps in the isolation procedure. However, the preparation of mica (modification and coating) typically takes two days. In 20% of all cases we also dealt with leakage from microfluidic channels during plasma injection. AFM scanning of the surface is also time-consuming. It takes at least an hour finding a right surface to position the AFM tip and scanning 10 images of 100 μm^2 at different locations on the surface.

Therefore, when this present method will be used as a diagnostic tool, the throughput needs to be increased by developing high speed AFM and automated sample handling. Additionally, if fluorescent labeling can be implemented efficiently, the number of particles captured should allow optical detection of these particles by means of fluorescence imaging. With the AFM technique being used for calibration, it should be possible to fluorescently tag the MPs to provide optical quantification of the number of MPs on the mica surface.

Conclusion

In this study, it is demonstrated that by using a removable microfluidic circuit, CD41-positive MPs can be captured directly from diluted blood plasma, and detected by AFM. Quantification of MPs is automated, to allow consistent and fast quantification. Use of the microfluidic system increases the sensitivity of MP detection considerably, leading to a higher surface concentration of attached MPs, reducing the AFM scanning time. Direct use of plasma as opposed to isolated MPs shortens the preprocessing time and enables the detection of MPs in a more natural state. Ten µL EDTA plasma is sufficient to quantify the number and determine the size distribution and shape of CD41-positive MPs using microfluidics and AFM.

In future experiments the characterization of MPs from other origins (endothelial cells, monocytes, tumor cells, etc) by using antigen-specific monoclonal antibodies will be addressed. This will help in monitoring subsets of MPs that may play a specific role in the development of certain diseases.

Acknowledgments

We thank G.J. van Baarle for assisting with the software that counts and measures the size of the particles. We thank Henk Verpoorten (Department of Fine Mechanics) for the construction of the microfluidic chip mold and the holder device. work was supported by the Dutch Cancer Research Society (KWF UL 2006-3618) and Cyttron, in the Besluit Subsidies Investeringen Kennisinfrastructuur program (J.S.), which in turn is financially supported by the Nederlandse Organisatie voor Wetenschappelijk Onderzoek.

References

1. **M.Diamant, M.E.Tushuizen, A.Sturk, and R.Nieuwland**, *Eur. J. Clin. Invest 34, 392 (2004).*

2. **P.Wolf,** *Br. J. Haematol. 13, 269 (1967).*

3. **E.Cocucci, G.Racchetti, and J.Meldolesi**, *Trends Cell Biol. 19, 43 (2009).*

4. **L.Burnier, P.Fontana, B.R.Kwak, and A.Angelillo-Scherrer**, *Thromb. Haemost. 101, 439 (2009).*

5. **E.Pap, E.Pallinger, M.Pasztoi, and A.Falus**, *Inflamm. Res. 58, 1 (2009).*

6. **S.Nomura, A.Shouzu, K.Taomoto, Y.Togane, S.Goto, Y.Ozaki, S.Uchiyama, and Y.Ikeda, J. Atheroscler**. *Thromb. 16, 878 (2009).*

7. **R.Lacroix, S.Robert, P.Poncelet, R.S.Kasthuri, N.S.Key, and F.Dignat-George**, *J. Thromb. Haemost. 8, 2571 (2010).*

8. **K.Aupeix, B.Hugel, T.Martin, P.Bischoff, H.Lill, J.L.Pasquali, and J.M.Freyssinet, J.** *Clin. Invest 99, 1546 (1997).*

9. **B.Furie and B.C.Furie**, *Blood Cells Mol. Dis. 36, 177 (2006).*

10. **Y.Yuana, T.H.Oosterkamp, S.Bahatyrova, B.Ashcroft, R.P.Garcia, R.M.Bertina, and S.Osanto**, *J. Thromb. Haemost. 8, 315 (2010).*

11. **J.M.Freyssinet, J. Thromb.** *Haemost. 1, 1655 (2003).*

12. **A.Habib, C.Kunzelmann, W.Shamseddeen, F.Zobairi, J.M.Freyssinet, and A.Taher**, *Haematologica 93, 941 (2008).*

13. **W.Jy, L.L.Horstman, J.J.Jimenez, Y.S.Ahn, E.Biro, R.Nieuwland, A.Sturk, F.Dignat-George, F.Sabatier, L.Camoin-Jau, J.Sampol, B.Hugel, F.Zobairi, J.M.Freyssinet, S.Nomura, A.S.Shet, N.S.Key, and R.P.Hebbel,** *J. Thromb. Haemost. 2, 1842 (2004).*

14. **H.F.Heijnen, A.E.Schiel, R.Fijnheer, H.J.Geuze, and J.J.Sixma**, *Blood 94, 3791 (1999).*

15. **M.Hughes, C.P.Hayward, T.E.Warkentin, P.Horsewood, K.A.Chorneyko, and J.G.Kelton**, *Blood 96, 188 (2000).*

16. **O.Aras, A.Shet, R.R.Bach, J.L.Hysjulien, A.Slungaard, R.P.Hebbel, G.Escolar, B.Jilma, and N.S.Key**, *Blood 103, 4545 (2004).*

17. **P.Harrison, R.Dragovic, A.Albanyan, A.S.Lawrie, M.Murphy, and I.Sargent**, "Application of dynamic light scattering to the measurement of microparticles," *(2009).*

18. **Y.Yuana, R.M.Bertina, and S.Osanto**, *Thromb. Haemost. 105, 396 (2011).*

19. **A.Piccin, W.G.Murphy, and O.P.Smith**, *Blood Rev. 21, 157 (2007).*

20. **A.K.Enjeti, L.F.Lincz, and M.Seldon, Semin.** *Thromb. Hemost. 33, 771 (2007).*

21. **S.Robert, P.Poncelet, R.Lacroix, L.Arnaud, L.Giraudo, A.Hauchard, J.Sampol, and F.Dignat-George**, *J. Thromb. Haemost. 7, 190 (2009).*

22. **L.L.Horstman and Y.S.Ahn**, *Crit Rev. Oncol. Hematol. 30, 111 (1999).*

23. **M.E.Tesselaar, F.P.Romijn, I.K.van der Linden, F.A.Prins, R.M.Bertina, and S.Osanto**, *J. Thromb. Haemost. 5, 520 (2007).*

24. **C.Gachet, D.Hanau, D.Spehner, C.Brisson, J.C.Garaud, D.A.Schmitt, P.Ohlmann, and J.P.Cazenave**, *J. Cell Biol. 120, 1021 (1993).*

25. **G.H.Rao, J.D.Peller, and J.G.White**, *Thromb. Res. 85, 23 (1997).*

26. **M.C.Belanger and Y.Marois, J. Biomed.** *Mater. Res. 58, 467 (2001).*

27. **P.W.Whitlock, S.J.Clarson, and G.S.Retzinger**, *J. Biomed. Mater. Res. 45, 55 (1999).*

28. **M.T.Khorasani and H.Mirzadeh, J.** *Biomater. Sci. Polym. Ed 15, 59 (2004).*

29. **S.Thorslund, J.Sanchez, R.Larsson, F.Nikolajeff, and J.Bergquist**, *Colloids Surf. B Biointerfaces. 46, 240 (2005a).*

30. **S.Thorslund, J.Sanchez, R.Larsson, F.Nikolajeff, and J.Bergquist**, *Colloids Surf. B Biointerfaces. 45, 76 (2005b).*

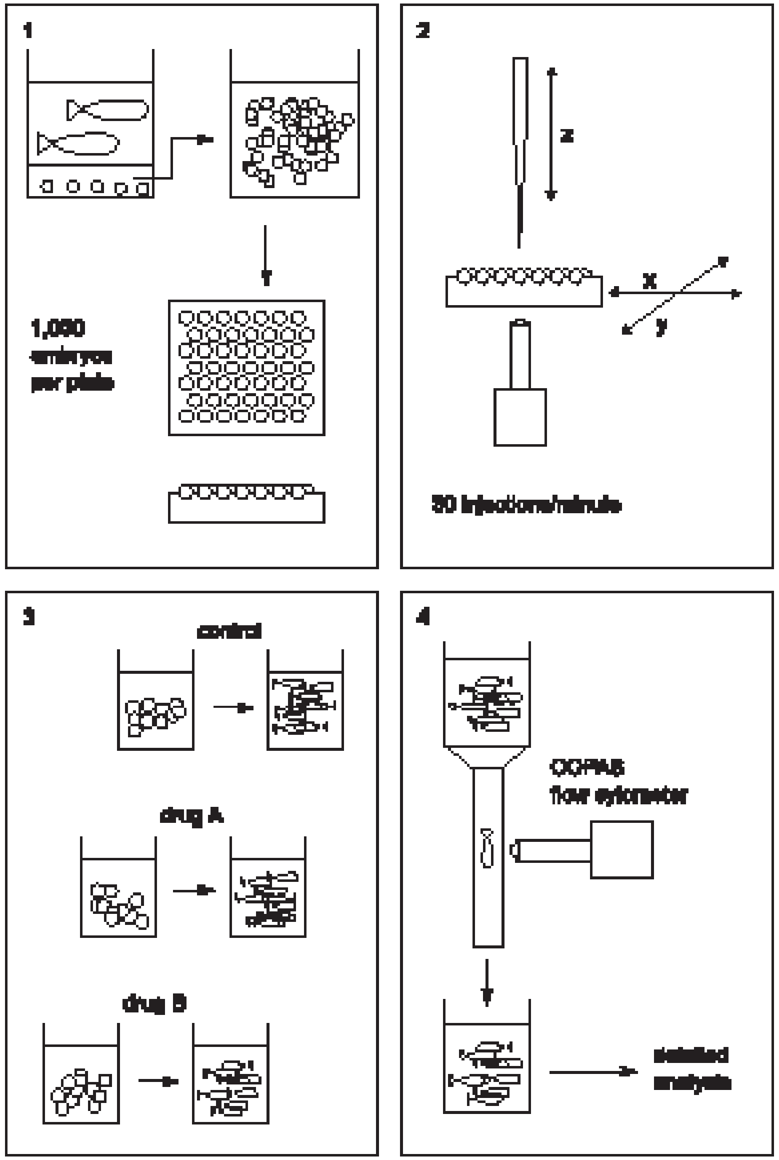
1
1,000
embryos
per plate
2
z
x
y
30 injections/minute
3
control
drug A
drug B
4
COPAS
flow cytometer
detailed
analysis

Chapter 4

A High-Throughput Screen for Tuberculosis Progression

Ralph Carvalho[a,c*], Jan de Sonneville[b*], Oliver W. Stockhammer[c], Nigel D. L. Savage[d], Wouter J. Veneman[c], Tom H. M. Ottenhoff [d], Ron P. Dirks[a], Annemarie H. Meijer[c], Herman P. Spaink[c]

---

*These authors contributed equally to this work.

a *ZF-screens B.V., Niels Bohrweg 11, 2333 CA Leiden, the Netherlands*
b *Leiden Institute of Chemistry, Einsteinweg 55, 2333 CC Leiden, the Netherlands*
c *Institute of Biology, Einsteinweg 55, 2333 CC Leiden, the Netherlands*
d *Department of Immunohematology and Blood Transfusion, Leiden University Medical Centre, Albinusdreef 2, 2333 ZA Leiden, the Netherlands*

PLoS ONE 6(2): e16779

Abstract

One-third of the world population is infected with *Mycobacterium tuberculosis* and multi-drug resistant strains are rapidly evolving. The noticeable absence of a whole organism high-throughput screening system for studying the progression of tuberculosis is fast becoming the bottleneck in tuberculosis research. We successfully developed such a system using the zebrafish *Mycobacterium marinum* infection model, which is a well-characterized model for tuberculosis progression with biomedical significance, mimicking hallmarks of human tuberculosis pathology. Importantly, we demonstrate the suitability of our system to directly study *M. tuberculosis*, showing for the first time that the human pathogen can propagate in this vertebrate model, resulting in similar early disease symptoms to those observed upon *M. marinum* infection. Our system is capable of screening for disease progression via robotic yolk injection of early embryos and visual flow screening of late-stage larvae. We also show that this system can reliably recapitulate the standard caudal vein injection method with a throughput level of 2,000 embryos per hour. We additionally demonstrate the possibility of studying signal transduction leading to disease progression using reverse genetics at high-throughput levels. Importantly, we use reference compounds to validate our system in the testing of molecules that prevent tuberculosis progression, making it highly suited for investigating novel anti-tuberculosis compounds *in vivo*.

Introduction

Tuberculosis (TB) is an ancient chronic disease caused by *M. tuberculosis*. With one-third of the world population infected, the predominant outcome is a latent and persistent infection controlled by type I immune responses[1 - 4]. An important characteristic of this infection is the formation of granulomatous lesions, consisting of clusters of infected macrophages and other immune cells[5,6]. Paradoxically, the main purpose of the host macrophages, which *M. tuberculosis* infects and where it persists, is to clear bacterial infection[7,8]. *M. tuberculosis* achieves persistent infection through rapid changes in its gene expression profile in order to counteract host cell biological and immune processes, such as antigen presentation, pro-inflammatory cytokine secretion and phagosome maturation[9].

The alarming rate of emergence of new drug resistant (MDR/XDR) *M. tuberculosis* strains isolated from patients, in particular HIV-infected individuals, is cause for global concern, and the race for more efficient vaccines, as well as novel antibiotics targeting either the pathogen or the host, has begun[3,10,11]. While *in-vitro* models have shed light on processes that are central to the uptake and survival of the bacterium, they cannot recapitulate the full phenotype of latent *M. tuberculosis* infection. This has been partly circumvented through the use of non-human primate models, which develop a form of TB that exhibits many of the hallmarks of the human infection[12]. However, although the guinea pig model has been used to validate anti-TB vaccines and drugs[13] and mouse models offer extensive arrays of genetic tools, neither rodent model fully recapitulates essential aspects of TB lesion progression in man, including granuloma formation and maturation[10,14].

The low-cost and high clutch-size zebrafish (D. rerio) is, at the embryonal and larval stages, optically transparent, permitting visualization of pathogens and lesions in real time[15], as well as offering exciting possibilities for high-throughput imaging[16]. Zebrafish are also amenable to forward genetic screening, or reverse genetics techniques such as injection of morpholinos (inhibitory of mRNA translation)[17,18]. As ectotherm, the zebrafish is one of the natural hosts of *M. marinum*, the closest relative of the *M. tuberculosis* complex[19]. Of crucial relevance, as shown by the pioneering work of the Ramakrishnan group, *M. marinum* infection of zebrafish closely mimics the mammalian TB pattern of infection, both in terms of bacterial numbers which increase rapidly in early infection, and of the formation of caseous granulomas which present characteristics typical of their human counterparts[20 - 23].

The indirect study of human TB via the infection of the zebrafish embryo with *M. marinum* has already led to the clarification of many important processes in the life cycle of the infection, in particular those underlying the mechanisms of granuloma formation[22 - 27]. The importance of studying mycobacterial infections at a whole organism level was highlighted in the report that induction of mmp9 expression, enhancing macrophage recruitment to granulomas, was localized to epithelial cells near infected macrophages[26]. Another example of the use of zebrafish larvae to uncover a host-pathogen interaction relevant to human mycobacterial infection is the recent forward genetic screen by Tobin and Ramakrishnan, who mapped a hypersusceptibility mutation to the leukotriene biosynthesis gene, lta4h, and showed that heterozygosity at the LTA4H locus correlated with susceptibility of human populations to both TB and leprosy[28]. It is therefore clear that the zebrafish mycobacterial infection model is quickly becoming an attractive and advantageous alternative for analyzing granuloma and disease progression *in vivo*.

The common route of infecting zebrafish embryos with *M. marinum* is the labour-intensive and low-throughput injection of the pathogen into the caudal vein of the 1 day old embryo[23]. This method is labour-intensive and generally considered to be a low-throughput technique, leading to major bottlenecks in drug discovery particularly in times of high-throughput technology. Since infection by immersion is not an effective alternative, we sought to achieve a reliable high-throughput automatic injection system, drastically reducing the man-hour requirement while vastly increasing the number of reproducibly infected embryos. Large quantities of similarly-injected/infected embryos would then allow testing of sizeable drug libraries for anti-bacterial activity targeting either the pathogen or the host itself.

Here we show that the automatic injector we developed provides a powerful and reliable high-throughput system for infecting embryos with *M. marinum*. We also show that we can couple the injector to a flow cytometer capable of sorting live multicellular organisms (Complex Object Parametric Analyzer and Sorter, COPAS) and rapidly test the efficacy of known anti-TB drugs in infected embryos. Finally, and importantly, we demonstrate that this system is ideally suited to test proliferation and tissue spreading of the human pathogen, *M. tuberculosis*.

Results and Discussion

Proof of principle of yolk sac as early-stage embryo injection site

We first demonstrated that the injection of 20-40 *M. marinum* colony-forming units (CFUs) into the yolk sac of embryos at several early developmental stages (up to the 1,024-cell stage) precisely mimics the infection obtained with the well-established caudal vein injection method. In our set-up, all injections were performed using polyvinylpyrrolidone as a polymer-based carrier for the bacteria, which showed several benefits: (1) restriction of early bacterial spread into the embryo, precluding developmental problems arising from the early injection stage; (2) higher concentration homogeneity; (3) clear visibility of injected inoculum as a spheroid (Video S1).

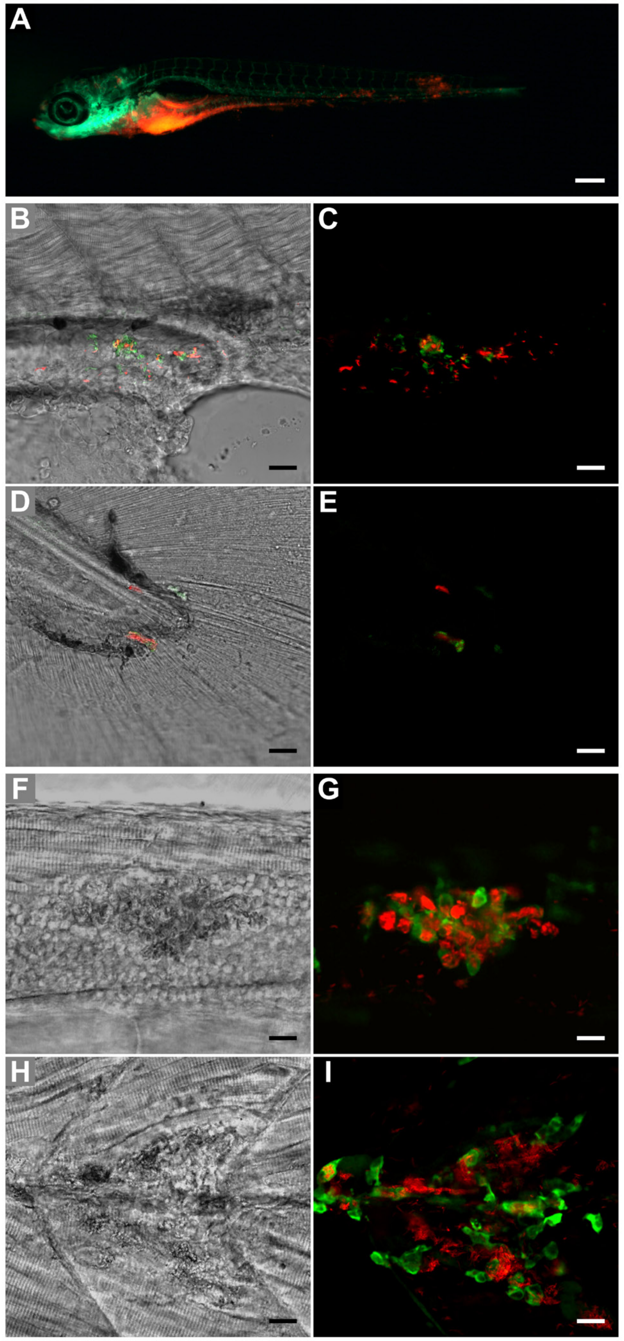

Figure 4.1 Outcome of *M. marinum* yolk sac injection of embryos between the 16- and the 512-cell stage.

(A) 5 days post-infection (dpi) fli1-egfp larva with gfp-labelled vasculature showing spread of bacteria (red) throughout the body (scale bar: 250 µm). (B and D) Bright-field/fluorescence overlay and (C and E) confocal z-stack of red-fluorescent bacteria showing activation of green-fluorescent gags at the (B and C) edge of the yolk extension and on the (D and E) tail of a 7 day-old larva (scale bar: 25 µm). (F and H) Bright-field confocal plane and (G and I) confocal z-stack of red-fluorescent bacteria co-localizing with green-fluorescent leukocytes detected by L-plastin immunostaining (scale bar: 25 µm). The lesions caused by the granulomas can be clearly seen in F and H.

Besides extensive bacterial growth within the yolk, we witnessed frequent formation of aggregates of infected cells outside the site of injection, namely in the head, body and tail of the larvae at 5 days post-infection (dpi) (**Figure 4.1A**). These aggregates were highly similar to those previously shown to represent initial stages of granuloma development[23]. No adverse developmental effects were seen in any of the conditions tested. Confirmation that yolk *M. marinum* injection resulted in granuloma formation was obtained through GFP-labelled granuloma-activated gene (gag)[23] activation at 7 dpi using an *M. marinum* strain also expressing mCherry (**Figure 4.1B-E**). Additionally, immunohistochemistry using L-plastin showed clear co-localization of *M. marinum* and leukocytes (**Figure 4.1F-I**). To functionally analyze the role of the immune system in the spreading and proliferation of mycobacteria after yolk injection, we co-injected a morpholino targeting pu.1[29] and *M. marinum* at the 1-2 cell stage. The results revealed the presence of extracellular *M. marinum* and increased bacterial proliferation in pu.1 morphants (**Figure 4.2A and B**), consistent with previous data demonstrating that macrophages in zebrafish embryos restrict mycobacterial growth[25]. At 2 dpi, we observed cording structures in Pu.1 morphants, characteristic of extracellular mycobacteria[27,28], in the tail region of infected embryos (**Figure 4.2C-E**). Using a mag49 (macrophage-activated gene)-GFP[23] construct in mCherry-labelled bacteria, we were able to confirm their extracellular location through the lack of mag49-GFP expression, previously shown to be active only after phagocytosis by macrophages[23] (**Figure 4.2C and D**).

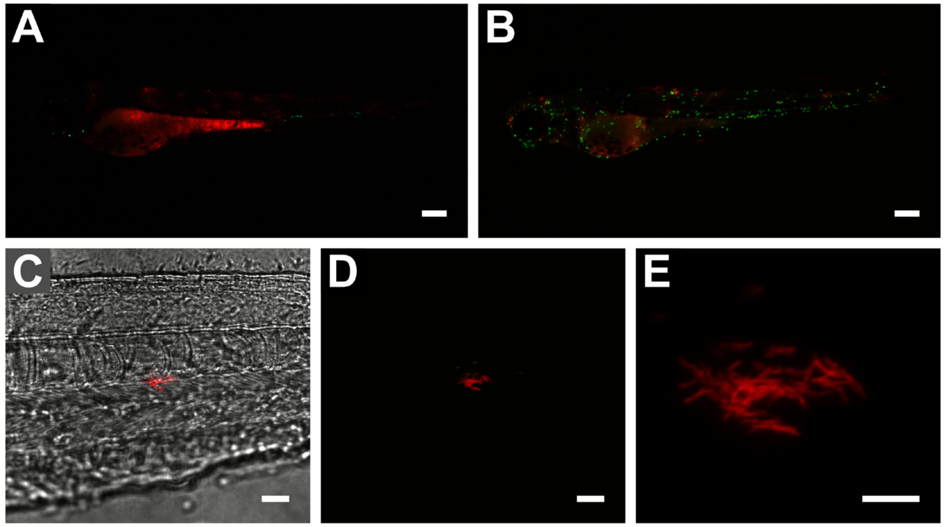

Figure 4.2 Effect of yolk sac co-injection of Pu.1 morpholino and *M. marinum* on bacterial localization and proliferation within embryos. (A and B) 3 day-old infected mpx-gfp transgenic embryos (A) with and (B) without Pu.1 morpholino (scale bar: 250 µm). Greater numbers of (extracellular) bacteria throughout body of morphant embryo seen in A contrast with lower amount of more localized (phagocytosed) bacteria seen in B. Very low number of mpx-gfp labelled neutrophils in A confirms Pu.1 morpholino effect. (C) Bright-field/fluorescence overlay and (D) confocal z-stack of mag49-GFP/mCherry bacteria in body of 2 dpi embryo (scale bar: 25 µm). Red-fluorescent bacteria form a cording structure adjacent to a few cells containing green-fluorescent (mag49-activated) bacteria. Lack of green fluorescence in cording bacteria indicates no phagocytosis by macrophages and extracellularity. (E) Close-up (digital zoom: 5.2) of cording structure formed by extracellular bacteria (scale bar: 10 µm; only red channel shown).

High-throughput *M. Marinum* injection and drug screen

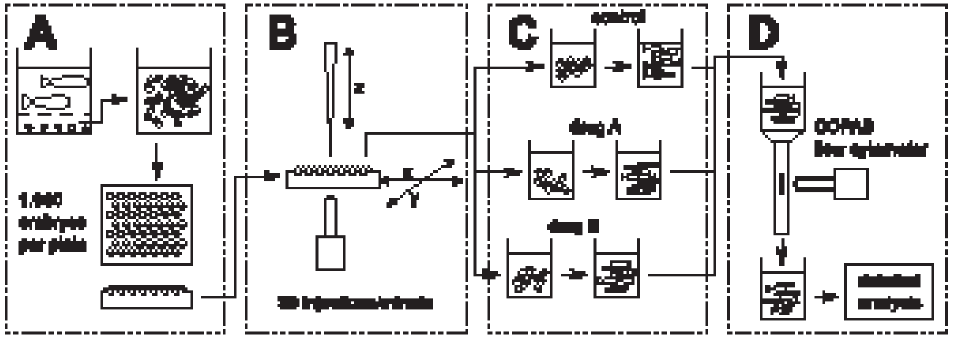

Figure 4.3 Pipeline of high-throughput infection of zebrafish embryos and subsequent drug testing. (A) After fertilization eggs are harvested, washed and distributed on injection plate. (B) Appropriate inoculum is injected in early stage embryos (up to 1,024-cell stage). (C) Injected embryos are dispensed into appropriate containers and drug screens take place between 3 and 6 dpi. (D) Groups of treated and untreated embryos are separately screened using COPAS during (when appropriate) and after drug exposure. Detailed optical analyses are performed on selected larvae.

We subsequently developed an automatic injector system around the yolk injection concept (**Figure 4.3 and 4.4**). All tests performed demonstrated that this injector design, capable of 1,024 consecutive injections per run of 30 minutes, reproducibly reached a success rate of over 99% (sample in Video S1) and produced identical results to manual yolk injections of embryos. Importantly, embryos occupied the hemi-spherical wells of the agarose cast (**Figure 4.S1**) in

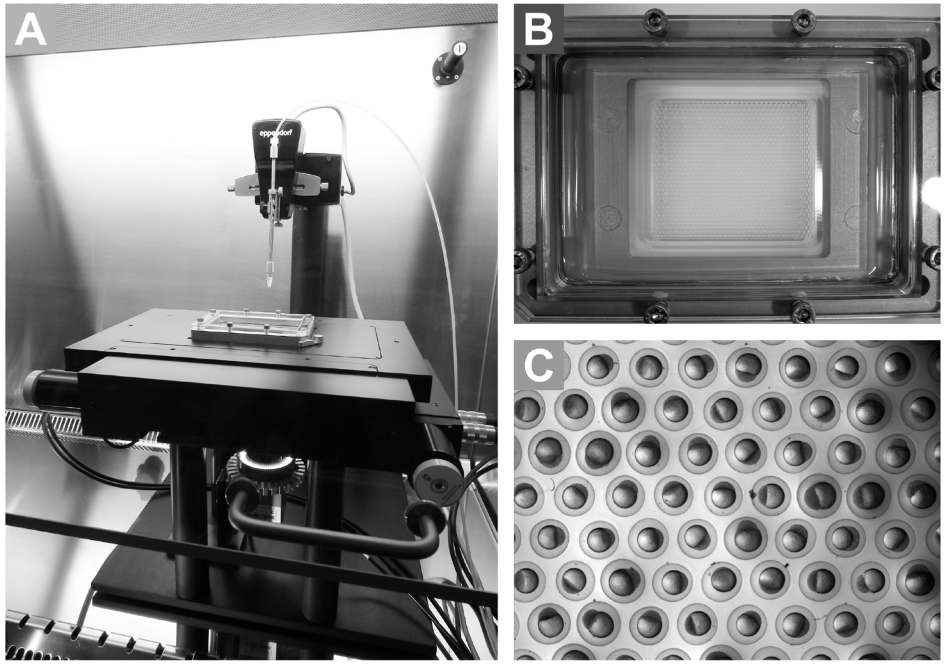

Figure 4.4 Pictures depicting automatic injector system. (A) the automatic injector system inside a laminar flow cabinet; (B) the embryo holder, showing the agarose grid within the steel support; (C) the embryo-filled grid, demonstrating the highly reproducible alignment of the embryos, with the cell mass resting to the side. Although size variation is observed, the embryos are always precisely in the centre of each well (the point of calibration for injection).

a centred and reproducible manner, with the cell mass always resting to the side. No image recognition was required for the injections, unlike a previously reported design that operates at a throughput level of 25 consecutive injections per run of 2 minutes[30]. The choice of agarose as the casting material dramatically reduced light refraction, resulting in a better image during calibration, and helped maintain embryos humid and viable.

To demonstrate the applicability of our system to drug screens, two independent large sets of embryos were injected with *M. marinum* and treated with a combination of first-line anti-TB drugs (Rifampicin and Isoniazid). After 3 days, immediately prior to the start of the antibiotic treatment, embryos were run through the COPAS flow cytometry system to determine the total level of red fluorescence, representative of bacterial load. The embryos were subsequently split into two randomly groups, whereby one was subjected to the combinatorial treatment for 3 days. At 5 dpi, the average signal per larva in the untreated group was approximately 3-fold higher than that of the treated group, and this difference was even more pronounced (4-fold) at 6 dpi (**Figure 4.5A and Table 4.S1**). These results attest both to the efficacy of the combinatorial drug treatment and to the ability of the COPAS to correctly discriminate treated and untreated groups.

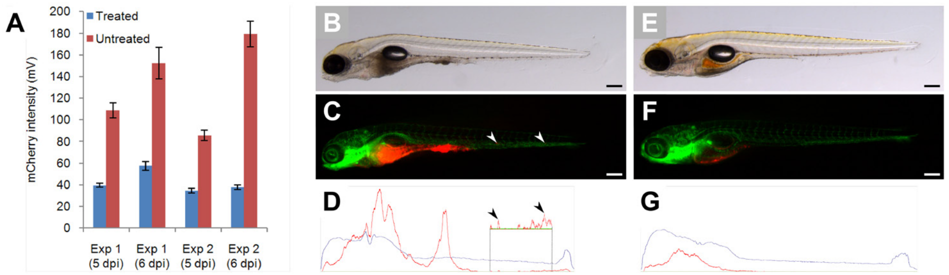

Figure 4.5 Automatic yolk sac injection of *M. marinum* and effect of treatment on infected larvae. (A) Effect of treatment on bacterial growth (measured by COPAS) in 5 and 6 day-old fli1-egfp larvae with gfp-labelled vasculature. Blue bars represent treated embryos, red bars represent untreated embryos. (B-D) Untreated versus (E-G) treated 5 day-old larvae, depicted whole in (B and E) bright-field and (C and F) fluorescent images, and (D and G) profiled by COPAS (scale bar: 250 μm). The localization of bacteria (red) in C and F correlates well with COPAS profile peaks in D and G, respectively (peaks in the tail region are shown enlarged in the inset; arrowheads depict two representative locations).

Epifluorescence and bright-field imaging revealed little to no red signal outside the yolk region of the treated larvae, which looked healthy and phenotypically normal. By contrast, untreated embryos displayed varying bacterial loads in the head, body and tail regions (**Figure 4.5B, C, E and F**). Additionally, the individual profiles generated by the COPAS correctly indicated whether bacteria were present in the body of infected larva (**Figure 4.5D and G**). L-plastin immunostaining further confirmed co-localization of *M. marinum* and leukocytes in the body of the untreated larvae (**Figure 4.1F-I**).

High-throughput *M. tuberculosis* injection and drug screen

It is clear that much can be learned about TB from the study of *M. marinum* infections in zebrafish, and the use of this pathogen offers practical advantages when compared to *M. tuberculosis*, such as lower biosafety restrictions and faster

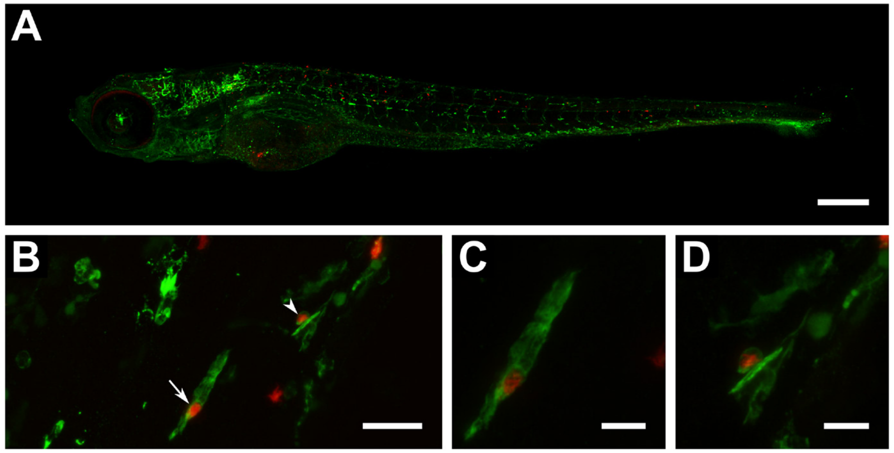

Figure 4.6 Automatic yolk sac injection of *M. tuberculosis* and effect of treatment on infected larvae. (A) Confocal z-stack (8x2 stitching) of a 6 day-old whole larva (fli1-egfp with gfp-labelled vasculature) showing spread of bacteria (red) throughout the body (scale bar: 250 µm). (B) Confocal z-stack of red-fluorescent bacteria co-localizing with green-fluorescent leukocytes detected by L-plastin immunostaining (scale bar: 25 µm). (C) Close-up (digital zoom: 4.2) of bacteria-containing leukocyte depicted in B by straight arrow (scale bar: 10 µm). (D) Close-up (digital zoom: 4.3) of bacteria-containing leukocyte depicted in B by arrowhead (scale bar: 10 µm).

growth rate. That notwithstanding, it was of interest to study the human pathogen, *M. tuberculosis*, directly in zebrafish. Using our system, we overcame all technical difficulties of manually injecting a BSL-3 pathogen into zebrafish embryos. Two independent sets of embryos were injected with *M. tuberculosis*, and were split at 3 dpi into treated (combinatorial Rifampicin and Isoniazid treatment) and untreated groups. To support growth of *M. tuberculosis*, embryos were maintained at a higher temperature (34°C) than in *M. marinum* infections (28°C).

Confocal imaging of fixed infected larvae revealed the presence of *M. tuberculosis* in their bodies after 5 dpi, indicating that the bacteria survived and were transported outside the injected area by macrophages, and that zebrafish larvae survive exposure to this pathogen (**Figure 4.6A**). There was a highly significant correlation (p=0.0004) between *M. tuberculosis* presence in the larvae and the absence of treatment (**Figure 4.S2**). Supporting the survival of *M. tuberculosis* in zebrafish, plating of lysates from 5 and 6 dpi larvae resulted in growth of *M. tuberculosis* colonies. Noteworthy, treated larvae did not yield any colonies, implying that the bacteria were eliminated during treatment.

L-plastin immunostaining showed leukocytes clustering around infected regions throughout the body, suggesting the formation of granuloma-like aggregates similar to those observed with *M. marinum* infections (**Figure 4.6B-D**). Leukocytes in these aggregates showed intracellular fluorescence of *M. tuberculosis* bacteria (**Figure 4.6C and D**). In addition, we also observed bacterial accumulation in cord-like structures characteristic of extracellular growth[27,28].

Concluding remarks

Our work has shown that the automatic injector, coupled with COPAS sorting, provides an extremely powerful high-throughput pipeline for infecting and analyzing zebrafish embryos and offers a new *in-vivo* tool for rapidly testing the efficacy of large panels of molecules on the propagation of the pathogen studied. Gene-disruption tools, such as morpholinos, can be easily integrated into our set-up. Moreover, our results clearly demonstrate, for the first time, the potential of using fish larvae to investigate *M. tuberculosis* directly, and highlight the importance of the automatic injector in enabling a high biosafety-level study that would otherwise be technically extremely difficult to accomplish. Interestingly, we have recently demonstrated the applicability of our robotic injection system for the xenotransplantation of human tumour cell lines into zebrafish embryos (data not shown), showing its general relevance in the high-throughput study of diseases that benefit from the use of whole vertebrate organisms.

Materials and Methods

Automated injection system

A polycarbonate substrate featuring a honeycomb pattern of 1,024 hemi-spherical wells (1.3 mm diameter) was used to create a negative mould in flexible polydimethylsyloxane (PDMS, Sylgard 184, Dow Corning) using standard moulding techniques. A 1% agarose gel (Sphaero) was poured onto an agarose-coated glass plate and the PDMS mould was pressed to touch the glass. After gelling the mould was removed and the grid was placed in a leakage-free steel support (sized to a 96-well plate) (**Figure 4.4B**).

The embryo grid was placed on a motorized stage (MTmot 200x100 MR, Märzhäuser) connected to a controller (Tango, Märzhäuser).
A motorized micro-manipulator (Injectman II, Eppendorf) was adjusted to a vertical position above the stage, and connected to a pump (Femtojet Express, Eppendorf) featuring an external compressor (lubricated compressor, model 3-4, JUN-AIR).

A firewire camera (DFK41BF02.H, The Imaging Source) equipped with a 4x macro lens (MR4/O, The Imaging Source) was placed beneath the stage for imaging.

All components were connected to the controlling computer (Ubuntu AMD64). A multi-threaded control program was written in Python, using PySerial and wxPython. Coriander software (http://damien.douxchamps.net/ieee1394/coriander) was used for imaging.

The camera height was adjusted to focus on the top plane of the agarose grid, and a grid calibration was performed.

The grid was removed for loading with embryos (**Figure 4.4C**). The injection needle (pulled borosilicate glass capillary, Harvard Apparatus) was placed in the Injectman and moved to the central focal position. The x and y coordinates were stored and the needle was elevated to replace the filled grid.

The injection height was calibrated using the first embryo by moving the needle downwards through the chorion until touching the yolk (400 µm above injection point).

Bacterial culture and inoculum preparation

M. marinum strain E11 stably expressing mCherry (pSMT3-mCherry vector)[31] was grown as previously described[32], in the presence of 50 µg/mL hygromycin. Injection inocula were prepared from glycerol stocks (frozen at OD600=0.75) by washing three times in sterile 0.05% Tween80/PBS solution (BD Difco), assessing optical density at 600 nm and resuspending in a 2% polyvinylpyrrolidone40 (PVP40) solution (CalBiochem) in PBS.

M. marinum Mma20 strains expressing, in addition to mCherry, mag49-GFP or gag7-GFP plasmids[23] were cultured in medium containing 20 µg/mL kanamycin and 50 µg/mL hygromycin.

M. tuberculosis strain H37Rv stably expressing mCherry was maintained in logarithmic phase at all times in 7H9 medium (BD Difco Middlebrook) containing 50 µg/mL hygromycin in a BSL-3 laboratory. Prior to injection, optical density at 600 nm was assessed, the bacteria were washed three times in sterile water and resuspended in 2% PVP40.

The number of CFU in each inoculum was verified by plating out serial dilutions and the injected inoculum in triplicate.

Ethics statement

Zebrafish lines (wild-type, albino/fli1-egfp[33] and mpx-gfp[34]) were handled in compliance with the local animal welfare regulations and maintained according to standard protocols (zfin.org). The breeding of adult fish was approved by the local animal welfare committee (DEC) of the University of Leiden. All protocols adhered to the international guidelines specified by the EU Animal Protection Directive 86/609/EEC.

Zebrafish infections

Infections including the Pu.1 morpholino[29] (1 mM, Gene Tools) were performed by yolk injection (1 nl) at the 1-2 cell stage, whereas all other injections of *M. marinum* (20-40 CFUs) or *M. tuberculosis* (100 CFUs) took place between 16 and 512 cells. Control embryos were injected with carrier solution.

After *M. marinum* infection, embryos were collected in 92x16 mm petri dishes (Sarstedt), with a maximum of 100 embryos per dish, and maintained at 28°C in egg water. At 3 dpi embryos were analyzed by the COPAS system (see below) and randomly split into two equal groups. One group was exposed to a combination of 200 µM Rifampicin (Sigma-Aldrich) and 2 mM Isoniazid (Sigma-Aldrich) for 3 days (exposure to the drugs achieved by adding compounds to egg water; antibiotics refreshed once daily) and the other was followed without treatment (water refreshed once daily). Uninjected controls were similarly split into treated and untreated groups to account for antibiotic effects. At 5 and 6 dpi, the different larva groups were analyzed by the COPAS system, and the bacterial load was assessed by the total red fluorescence detected.

After *M. tuberculosis* infection, embryos were collected in tanks containing 1 litre of egg water with a maximum of 300 embryos per tank, and maintained at 34°C. At 3 dpi embryos were randomly split into treated and untreated groups as described above. Twenty larvae per group were homogenized at 5 and 6 dpi and plated out to assess the number of live bacteria per larva. Batches of 40-100 larvae per group were fixed at 5 and 6 dpi for optical analyses.

Immunohistochemistry

Larvae were fixed in 4% paraformaldehyde in PBS overnight at 4°C and immunolabeled using the L-plastin antibody as previously described[35].

Microscopy

Fluorescence in embryos and larvae was observed using a Leica MZ16 FA fluorescence stereomicroscope equipped with LAS AF software (Leica Microsystems), a Leica DMI400 B confocal microscope equipped with LAS AF software (Leica Microsystems) and a Zeiss LSM5 Exciter / Axio Observer confocal microscope equipped with ZEN software (Carl Zeiss). The following objectives were used: Leica stereomicroscope PlanaP0 1x (**Figure 4.1A, 4.2A and B and 4.5B, C, E and F**); Leica confocal HCX PL Fluotar 40x/0.75 dry (**Figure 4.1B-I, 4.2C-E and 4.6B-D**); Zeiss confocal EC Plan-Neofluar 10x/0.30 dry (**Figure 4.6A**). Images were processed using the public domain program ImageJ (W. Rasband, ImageJ 1.42q, http://rsb.info.nih.gov/ij/).

Complex Object Parametric Analyzer and Sorter (COPAS)

The COPAS™ XL (Union Biometrica) large particle sorter has been designed for the analysis, sorting and dispensing of objects up to 1.5 mm in diameter based on size, optical density and fluorescence intensity. It is equipped with 488 nm and 561 nm Solid State lasers, and mCherry is detected through a 615/24 Band-Pass filter.

The Profiler II Option simultaneously detects and analyzes up to 8,000 data points per object for each of the channels of extinction and fluorescence, and includes advanced imaging options. The resulting profiles can be used to set sorting parameters.

The COPAS parameters used were as follows: optical density threshold (extinction) = 390 mV (COPAS value: 20); minimum time of flight = 280 µs (COPAS value: 700); red photomultiplier tube (PMT) voltage = 450 V; green PMT voltage = 0 V; yellow PMT voltage = 0 V.

Statistics

The effect of drug treatment on *M. marinum* mCherry fluorescence in zebrafish larvae was statistically analyzed using a 2-tailed T-test. The correlation between drug treatment and the presence or absence of *M. tuberculosis* was determined by a χ^2-test.

Acknowledgements

We thank the following colleagues for generously contributing to our work: Dr. Lalita Ramakrishnan (University of Washington) for providing *M. marinum* gag and mag plasmids, Dr. Anna Huttenlocher (University of Wisconsin) for providing the L-plastin antibody and Dr. Astrid van der Sar (Vrije Universiteit, Amsterdam) for fluorescent *M. marinum* strains and growth and transformation protocols. We also thank Rico Bongaarts and Angela Comas (Union Biometrica) for all their COPAS help and advice. Lastly, we are very grateful to the following colleagues from Leiden University: Davy de Witt, Ulrike Nehrdich and Karen Bosma for fish care-taking, Gerda Lamers for assistance with confocal microscopy, Fred Schenkel and Ewie de Kuyper (FMD) for the technical help and discussions, and Erica Benard, Wietske van der Ent and Dr. Anna Zakrzewska for help with experimental work and reading of the manuscript.

References

1. **Ottenhoff TH, Verreck FA, Lichtenauer-Kaligis EG, Hoeve MA, Sanal O, et al.** (2002) Genetics, cytokines and human infectious disease: lessons from weakly pathogenic mycobacteria and salmonellae. *Nat Genet 32: 97 - 105.*

2. **van de Vosse E, Hoeve MA, Ottenhoff TH** (2004) Human genetics of intracellular infectious diseases: molecular and cellular immunity against mycobacteria and salmonellae. *Lancet Infect Dis 4: 739 - 749.*

3. **Russell DG, Barry CE, 3rd, Flynn JL** (2010) Tuberculosis: what we don't know can, and does, hurt us. *Science 328: 852 - 856.*

4. **van Crevel R, Ottenhoff TH, van der Meer JW** (2002) Innate immunity to *Mycobacterium tuberculosis. Clin Microbiol Rev 15: 294 - 309.*

5. **Russell DG** (2007) Who puts the tubercle in tuberculosis? *Nat Rev Microbiol 5: 39 - 47.*

6. **Adams DO** (1976) The granulomatous inflammatory response. A review. *Am J Pathol 84: 164 - 192.*

7. **Pieters J** (2008) *Mycobacterium tuberculosis* and the macrophage: maintaining a balance. *Cell Host Microbe 3: 399 - 407.*

8. **Bold TD, Ernst JD** (2009) Who benefits from granulomas, mycobacteria or host? *Cell 136: 17 - 19*.

9. **Schnappinger D, Ehrt S, Voskuil MI, Liu Y, Mangan JA, et al**. (2003) Transcriptional Adaptation of *Mycobacterium tuberculosis* within Macrophages: Insights into the Phagosomal Environment. *J Exp Med 198: 693 - 704*.

10. **Ottenhoff TH** (2009) Overcoming the global crisis: "yes, we can", but also for TB ... ? *Eur J Immunol 39: 2014 - 2020*.

11. **Kuijl C, Savage ND, Marsman M, Tuin AW, Janssen L, et al**. (2007) Intracellular bacterial growth is controlled by a kinase network around PKB/AKT1. *Nature 450: 725 - 730*.

12. **Flynn JL** (2006) Lessons from experimental *Mycobacterium tuberculosis* infections. *Microbes Infect 8: 1179 - 1188*.

13. **Williams A, Hall Y, Orme IM** (2009) Evaluation of new vaccines for tuberculosis in the guinea pig model. *Tuberculosis (Edinb) 89: 389 - 397*.

14. **O'Toole R** (2010) Experimental models used to study human tuberculosis. *Adv Appl Microbiol 71: 75 - 89*.

15. **Lesley R, Ramakrishnan L** (2008) Insights into early mycobacterial pathogenesis from the zebrafish. *Curr Opin Microbiol 11: 277 - 283*.

16. **Pardo-Martin C, Chang TY, Koo BK, Gilleland CL, Wasserman SC, et al**. (2010) High-throughput in vivo vertebrate screening. *Nat Methods 7: 634 - 636*.

17. **Amsterdam A, Hopkins N** (2006) Mutagenesis strategies in zebrafish for identifying genes involved in development and disease. *Trends Genet 22: 473 - 478.*

18. **Nasevicius A, Ekker SC** (2000) Effective targeted gene 'knockdown' in zebrafish. *Nat Genet 26: 216 - 220*.

19. **Tobin DM, Ramakrishnan L** (2008) Comparative pathogenesis of *Mycobacterium marinum* and *Mycobacterium tuberculosis*. Cell Microbiol 10: 1027 - 1039.

20. **Swaim LE, Connolly LE, Volkman HE, Humbert O, Born DE, et al**. (2006) *Mycobacterium marinum* infection of adult zebrafish causes caseating granulomatous tuberculosis and is moderated by adaptive immunity. *Infect Immun 74: 6108 - 6117.*

21. **Volkman HE, Clay H, Beery D, Chang JC, Sherman DR, et al**. (2004) Tuberculous granuloma formation is enhanced by a *mycobacterium* virulence determinant. *PLoS Biol 2: e367.*

22. **Davis JM, Ramakrishnan L** (2009) The role of the granuloma in expansion and dissemination of early tuberculous infection. *Cell 136: 37 - 49*.

23. **Davis JM, Clay H, Lewis JL, Ghori N, Herbomel P, et al**. (2002) Real-time visualization of *mycobacterium*-macrophage interactions leading to initiation of granuloma formation in zebrafish embryos. *Immunity 17: 693 - 702*.

24. **Agarwal N, Bishai WR** (2010) Microbiology. Subversion from the sidelines. *Science 327: 417 - 418*.

25. **Clay H, Davis JM, Beery D, Huttenlocher A, Lyons SE, et al**. (2007) Dichotomous role of the macrophage in early *Mycobacterium marinum* infection of the zebrafish. *Cell Host Microbe 2: 29 - 39*.

26. **Volkman HE, Pozos TC, Zheng J, Davis JM, Rawls JF, et al**. (2010) Tuberculous granuloma induction via interaction of a bacterial secreted protein with host epithelium. *Science 327: 466 - 469*.

27. **Clay H, Volkman HE, Ramakrishnan L** (2008) Tumor necrosis factor signaling mediates resistance to mycobacteria by inhibiting bacterial growth and macrophage death. *Immunity 29: 283 - 294*.

28. **Tobin DM, Vary JC, Jr., Ray JP, Walsh GS, Dunstan SJ, et al**. (2010) The lta4h locus modulates susceptibility to mycobacterial infection in zebrafish and humans. *Cell 140: 717 - 730*.

29. **Rhodes J, Hagen A, Hsu K, Deng M, Liu TX, et al**. (2005) Interplay of pu.1 and gata1 determines myelo-erythroid progenitor cell fate in zebrafish. *Dev Cell 8: 97 - 108*.

30. **Wang W, Liu X, Gelinas D, Ciruna B, Sun Y** (2007) A fully automated robotic system for microinjection of zebrafish embryos. *PLoS One 2: e862*.

31. **Meijer AH, van der Sar AM, Cunha C, Lamers GE, Laplante MA, et al**. (2008) Identification and real-time imaging of a myc-expressing neutrophil population involved in inflammation and mycobacterial granuloma formation in zebrafish. *Dev Comp Immunol 32: 36 - 49*.

32. **van der Sar AM, Spaink HP, Zakrzewska A, Bitter W, Meijer AH** (2009) Specificity of the zebrafish host transcriptome response to acute and chronic mycobacterial infection and the role of innate and adaptive immune components. *Mol Immunol 46: 2317 - 2332*.

33. **Lawson ND, Weinstein BM** (2002) In vivo imaging of embryonic vascular development using transgenic zebrafish. *Dev Biol 248: 307 - 318*.

34. **Renshaw SA, Loynes CA, Trushell DM, Elworthy S, Ingham PW, et al**. (2006) A transgenic zebrafish model of neutrophilic inflammation. *Blood 108: 3976 - 3978*.

35. **Mathias JR, Dodd ME, Walters KB, Rhodes J, Kanki JP, et al**. (2007) Live imaging of chronic inflammation caused by mutation of zebrafish Hai1. *J Cell Sci 120: 3372 - 3383*.

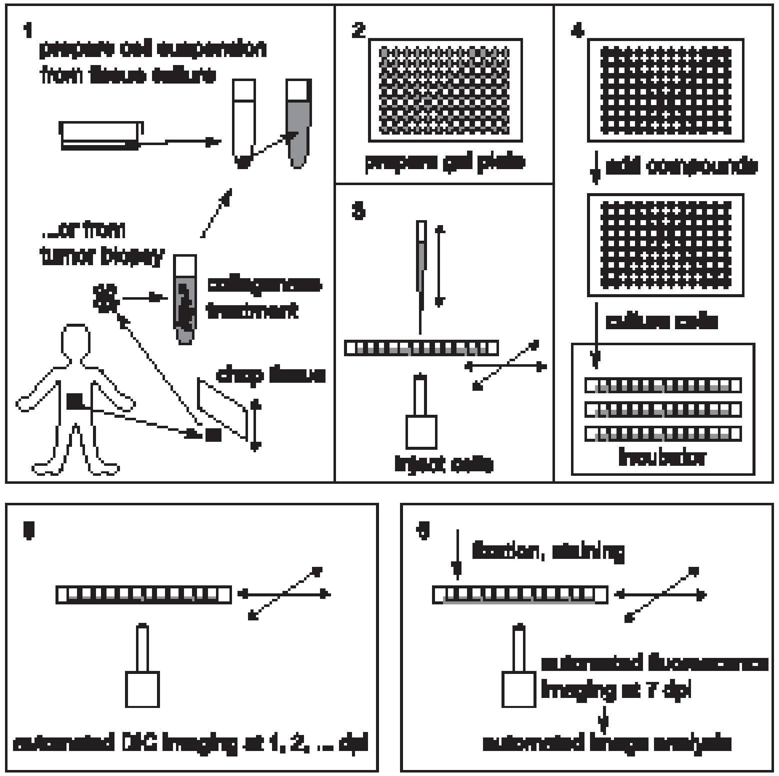
1
prepare cell suspension from tissue culture
...or from tumor biopsy
collagenase treatment
chop tissue
2
prepare gel plate
3
inject cells
4
add compounds
culture cells
incubator
5
automated DIC imaging at 1, 2, ... dpi
6
fixation, staining
automated fluorescence imaging at 7 dpi
automated image analysis

Chapter 5

Automated microinjection of cell-polymer suspensions in 3D ECM scaffolds for high throughput quantitative cancer invasion screens

Hoa H Truong[a*], Jan de Sonneville[b*], Veerander PS Ghotra[a], Jiangling Xiong[a], Leo Price[a], Pancras Hogendoorn[c], Herman Spaink[d], Bob van de Water[a], Erik HJ Danen[a]

[*] These authors contributed equally to this work.
[a] *Division of Toxicology, Leiden Amsterdam Center for Drug Research, Leiden University, Einsteinweg 55, 2333 CC, Leiden, the Netherlands*
[b] *Division of Biophysical Structural Chemistry, Leiden Institute of Chemistry, Leiden University, Einsteinweg 55, 2333 CC Leiden, the Netherlands*
[c] *Department of Pathology, Leiden University Medical Center, Albinusdreef 2, 2333 ZA, Leiden, the Netherlands*
[d] *Institute of Biology, Leiden University, Einsteinweg 55, 2333 CC, Leiden, the Netherlands*

Biomaterials, in press

Abstract

Cell spheroids (CS) embedded in 3D extracellular matrix (ECM) serve as *in vitro* mimics for multicellular structures *in vivo*. Such cultures, started either from spontaneous cell aggregates or single cells dispersed in a gel are time consuming, applicable to restricted cell types only, prone to high variation, and do not allow CS formation with defined spatial distribution required for high-throughput imaging. Here, we describe a novel method where cell-polymer suspensions are microinjected as droplets into collagen gels and CS formation occurs within hours for a broad range of cell types. We have automated this method to produce CS arrays in fixed patterns with defined x-y-z spatial coordinates in 96 well plates and applied automated imaging and image analysis algorithms. Low intra- and inter-well variation of initial CS size and CS expansion indicates excellent reproducibility. Distinct cell migration patterns, including cohesive strand-like- and individual cell migration can be visualized and manipulated. A proof-of-principle chemical screen is performed identifying compounds that affect cancer cell invasion/migration. Finally, we demonstrate applicability to freshly isolated mouse and human tumor biopsy material - indicating potential for development of personalized cancer treatment strategies.

Introduction

Cells grown under classical 2D culture conditions behave differently from the same cell types grown *in vivo*. In addition to soluble factors produced in the *in-vivo* microenvironment, differences in cell shape, intercellular contacts, and connections to ECM have striking effects on gene expression, cell survival, proliferation, differentiation, cytoarchitecture, and migration. Various systems have been developed to culture cells within 3D ECM environments, aimed at more closely mimicking the *in-vivo* context[1,2]. Several of these systems produce 3D cell aggregates in which, after compaction, depletion of oxygen, nutrients, and growth factors occurs in the core, leading to cell heterogeneity depending on the position in the resulting CS[3,4]. Multistep methods are used in which aggregates are allowed to form spontaneously and, following a compaction phase, can subsequently be transferred to a 3D ECM. The best-known example of this approach is the "hanging drop assay" that was developed to create embryoid bodies from ES cells and has also been applied to cancer cell lines to produce tumor-like structures[5,6]. Alternative methods involve mixing of single cell suspensions with a solidifying ECM, resulting in individual cells that eventually form spheroids randomly within a 3D ECM structure[7], or seeding polymeric scaffolds with cell/ECM suspensions[2].

Cell behavior in 3D cultures is controlled by chemical (composition) and physical (rigidity, cross-linking) properties of the gel. Natural ECM proteins can be used such as collagen, fibrinogen, or the laminin-rich matrigel to represent the *in-vivo* ECM composition most relevant to a given cell type. More recently, synthetic polymers have been developed for 3D CS culture environments although it remains to be established how well these support a variety of cell behavioral outputs, including cell migration[8]. Collagen type I is an abundant polymer in ECM *in vivo*, and it is widely used for 3D cultures. Various physical properties of the collagen gel, such as rigidity and pore size modulate stem cell differentiation, cancer growth, and cell migration[9-11]. Cells can use various migration strategies in 3D environments, including mesenchymal or amoeboid individual cell migration modes or collective invasion strategies, depending on properties of the cells and of the matrix[10]. Changes in matrix pore size can force cells to adopt alternative migration strategies or - if too extreme - pose a barrier to cell migration. Importantly, cells can modify the ECM by physical deformation and proteolysis, to overcome such barriers[12].

Chemical compound screens as well as RNAi screens for various types of cellular functions, including survival, growth, differentiation, and migration are mostly performed in 2D culture conditions. Methods to analyze cells in 3D based on the hanging-drop assay are labor and time intensive; are limited to cell types that are cohesive and aggregate spontaneously; and are prone to high variability between experiments due to variation in aggregation and compaction time and CS size. Alternative methods in which single cell suspensions are mixed with soluble ECM substrates that are subsequently allowed to form a gel are relatively easy to perform but also have several major disadvantages: formation of CS depends on the ability of a cell type to survive and proliferate as single cells in low adhesion conditions for extended periods; CS formation is time consuming; CS show a large variation in size; and CS form at random locations, which is disadvantageous for imaging purposes.

To allow for CS formation that is relatively fast and easy, highly reproducible, and overcomes the disadvantages described above we have developed a novel method where cell-polymer suspensions are microinjected into multiwell plates containing a collagen gel. This method has been automated to produce CS arrays with highly reproducible properties in large quantities in 96 well plates. We use this system to visualize distinct 3D migration strategies and regulation of those strategies by ECM properties and actomyosin contractility. We demonstrate applicability in high-throughput screening platforms in a chemical screen for compounds that affect breast cancer invasion/migration. Finally, we apply the method to cell suspensions derived from fresh tumor biopsies, which opens the possibility to test therapeutic strategies on freshly isolated material from individual patients.

Results

Development and characterization of the method

To design a protocol that rapidly produces CS with highly reproducible characteristics we developed a novel method based on microinjection. For the microinjection method we mixed cells with polyvinylpyrrolidone (PVP), which is an inert (hydrophilic) water-soluble synthetic polymer, also used as emulsifier, food-additive (E1201) and as solubilizing agent for injections[13]. In our application it was used to delay cell sedimentation within the capillary needle. Furthermore, in our experience cells rapidly disperse in the absence of PVP while cells injected in the presence of PVP remained localized (e.g. trapped by the polymer) at the site of injection, allowing time for aggregation and CS formation.

We first compared our method to the established hanging drop assay 5. Twenty µl drops containing 5x10^3 GEß1 cells were used to create hanging drops in an inverted 10 cm dish (**Fig. 5.1a**). The time required to form cell aggregates was 24h. These cell aggregates were transferred to agarose-coated dishes where they formed tightly packed spheroids over a period of 48h. Next, the spheroids were embedded in 2.4 mg/mL collagen solution that was subsequently allowed to solidify. For microinjection, GEß1 cells were suspended in 2% PVP, loaded into a pulled glass needle, and ~80nL droplets containing ~1x10^4 cells were injected directly into preformed 2.4 mg/mL collagen gels where they formed tightly packed spheroids within 1h (**Fig. 5.1a**). Microinjection-derived CS at 24h post-injection and hanging-drop-derived CS at 96h post initiation (24h in collagen) displayed similar cell migration the following days (**Fig. 5.1b**). Microinjection-derived CS

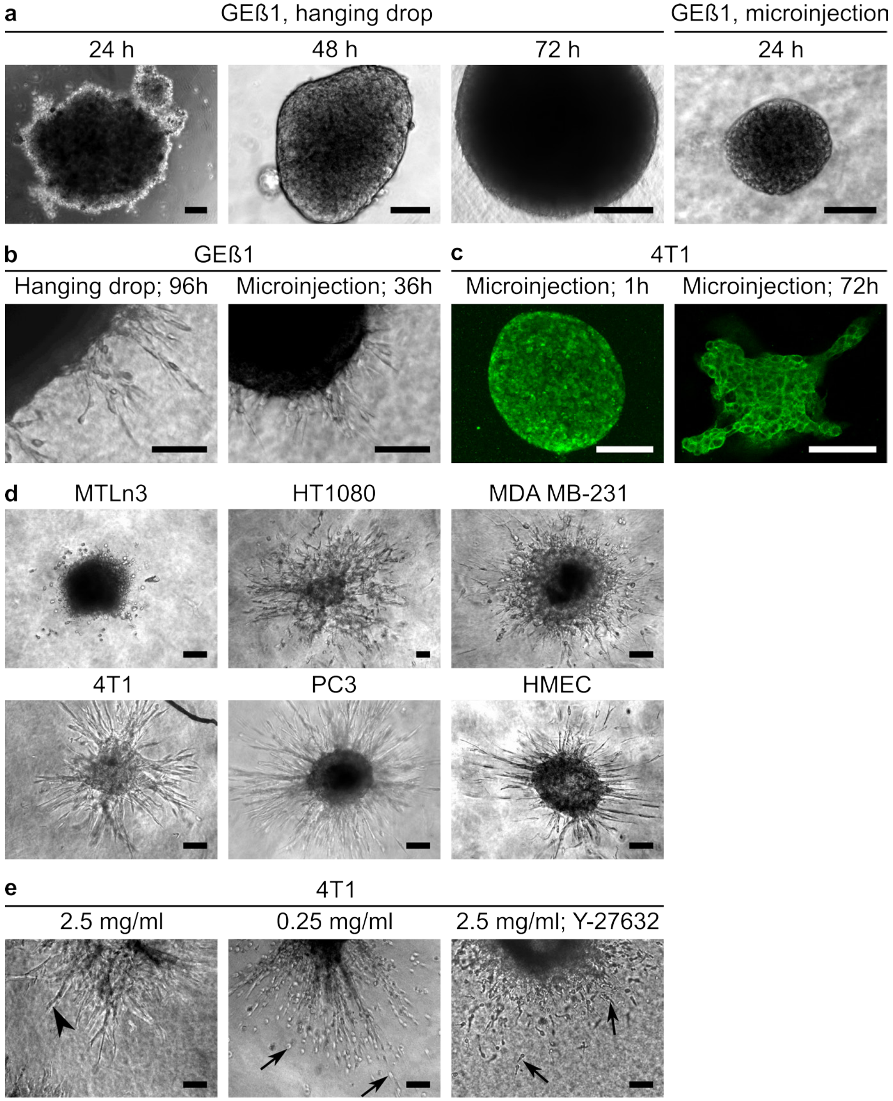

Figure 5.1 Characteristics of microinjection-derived speroids. a, Comparison of hanging-drop and microinjection method for GEß1 cells. b, Migration of GEß1 cells from hanging-drop and microinjection-derived spheroids. c, E-cadherin staining in spheroids at indicated timepoints post- injection for 4T1 cells. d, Different modes of cell migration from spheroids for indicated cell types showing individual (top row) and cohesive strand migration (bottom row). e, Modulation of cell migration modes by alterations in collagen gel network (left and middle) or interfering with cytoskeletal network (right image, ROCK inhibitor, Y-27632). Arrowheads indicate cohesive migration strands; arrows indicate individual migrating cells. Scales, 120 µm.

were also established from 4T1 mouse breast carcinoma cells where E-cadherin staining marked cell-cell contacts within the first day post-injection that were maintained for at least 96h (**Fig. 5.1c**).

CS derived by microinjection of different cancer- or non-cancerous cell types allowed analysis of various distinct motile strategies in 3D (**Fig. 5.1d**). Cell types that do not typically form cell-cell contacts in 2D cell culture (and that are typically difficult to study in 3D using the hanging-drop-, liquid overlay-, or other assays in absence of additives like matrigel[14,15]) such as MTLn3 and MDA-MB-231 breast cancer cells and HT1080 fibrosarcoma cells, displayed amoeboid (MTLn3) or mesenchymal (HT1080 and MDA-MB-231) movement of individual cells. On the other hand, 4T1 breast cancer, PC-3 prostate cancer, and human microvascular endothelial cells (HMEC) that grow as islands in 2D culture, invaded as cohesive strands into the collagen matrix.

ECM rigidity influences cell behavior in 3D and the actin cytoskeleton is believed to be essential for sensing and responding to such physical ECM properties[12]. We used these CS to study the effect of alterations in ECM network composition or intracellular cytoskeletal network properties on migration strategies in 3D. Lowering ECM rigidity by decreasing collagen concentration from 2.5 to 0.25 mg/mL or lowering cytoskeletal tension by application of a ROCK inhibitor, both caused a switch from cohesive strand invasion to individual cell migration in 4T1 cells (**Fig. 5.1e**). This suggests that tension exerted on cell-cell adhesion structures either from outside or inside the cell is required for cohesive 3D movement.

Altogether, these results demonstrate that the microinjection method produces CS for 3D growth and migration studies rapidly (hours versus days), conveniently (one step), with a broad spectrum of cell types including those that are incompatible with previous methods, and displaying a variety of migration patterns.

Method automation

Since this method has the potential to rapidly create CS with high reproducibility for large- scale analysis in 3D ECM of cell growth and migration/invasion we set up a procedure to automate the CS formation process. For this purpose, a 96 well plate containing 60 µL collagen gel per well was placed on a motorized stage and the glass needle containing the cell/PVP suspension described above was placed vertically in a motorized micromanipulator above the stage (**Fig. 5.2a**). After calibration of needle and 96-well plate using camera vision from under the stage, a computer script was used to automate the injection process with various macros.

Figure 5.2 Automated production of spheroid arrays. a, Automated injection system (left) and cell/PVP suspension containing needle during injection (right). b, Bottom view of multiple wells with 4T1 spheroid arays 96 hours post-injection. Scale, 10mm. c, Upper row shows stitched brightfield images showing spheroid arrays at indicated timepoints. Scale, 1 mm. Bottom row shows cell migration from single bright-field images of spheroids marked by dashed rectangle in upper row. Scale, 100 µm. d, Mean and SD for initial spheroid size 4h post-injection (black bars) and CS migration over ~4 days determined from outline of migration strands (grey bars) obtained from all 7 spheroids /well for indicated wells of a 96-well plate.

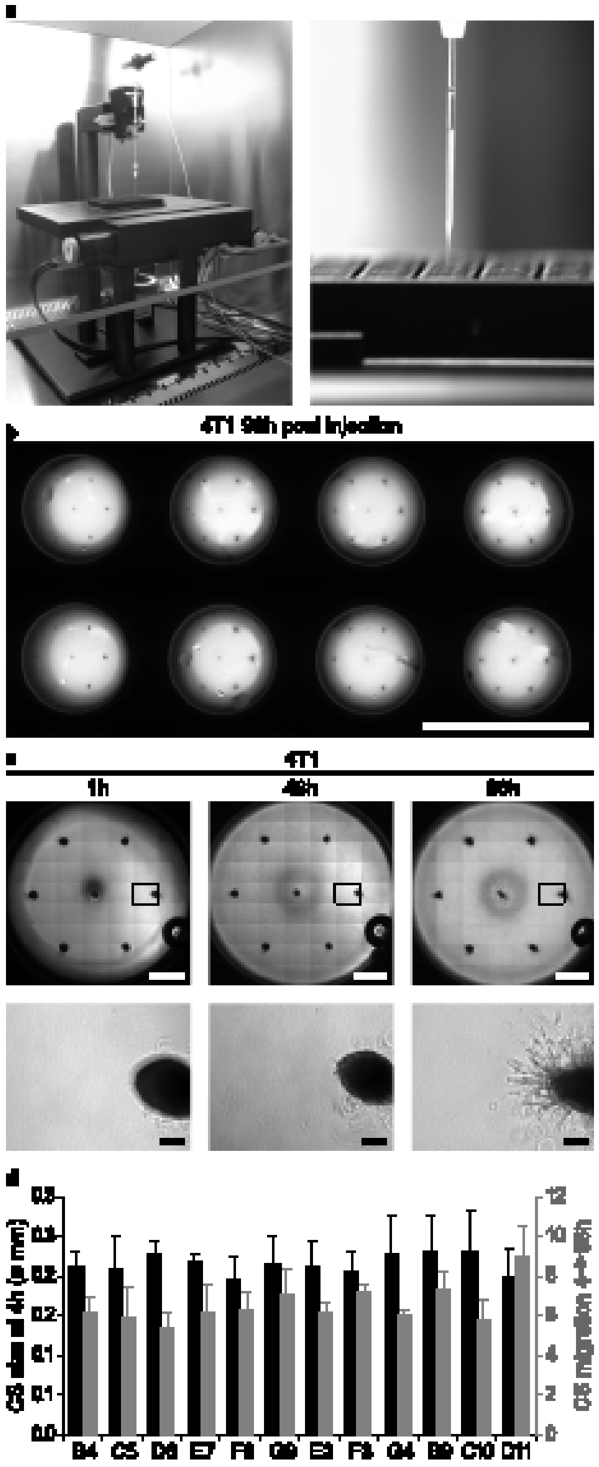

With this set up, cell droplets were injected resulting in spheroids of ~300 µm diameter (**Movie S1**). To increase reproducibility, using commercial needles reduced needle tip diameter variance and gels were prepared from a single large batch of collagen isolated in-house from rat-tail. Various layouts of injection patterns were tested. A hexagonal pattern of 19 spheroids spaced at 1.2 mm started to show interaction between migration strands of CS at day 4 but a less dense hexagon pattern of 7 spheroids at 2 mm spacing provided sufficient spacing for 96h analysis of CS migration (**Fig. 5.2b,c**). Visual inspection indicated reduced CS migration on the most outer rows and columns of each plate, pointing to edge effects. We therefore chose to exclude these wells in all further experiments. We determined reproducibility in all other wells and detected no significant intra- or inter-well variation in initial CS size (ANOVA, P>0.5) or CS expansion over ~92h (ANOVA, P>0.5) (**Fig. 5.2d**).

These data demonstrate that the microinjection method can be automated to create with high reproducibility and predefined x-y-z coordinates CS arrays in 96 well plates. Such properties make this protocol ideal for automated imaging strategies.

Application of the method to automated drug screens

A proof of principle drug screen was performed to test the applicability of this procedure to automated high-throughput drug screening assays (HTS). 4T1 CS were generated and various previously described inhibitors, including AG1478 (EGFR), PP2 (Src), ML-7 (MLCK), Y-27632 (ROCK), NSC23766 (Rac), SB-431542 (TGFβR activin-like kinases), AG-82 (EGFR), LY-294002 (PI3K), JSI-124 (STAT3) were added one hour later at different concentrations (4, 10, 20 µM) in duplicate. Effects on cell migration could be clearly observed by DIC imaging after 2 and 4 days for ML-7 and JSI-124 (**Fig. 5.3a**). For automated imaging and image analysis protocols, we labeled the actin cytoskeleton at day 4 of all 10 µM-treatments and controls (**Fig. 5.3b**). This allowed automated capture of Z-stacks that were converted to maximum projection images, thresholded, and used for automated multiparameter analysis including Feret's diameter and circularity.

Visual inspection and manual assessment of Feret's diameter from DIC images at day 0 and 4 demonstrated that initial CS size, CS expansion, and inhibition of invasion by ML-7 and JSI-124 were highly reproducible (**Fig. 5.3a,c**). Automated image analysis fitted well with these data showing that ML-7 and JSI-124 caused significantly reduced Feret's diameters (p<0.05) (**Fig. 5.3d**). For JSI-124 this correlated with increased circularity (p<0.05) in agreement with inhibition of invasion and a remaining round CS. The extremely low values observed for

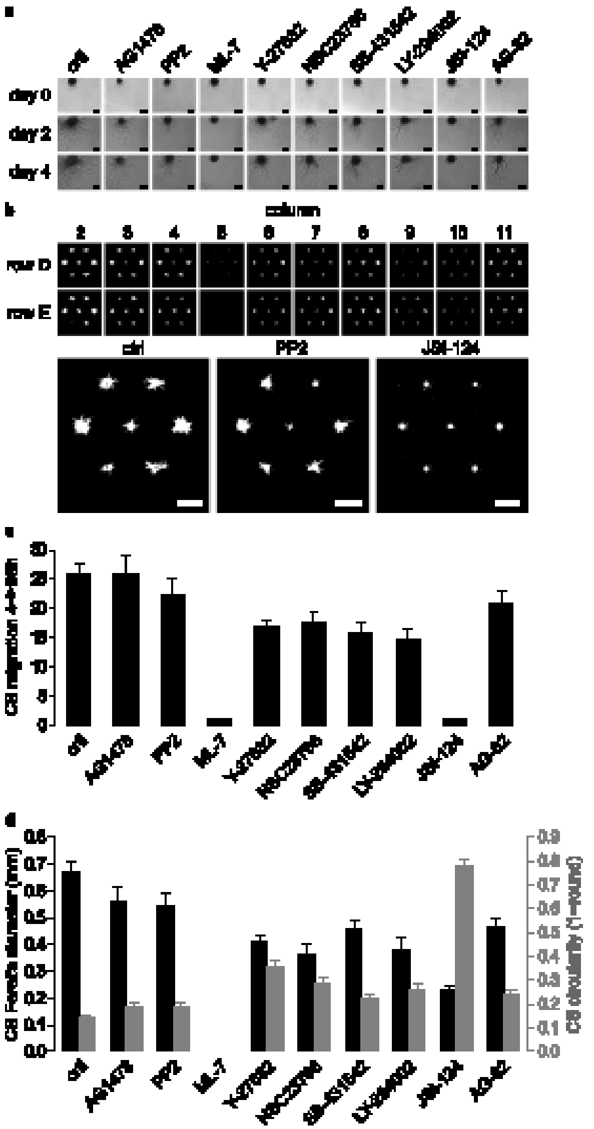

Figure 5.3 Results from a drug screen performed on 4T1 cells in a 96 well plate.
a, DIC images showing tumor cell migration in the presence of indicated inhibitors at indicated timepoints (scale = 100 µm). b, Top 2 rows, rhodamine-phalloidin staining and thresholding for indicated wells at 4 dpi (columns correspond to treatments from a; rows represent duplicates); bottom row, zoom in on well D2 (Ctr), D4 (PP2), and D10 (JSI-124). Scale, 1 mm. c, effect of indicated inhibitors on CS migration over ~4 days determined from outline of migration strands derived from DIC images in a (mean and SEM for 14 spheroids derived from 2 wells is shown). d, Quantification of data derived from automated analysis of fluorescent images shown in B (mean and SEM for 14 spheroids derived from 2 wells is shown).

ML-7 (**Fig. 5.3d**) despite the fact that a CS was observed by DIC (**Fig. 5.3a**) can be explained by ML-7-induced loss of filamentous actin fibers causing reduced staining in this particular method. Alternative staining procedures should lead to improvement and compatibility with real-time analysis. Nevertheless, the reproducibility of the injection procedure (**Fig. 5.2 and 5.3**) combined with the similarity between visual inspection and automated imaging (**Fig. 5.3c,d**), demonstrates that this automated injection system can be coupled to fully automated imaging and image analysis methodology that is accurate and reproducible.

Compatibility of the method with primary biopsy material

We determined if this methodology is compatible with freshly isolated biopsy material. First, a cell suspension was generated from 4T1-GFP orthotopic breast tumors in mice using collagenase- treatment. In contrast to alternative methods, the microinjection method circumvents any 2D tissue culture steps, which may cause altered cell behavior[16-20]. Following injection, these cells rapidly formed CS from which migration was analyzed after 3 days (**Fig. 5.4a**). CS were stained for actin and DNA and the near complete overlap between actin and GFP staining demonstrates that these CS consist mainly of tumor cells.

Next, cell suspensions were derived by collagenase treatment of freshly isolated human osteosarcoma and chondrosarcoma tissue. Following injection, CS readily formed from these human biopsies and survival and migration could be studied for up to one week with the two tumor types showing distinct migratory behavior (**Fig. 5.4b**). Osteosarcoma mainly displayed individual amoeboid movement whereas chondrosarcoma showed predominantly individual mesenchymal movement. We treated these CS with the range of compounds described above at 10 μM starting one day post-injection. Several of the chemical inhibitors effectively inhibited migration of both tumor types (**Fig. 5.4b,c**). Notably, the ROCK inhibitor Y-27632 did not affect mesenchymal movement but caused switching from amoeboid to mesenchymal movement in the osteosarcoma cells, in line with the described requirement for ROCK activity only in amoeboid single cell movement[21].

Taken together, these data indicate that the automated CS injection methodology has the potential to be used for drug testing on tumor cells freshly isolated from individual patients.

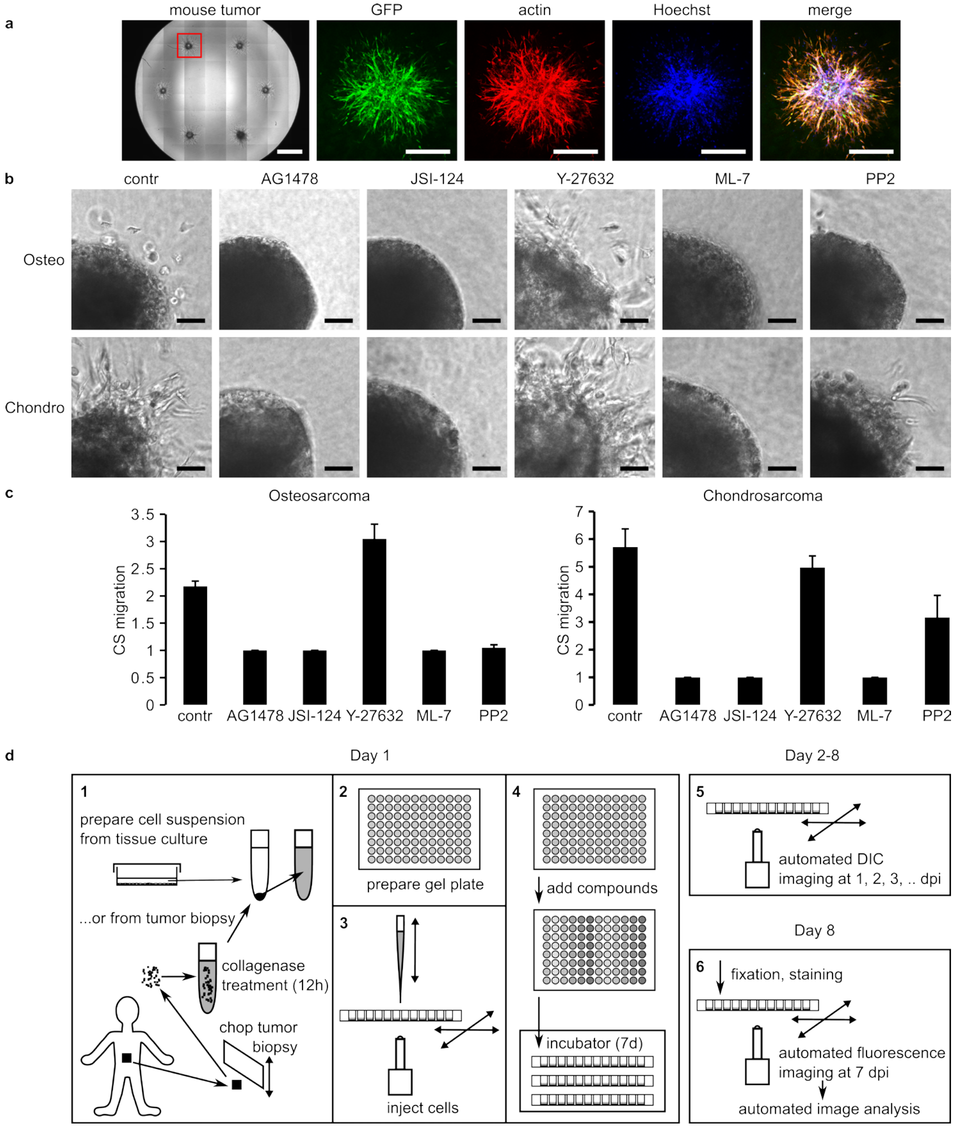

Figure 5.4 Application to tumor biopsies. a, Overview DIC image (left) and zoom in on individual spheroid obtained from 4T1-GFP orthotopic mouse breast tumor. Scales, 1 mm (left DIC); 500μm (fluorescent images). b, DIC images showing spheroids derived from osteosarcoma (top) and chondrosarcoma biopsy (bottom) treated with indicated inhibitors. Scale, 100μm. C, effect of 14 indicated inhibitors on CS migration over ~4 days determined from outline of migration strands derived for DIC images in a (mean and SD 12 spheroids derived from 2 wells is shown). d, Schematic overview of high-throughput spheroid screening indicating procedure at day 1 (steps 1- 3) and imaging in absence or presence of compounds at days 2-8 (steps 4-6).

Discussion

Here, we describe a method for generation of 3D CS cultures based on microinjection of cell suspensions into premade gels, that has a number of features making it highly useful for drug screening applications: compared to previous methods it is easy (one step procedure) and fast (minutes instead of days); CS are generated with high accuracy at predetermined x-y-z positions in multiwell plates; it is applicable to many different cell types irrespective of the ability of cells to form spontaneous cell-cell contacts; it shows good intra- and inter-well reproducibility with respect to CS size and migration; because of the predefined coordinates of each individual CS the method can easily be combined with fully automated imaging and image analysis protocols (**Fig. 5.4d**).

2D culture conditions are a very poor representation of the environment cells encounter *in vivo*. Besides implications for cell biology studies, this has important consequences for the interpretation of genetic - and drug screens[22]. So far, these have mostly been performed on 2D cultures. For the study of tumor cell invasion the Boyden chamber assay (trans-well migration assay) is also commonly used. Here, a monolayer of cells migrates through a thin layer of gel to reach the bottom of a filter. This particular assay does not resemble cells disassociating from a solid tumor. For this purpose, CS cultures have been developed that provide a pathophysiological context that mimics solid cancer microenvironments. However, these have not been used for large-scale drug screens due to the complicated procedures, which negatively affect reproducibility of results and lead to higher costs. Reproducibility of CS size is critical for a reliable 3D culture platform. Size and compactness of CS will inevitably affect drug penetration and previous studies have indicated that CS with diameters between 200 and 500µm are required to develop chemical gradients (e.g. of oxygen, nutrients, and catabolites) that may represent conditions found in tumors[3,4,23 - 26]. Our automated approach yields spheroids with a diameter of ~300µm, a size that may thus represents solid tumor traits.

We have used collagen-based gels but the same method could be easily adapted to studies using alternative 3D matrices. The type and concentration of matrix proteins will have considerable influence on scaffold structure, rigidity, and porosity, which will impact on cell morphology, survival, proliferation, and migration efficiency[8,27,28]. We find that changing collagen concentrations has a major impact on CS cell migration and that optimal conditions differ for distinct cell types, in agreement with findings from others[8,27-30]. Hence, it is essential that gel formation is standardized and optimized for each cell type. The use of ECM proteins such as collagen has some limitation in terms of controlling batch-to-batch variation. Therefore, stabilization by chemical crosslinking may be applied to better control mechanical properties as porosity and mechanical strength. A number of different cross-linking agents that react with specific amino acid residues on the collagen molecule, synthetic biopolymer scaffolds, and self-assembling synthetic oligopeptide gels are available to address this[27,28,31,32].

We demonstrate that we can automate each step of the procedure, from injection of cell suspensions to imaging and image analysis, while maintaining reproducibility. Our method not only accelerates and simplifies CS formation but by generating up to 7 CS per well at predefined x-y-z coordinates it is compatible with fully automated imaging procedures, enhanced data collection, and robust statistical analysis. We present a small drug screen to demonstrate such properties. Finally, we show that the method presented here can be used for CS formation directly from freshly isolated tumor biopsy material without the need of any intermediate culture steps. This eliminates artificial traits induced by 2D culture. A fully analyzed CS cancer migration screen in 96 well plates can be derived from a biopsy within 1 week. This opens the door to screening on a patient-by-patient basis for drug sensitivity of tumor cells under conditions that may closely mimic the *in-vivo* pathophysiological situation. Clinical tests to validate inhibitor effects in CS screens by comparing with therapeutic efficacy can be performed without further modifications of the presented system. Moreover, expansions of this method can be envisioned in which multiple cell types are combined (e.g. cancer cells and cancer-associated fibroblasts and/or endothelial cells) to further improve representation of the complex tumor microenvironment.

Materials and methods

Cell culture

The following cell lines were obtained from ATCC: MDA-MB-231, MTLn3, PC-3, HT1080, 4T1, and MAE. GEβ1 was described earlier[33]. All cell lines were cultured under standard cell culture conditions indicated by ATCC or as described[33] at 37°C, 5% CO_2 in a humidified incubator. Primary mouse tumor cell suspensions were derived from surplus mouse breast tumor material by mincing using scalpel and tissue chopper followed by 2-hour collagenase treatment at 37°C. Human biopsy material was obtained from surplus material from patients that were surgically treated for chondrosarcoma or osteosarcoma. Tumor cell suspensions were derived from biopsies by 12h collagenase treatment at 37°C.

Preparation of collagen

Collagen type I solution was obtained from Upstate-Milipore or isolated from rat-tail collagen by acid extraction as described previously[34]. Collagen was diluted to indicated working concentrations of ~2.4 mg/mL in PBS containing 1xD-MEM (stock 10x, Gibco), 44 mM $NaHCO_3$ (stock 440 mM, Merck), 0.1 M Hepes (stock 1M, BioSolve).

Hanging drop method

N $5 \cdot 10^3$ cells in 20 µL droplets were dispensed onto a 10 cm dish that was inverted over a dish containing 10 mL DMEM. After 24h, cell aggregates were harvested using a Pasteur pipette and transferred into 10 cm dishes coated with 0.75% agarose submerged in 10mL DMEM. After 48h, spheroids had formed and these were embedded into a 2.4 mg/mL collagen solution using a Pasteur pipette. Collagen gels were allowed to solidify at 37°C for 30 min and overlaid with DMEM. Cell invasion was recorded for 3 days using an inverted phase contrast light microscope (Nikon Eclipse E600).

Cell preparation for injection method

Cell suspensions derived from trypsin-detached adherent cultures or from collagenase-treated biopsies were filtered to remove clumps, centrifuged at 1000 rpm for 5 minutes, and washed twice with PBS. ~7×10^6 cells were re-suspended in 30 µL PBS containing 2% polyvinylpyrrolidone (PVP; Sigma-Aldrich). The PVP/cell suspension was loaded into a beveled pulled glass needle (Eppendorf CustomTip Type III, OD [µm] 60, Front surface 40, Flexibility: rigid).

Manual injection

Cell suspensions in 2% PVP were microinjected (~1×10^4 cells/droplet) with a microinjector (20 psi, PV820 Pneumatic PicoPump, World Precision Instruments, Inc) into solidified collagen gels in 8 well µslides (IBIDI).

Automated injections

A glass-bottom 96 well plate (Greiner) containing 60 µL solidified 2.4 mg/mL collagen gel per well was placed in a motorized stage (MTmot 200x100 MR, Märzhäuser) connected to a controller (Tango, Märzhäuser). A motorized micro-manipulator (Injectman II, Eppendorf) was positioned above the stage and connected to a pump (Femtojet Express, Eppendorf) featuring an external compressor (lubricated compressor, model 3-4, JUN-AIR). A firewire camera (DFK41BF02.H, The Imaging Source) equipped with an 8x macro lens (MR8/O, The Imaging Source) was placed beneath the stage for calibration and imaging. All components were connected to the controlling computer (Ubuntu AMD64). A multi-threaded control program was written in Python using PySerial and wxPython. Coriander software (http://damien.douxchamps.net/ieee1394/coriander) was used for imaging.

After the program was calibrated for the 96 well plate the camera height was adjusted to focus on the bottom of the 96 well plate. The plate was then removed for needle calibration: the injection needle was fixed in the Injectman and moved, using the Injectman controller, into the center of the image. The injection height was set to 200µm above the bottom of the (virtual) plate.

After the needle was moved up, the plate was placed back in position and the upper left well was used for multiple test injections to adjust pump pressure and injection time for optimization of the droplet size (~8nL ~ 300µm diameter) using video inspection. Subsequently, using a pre-defined macro defining x-y coordinates and number of injections per well, all wells were injected with the same pressure and injection time.

Microscopy and image analysis

Manually injected CS were monitored daily using a Nikon Eclipse E600 microscope. CS generated by automated injection were used for montage imaging using a Nikon TE2000 confocal microscope equipped with a Prior stage controlled by NIS Element Software and a temperature and CO_2-controlled incubator.

Differential interference contrast (DIC) images were captured using a charged coupled device (CCD) camera with NIS software at 10x dry objective. Quantification of CS invasion area was analyzed from DIC images using ImageJ. The CS ellipsoidal area after three days was estimated using the diameter in x and y axis (pi*radius-x*radius-y) occupied by cells in the 10x montage image in the midplane of each spheroid and normalizing to the occupied area 1h after injection. One-way ANOVA was performed to test the significance of the data. The data are presented and plotted as average and standard error of the mean.

For automated imaging, wells containing gel-embedded spheroids were treated with a fixation and staining cocktail containing 3.7% paraformaldehyde, 0.2% Triton X-100 (Sigma) and 0.1 µM rhodamine Phalloidin (Sigma) for 3 hrs. Wells were washed extensively with PBS and plates were imaged on a Becton Dickinson Pathway 855 using a 4X lens. A montage of 12 frames was made for each Z plane, with a total of 24 Z planes at an interval of 50 µm. Image stacks were converted into 2D maximum fluorescence intensity projections using ImagePro 7.0. CS were then digitally segmented using ImageJ to identify the outline of individual CS and multiple parameters were measured, including Feret's diameter, roundness, and number of CS scored in each well.

For immunostaining of E-cadherin, gels were incubated for 30 mins with 5 µg/mL collagenase (Clostridium histolyticum, Boehringer Mannheim) at room temperature, fixed with 4% paraformaldehyde, permeabilized in 0.2% Triton X-100, and blocked with 10% FBS. Gels were incubated with E-cadherin antibody (BD Transduction Laboratories) overnight at 4°C followed by Alexa 488-conjugated secondary antibody (Molecular Probes/Invitrogen) for 2 hrs at room temperature and Hoechst 33258 nuclear staining (Molecular Probes/Invitrogen) for 30 min at room temperature. Preparations were mounted in Aqua-Poly/Mount solution (Polysciences, Inc) and analyzed using a Nikon TE2000 confocal microscope. Z-stacks (~100 stacks, step of 1 µm) were obtained using a 20x dry objective, imported into ImageJ, and collapsed using extended depth of field plugin (Z projection) into a focused composite image.

Drug Treatment

LY-294002 (phosphatidylinositol 3-kinase), JSI-124-cucurbitacin (STAT3/Jak2), NSC23766 (Rac1), and AG-82 (general protein tyrosine kinases) were purchased from Merck/CalBiochem. PP2 (Src) and ML-7 (MLC kinase) were purchased from ENZO. Y-27632 (Rock), SB-431542 (TGFβ) and AG1478 (EGFR) were purchased from BioMol Tocris. Cell migration was analyzed in the absence and presence of inhibitors for 4 days.

Acknowledgments

We thank ZF-screens B.V. (Leiden, NL) for permitted use of the microinjector-system, which was modified for this project, with the technical help of Fred Schenkel and Ewie de Kuyper (Department of Fine Mechanics). We thank Wies van Roosmalen and Sylvia le Dévèdec for mouse tumor biopsy material. We acknowledge financial support from the Netherlands Organization for Science (NWO; Cyttron project), the Dutch Cancer Society (project UL-2006- 3521), and EU FP7 (HEALTH-F2-2008-201439).

References

1. **Kenny PA, et al**. The morphologies of breast cancer cell lines in three-dimensional assays correlate with their profiles of gene expression. *Mol Oncol. 1: 84 - 96, (2007).*

2. **Fischbach C, et al**. Engineering tumors with 3D scaffolds. *Nat Methods 4: 855 - 860 (2007).*

3. **Mueller-Klieser W.** *Multicellular spheroids. J Cancer Res Clin Oncol 113: 101 - 122 (1987).*

4. **Sutherland RM.** Cell and environment interactions in tumor microregions: the multicell spheroid model. *Science, 240: 177 - 184 (1988).*

5. **Keller GM**. In vitro differentiation of embryonic stem cells. *Curr Opin Cell Biol, 7: 862 - 869 (1995).*

6. **Kelm JM, Timmins NE, Brown CJ, Fussenegger M & Nielsen LK.** Method for generation of homogeneous multicellular tumor spheroids applicable to a wide variety of cell types. *Biotechnol Bioeng, 83: 173 - 180 (2003).*

7. **Lee GY, Kenny PA, Lee EH & Bissell MJ**. Three-dimensional culture models of normal and malignant breast epithelial cells. *Nat Methods, 4: 359 - 365 (2007).*

8. **Loessner D, et al**. Bioengineered 3D platform to explore cell-ECM interactions and drug resistance of epithelial ovarian cancer cells. *Biomaterials 31: 8494 - 8506 (2010).*

9. **Buxboim A & Discher DE**. Stem cells feel the difference. *Nat Methods, 7: 695 - 697 (2010).*

10. **Friedl P & Wolf K**. Plasticity of cell migration: a multiscale tuning model. *J Cell Biol, 188: 11 - 19 (2010)*

11. **Levental KR, et al**. Matrix crosslinking forces tumor progression by enhancing integrin signaling. *Cell, 39: 891 - 906 (2009).*

12. **Lammermann T & Sixt M**. Mechanical modes of 'amoeboid' cell migration. *Curr Opin Cell Biol, 21: 636 - 644 (2009).*

13. **Haaf F, Sanner A & Straub F**. Polymers of N-Vinylpyrrolidone: Synthesis, Characterization and Uses. *Polymer J, 17: 143 - 152 (1985).*

14. **Ivascu A & Kubbies M**. Rapid generation of single-tumor spheroids for high-throughput cell function and toxicity analysis. *J Biomol Screen, 11: 922 - 932 (2006).*

15. **Ivascu A & Kubbies M**. Diversity of cell-mediated adhesion in breast cancer spheroids. *Int J Oncol, 31: 1403 - 1413 (2007).*

16. **Bjerkvig R, Tonnesen A, Laerum OD & Backlund EO**. Multicellular tumor spheroids from human gliomas maintained in organ culture. *J Neurosurg, 72: 463 _ 75 (1990).*

17. **Bissell, M.J.** The differentiated state of normal and malignant cells or how to define a "normal" cell in culture. *Int Rev Cytol, 70: 27 - 100 (1981).*

18. **Walpita D & Hay E**. Studying actin-dependent processes in tissue culture. *Nat Rev Mol Cell Biol, 3: 137 - 141 (2002).*

19. **Corcoran A, et al**. Evolution of the brain tumour spheroid model: transcending current model limitations. *Acta Neurochir, 145: 819 - 824 (2003).*

20. **Beliveau A, et al**. Raf-induced MMP9 disrupts tissue architecture of human breast cells in three-dimensional culture and is necessary for tumor growth in vivo. *Genes Dev, 15: 2800 - 2811 (2010).*

21. **Sahai E & Marshall CJ**. Differing modes of tumour cell invasion have distinct requirements for Rho/ROCK signalling and extracellular proteolysis. *Nat Cell Biol, 5: 711 - 719 (2003).*

22. **Pampaloni F, Reynaud EG & Stelzer EH**. The third dimension bridges the gap between cell culture and live tissue. *Nat Rev Mol Cell Biol, 10: 839 - 45 (2007).*

23. **Friedrich J, Ebner R & Kunz-Schughart LA**. Experimental anti-tumor therapy in 3-D: spheroids--old hat or new challenge? *Int J Radiat Biol, 83: 849 - 871 (2007).*

24. **Kunz-Schughart LA, Freyer JP, Hofstaedter F & Ebner R**. The use of 3-D cultures for high- throughput screening: the multicellular spheroid model. *J Biomol Screen, 9: 273 - 285 (2004).*

25. **Mueller-Klieser,W**. Three-dimensional cell cultures: from molecular mechanisms to clinical applications. *Am J Physiol, 273: C1109 - 1123 (1997).*

26. **Mueller-Klieser,W**. Tumor biology and experimental therapeutics. C*rit Rev Oncol Hematol, 36: 123 - 139 (2000).*

27. **Bott K, et al**. The effect of matrix characteristics on fibroblast proliferation in 3D gels. *Biomaterials, 32: 8454 - 8464 (2010).*

28. **Sung KE, et al**. Control of 3-dimensional collagen matrix polymerization for reproducible human mammary fibroblast cell culture in microfluidic devices. *Biomaterials, 27: 4833 - 4841 (2009).*

29. **Cross VL, et al**. Dense type I collagen matrices that support cellular remodeling and microfabrication for studies of tumor angiogenesis and vasculogenesis *in vitro*. *Biomaterials, 31: 8596 - 8607 (2010).*

30. **Zaman MH, et al**. Migration of tumor cells in 3D matrices is governed by matrix stiffness along with cell-matrix adhesion and proteolysis. *Proc Natl Acad Sci, 103: 10889 - 10894 (2006).*

31. **Rosso F, et al**. Smart materials as scaffolds for tissue engineering. *J Cell Physiol, 203: 465 - 470 (2005).*

32. **Peppas, NA, Hilt JZ, Khademhosseini A & Langer R**. Hydrogel in Biology and Medicine: From Molecular Principles to Bionanotechnology. *Adv. Mater, 18: 1345 - 1360 (2006).*

33. **Danen EH, Sonneveld P, Brakebusch C, Fassler R & Sonnenberg A**. The fibronectin-binding integrins alpha5beta1 and alphavbeta3 differentially modulate RhoA-GTP loading, organization of cell matrix adhesions, and fibronectin fibrillogenesis. *J Cell Biol, 159: 1071 - 1086 (2002).*

34. **Rajan N, Habermehl J, Cote M, Doillon CJ, & Mantovani D**. Preparation of ready-to-use, storable and reconstituted type I collagen from rat-tail tendon for tissue engineering applications. *Nat Protocols, 1: 2753 - 2758 (2007).*

Chapter 6

Appeal for better data management

Abstract

Academic research results are shared digitally since many years, yet there is a lack of uniformity in management of research data. Recent advances in social media are used to a limited extent in research. Here, we examine the specific requirements of information sharing in research, and show how social media can help to improve reproducibility, communication and data storage. When available, the adoption of a new social media platform to share knowledge can have huge impact on our daily research practice.

Introduction

At the start of a scientific project much of the work builds upon previous or similar work and ideas. This includes not only literature, protocols and methods, but also daily research practice such as writing a lab journal, data handling including filtering and analysis, preparing work discussions and/or presentations. Much effort is spent on data analysis, interpretation and model building. Research is part of an iterative process, where each step is made based on recent results in discussion with a peer group and/or collaborators. Unless the collaboration requires it, raw data is usually kept personal and accessible to experts only. During research work, there is a huge accumulation of information. Before managing this information, one has to look at the origin and the objective of gathering information. What information is important, what is neglected, and what information can be safely thrown away? In this chapter some ideas are presented which may lead to better data management to make research more efficient and accessible for future PhD students.

Research

Scientific knowledge can originate from personal projects, for example as in a PhD project, and/or can be part of larger projects conducted mostly in research groups. Both situations have a specific influence on how research knowledge is accessible and disseminated to other (future) researchers. To unravel this influence, one has to look at how the data is generated and stored for future use.

PhD students

The final result of a PhD project is the thesis. Next to the thesis, many of the results are also shared in journal articles, in conference proceedings and workshops. Sometimes results and ideas are published in patent applications. During a PhD project most candidates are involved in teaching bachelor and master students. Protocols and specific experimental information is archived in lab journals. Raw experimental data is generally not stored for a long time, and is usually not very well documented. Data remaining after the thesis project is completed, can be scattered and unorganized. Data recorded during experiments is not published and data with a negative result is often discarded or even thrown away. Changes in protocols for specific experiments are sometimes published, or only available in the lab journals. The content of a lab journal is mostly ordered on time, not on topic or experiment. Therefore, it is hard to search in lab journals for previous work.

Research groups

The methodologies used in a group are shared and discussed on a regular basis. Methodologies are the group's most valuable assets, as they determine both the success rate of experiments and the scientific value of the experimental data. Results that can not easily be repeated or reproduced by others gradually loose their value. Many factors contribute to modifications in the commonly used methods, for example the personal experiences of individual workers, i.e. a personal way of doing things, improved methods taken from literature or collaborators, and progress in available technology. New methods are not immediately adopted and have to convince the research group first and the peer group later. A new method usually requires at least one or more cycles of successful use before it becomes accepted. Here, experiments which do not work, produce negative results or take too much effort, are usually forgotten as soon as a more reproducible or easier methodology is established or published. Only people with hands-on experience will remember the original pitfalls and points of care of abolished methods. Experience mostly determines whether a certain method is being applied in a particular area. It is mostly here where negative results don't have any value, and are simply thrown away. A group, mostly professors and/or principal investigators, prevent that these experiments are tried again. However, as this information is not shared on a larger scale, many researchers in other laboratories will try similar experiments and mostly reach the same conclusion(s). This process itself is not without value as perseverence of (PhD) students may reintroduce methods that were abandoned earlier in a (slightly) modified form. Sometimes new materials, improved instruments, alternative methods or additional funding make experimental approaches feasible and viable later. A good example is the analysis of the samples obtained in the original Miller experiments on the creation of aminoacids[1].

Research knowledge

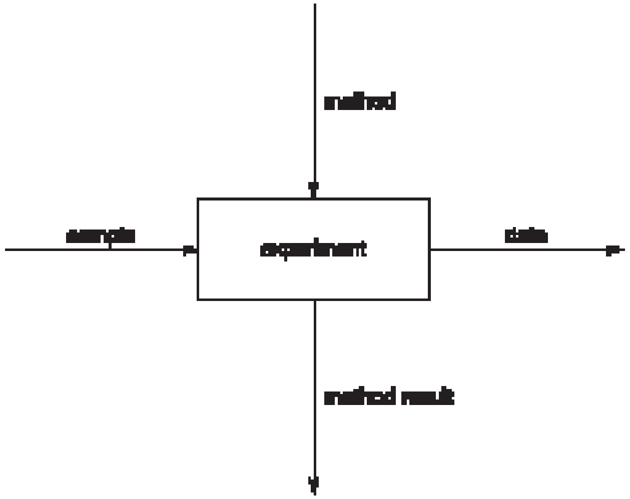

Figure 6.1 An experiment yields two results, the acquired data and method result that together determine the validity of the experiment.

A considerable part of research consists of repetition of the same basic procedures inherently required by the necessary reproducibility. When a research protocol is invented and published, others can reuse the protocol to generate more data from different samples, improve the protocol, or use parts of it in other protocols for other experiments. Experiments are often performed to find new results, each time the generalized form of such scientific experiments is the same. This generalized form is illustrated in **Figure 6.1**. The illustrated 'method result', for example a 'log file' in scientific computing or a human observation in biological or chemical experiments, is used in experiments to validate the data of the experiment. In research, often, many experiments are performed, of which the 'method result' is observed and used as a control measure to further substantiate to the data and/or method. When the method is unaltered, different experiments are performed to either test multiple different samples, to get different data sets, or multiple similar samples to increase the sensitivity of a single dataset[2].

Research method development

Research is based on a collection of basic procedures that is used over and over. The basic procedures which are often called "methods" or "protocols" are not fixed but improved to achieve two aims: to compare multiple (different) experiments or to increase the sensitivity and/or accuracy of the method. Next to the methods and protocols the analysis of results is becoming more and more predominant due to the availability of numerous automated, more complex, and faster analysis methods.

In method development the experimental method or protocol is changed (often by only one change at a time) between experiments, to observe the different data outcomes for each method or protocol change, while the sample remains unchanged or changed as little as possible. Note that differences between samples affect the reproducibility, not only of the obtained research data, but also of the method result (methodology data).

When part of the experiment is automated, such as the data analysis, the reproducibility & reliability are affected by the software version and installation. A different version of the software might give another result because of rewrites, bug fixes, replacement of software libraries and/or hardware modules. For reproducibility it is pertinent to know exactly what happened with the raw experiment data during processing, and for this reason open source software must always be preferred over closed source software. The source code should have version numbering, such that the version can be documented, and mentioned in the lab journal and/or method section of a publication. Noteworthy, small project specific changes in the source should not be forgotten. Source code control systems can be used to automate this process.

We can conclude that there is much repetition in research. Experiments should be repeatable, thus when the method is preserved, the data can be reused or regenerated. How is method development currently stored and communicated through the research community?

Preserving research knowledge

Taken from **Figure 6.1**, researchers deal with two interdependent data flows, the methodology and research data. What happens with these data flows over time is depicted in **Figure 6.2**.

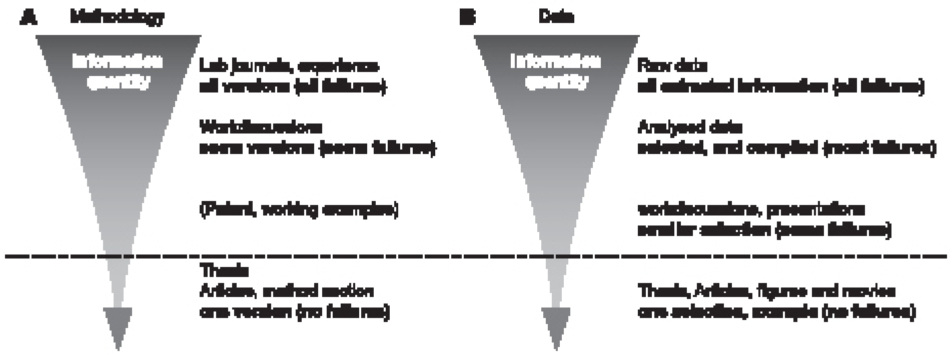
A
Methodology
Information quantity
Lab journals, experience
all versions (all failures)
Workdiscussions
some versions (some failures)
(Patent, working examples)
Thesis
Articles, method section
one version (no failures)
B
Data
Information quantity
Raw data
all extracted information (all failures)
Analysed data
selected, and compiled (most failures)
workdiscussions, presentations
smaller selection (some failures)
Thesis, Articles, figures and movies
one selection, example (no failures)

Figure 6.2 Visualisation of Information flow for (A) methodology development and (B) data acquisition.

The added value of a group specialized in a specific research methodology, is the extra information above the horizontal line of thesis and article information. As this knowledge is generally not published, one can only learn this from within a group. To reproduce or learn a specific method it is therefore best to visit the group and do the experiments on location. In that case the complete data flow, located on the right side of **Figure 6.2** can be studied and understood. Still, when returning to your laboratory, or trying to perform the same experiment elsewhere, part of the information (**Figure 6.2**, left, above the working examples), equipment or expertise is still missing. Then, when the experiment is not working the first time, the easiest route is to call someone in the laboratory visited. Sometimes, in practice, groups exchange this more detailed information by exchanging scientists. The complexity of research projects has similarities with Lifecycle Knowledge Management in the manufacturing industry, dealing with multiple information sources, multiple media, multiple versions and multiple communities[3].

The above showed an idealized situation, in a specialized laboratory, fully sharing its newly developed methods among the research community. Not every group experiences visiting researchers on a regular basis. The ability to preserve knowledge in the group is challenging, especially in a small group of specialists. Regularly, people leave a group before all knowledge is transferred in sufficient detail to the (new) group members. In that case, new people solely rely on the theses, lab-journals and knowledge of the PIs. As a PhD student, one could ask a group leader: Where is the actual list of well defined working protocols?

Who has expert knowledge on which protocol? It is of importance that such information is not only directly available from within a group, but also within an institute, or maybe even worldwide. This information is, in part, preserved by group members that write review papers describing the accepted state of the art methods, used in a research field. Unfortunately, review papers do in general not contain enough detail to reproduce experiments.

Communication in research

To find more information about a scientific topic, protocol or method, the literature is searched, and articles are ranked according to journal type, and more importantly, the number of citations. The citation system is problematic as it is slow and inaccurate. Slow, because only after a couple of years an article will have received enough citations to be significantly 'better' than other articles in the field. And inaccurate, because the citations usually target only a specific part of an article. This makes it difficult and at least time-consuming for the reader to find out how many articles cite a specific part of an article, like a method, part of a discussion section or result. Citation is an overall property.

Sharing research data

Figure 6.3 Books ordered using different schemes

Within science, as well as in other fields, data is organized by many people. Each person has his or her own data storage structure based on personal efforts to organize, which in part is also dependent on the time a project is running and possible reuse of information from other projects. The personal storage structure of data per project can be influenced by the active time one spends in a project, the number of collaborators, the amount and methods of communication used in the project and by project specific properties such as the connection with other (previous) projects and the overall project flow, the project growth, change of goals and collaborators. In essence, the data storage structure is personal, but influenced by available software, collaborators, project specifics and legal constraints (for example in medical research). More on information acquisition, creation, storage, maintenance, retrieval, use and distribution of information can be found in the article "Personal Information Management" by William Jones[4].

The personal storage structure and strategy is only partially shared with other people. This has a clear reason, as sharing things between people often creates an ordering problem.

Every person likes his or her own ordering scheme. Take for example a bookshelf, as shown in **Figure 6.3**. Some people like to order books on titles, other people like to order books on topics, then there is a possibility to order on authors or date when the book was bought or used. Next to that there are people that like to put little pieces of art in a bookshelf or handicrafts bought in the same country where the book was bought. Ask a person, unfamiliar with the ordering system used, to take out a specific item. Suppose this person succeeded, the next step is to ask this same person to put a new item in this bookshelf. Clearly, sharing a bookshelf with multiple people may give rise to conflicts about the preferred ordering of objects. Librarians and book shop owners face this on a daily basis and spend time in creating and preserving an optimal system for their customers. Simple object classification and successful object retrieval are crucial factors that determine the success of a storage system.

When working with computers, sharing files or other pieces of information, creates a similar problem. A file is like a book and has associated metadata. The fuzziness of the metadata and the personal usage of the metadata is the true problem at hand. People like to use the hierarchy of a file system, but just like the bookshelf case, this putting files in folders creates an ordering problem. The ordering in a file tree is even worse as files are not even visible from outside a folder. Although the first vertical filing cabinet was available in the end of the 18th century[5], the personal folder system and shared file servers still bear the same principle of a single label per folder. One response to ordering problems is the creation of search agents like Google desktop or grep and locate (macosx, unix, linux). While these search programs are getting smarter and better they do not solve the real problem of simultaneously ordering and sharing (large amounts of) data. When asked if a folder system can be replaced with a search functionality, many reasons pop-up why a folder system is crucial. Primary reasons given are trust, quote: "I'm just not willing to depend on search alone", and control, quote: "I want to be sure all the files I need are in one place", as well as visibility and understandability of the structure of the data[6]. In general, humans are uncomfortable when handling large dynamic unstructured data.

Metadata

Currently, when working on a project, all project data is accessed via software; emails are enclosed by an email program. The files are stored in folders and usually synchronized by email. The timeline is in an agenda, some people use agenda programs. The people information is hidden in a list in an email program or address book. The websites used are stored in a web-browser, and references are stored as pdf or word documents, or in a list in a word file describing the project. Some images are stored in powerpoint files or word documents. Operating systems such as Windows, Linux and Mac-OS X, and many different programs on these systems lack the possibility to share the storage structure of different types of data together in a flexible, adoptable way. In fact data sharing often appears blocked for commercial reasons. As such the ordering problem is intensified on the computer, called information fragmentation, caused by reuse of a similar structures in multiple tree hierarchies, e.g. in email programs, personal and shared file systems, address books etc[4].

From a birds-eye perspective, one can look at the data flows of projects between people, and see many repetitive schemes. This repetitive use of different communication methods in research is not yet optimized. The specific properties of scientific project data can be used to automate communication methods. For example, take a project file, a protocol, or a data file like an image. When a measurement is made, and data is added or modified, many people could benefit from this information. Therefore such a file, or the added information, should be communicated to other people. Which people should be addressed? Currently, these choices are made repetitively, while this list of interested people could have been added as metadata to this project file, and reused as such. In a sense, references in the scientific literature form a part of the metadata associated with an article. Publishers added a suggestion functionality (based on keywords assigned by authors), similarly used by google, booksellers and webshops, to find other works or articles of interest to the user. For published articles that one reads on-line one can already establish a link to the article to get alerted if new people cite the article or the article is corrected. This can be convenient as it brings you in contact with work of people that cite a paper that you consider to be interesting.

Example: DICOM

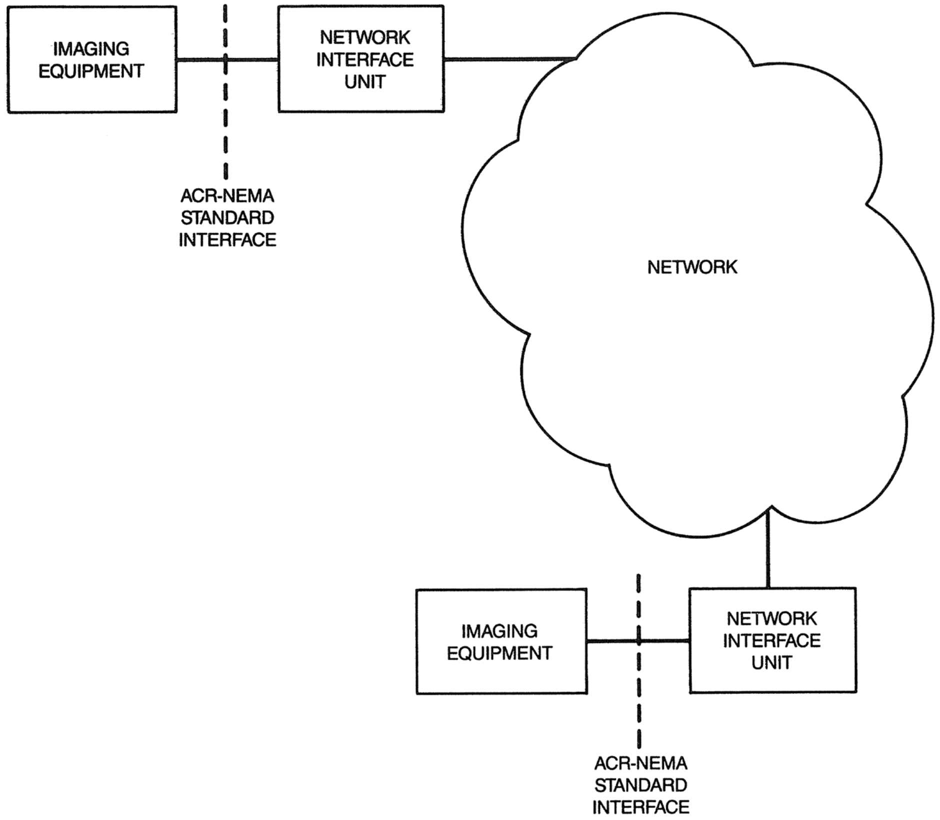

Figure 6.4 Illustrating the use of the DICOM standard in 1985, taken from page iv of ACR-NEMA standards publication/ No. 300-1985

In medicine, the digital imaging and communication is standardized in a file format and communication protocol called DICOM, developed by the American College of Radiology (ACR) and the National Electrical Manufacturers Association (NEMA) in 1985[7]. Originally DICOM was developed as a communication protocol, now the main purpose of the DICOM is to allow for standardization of data storage, such that many people can view and or adjust the data using the same methods. When the internet was still at its infancy the benefits of data sharing across networks was already clear, as illustrated in **Figure 6.4**. The aim of DICOM was to store all experimental information, the machine settings, other metadata and data files belonging to radiology experiments, in a single file, which could be communicated over a network. Since then, many different file formats and imaging modalities have been added to use DICOM in other medical measurements. All these changes and additions have been approved by the standards committee. Currently, even medical reports are created using the DICOM file format to allow for direct links to the imaging data. A similar standard does not exist in research and the DICOM approach is not adapted. DICOM is considered a file based information sharing system, all information is contained in DICOM files, and metadata is directly and uniquely linked to the data. When stored on a computer, a program similar to 'desktop search' can be used to collect all DICOM files and sort and search using the metadata. The standardization of this metadata might pose problems when using DICOM for not yet anticipated purposes. Although open 'free to use' field exist, and undocumented metadata can be added, it is therefore not certain that someone else will discover and follow the same scheme. When a vendor/producer of DICOM files decides to use new undocumented tags and wants to inform other people about this existence, he will also write a DICOM conformance statement in which these additional tags are explained. So other people can use this information for e.g. searching specific information. The tiff file format, used to store image data, also offers a “free to use” metadata field, but suffers from the same access problem.

Social Media for Research

After search engine development, it is now the age of social media. Facebook, Twitter, YouTube, Flickr, Wikipedia, Hyves (in the Netherlands) and LinkedIn offer direct user-user interaction, giving the opportunity to share messages, discussions, photos, videos, links, or other information with other people. The user-user interaction, monitored on social media sites is used to rate changes directly and develop the system itself. Many of the features of Facebook were added using the direct quality control of the users of the system. Not even the business plan was developed before the system became a huge success.

It could be a giant leap in science if method development and research could be performed in a similar way, instead of the slow process of writing research proposals, peer review on proposals, finding people to perform the research, doing the research, finding references, reporting on the research, submission of an article, peer review, changes, acceptance, waiting and publication. It often takes many years before a research idea is published in an article. In a "Facebook-science-world" the research would be discussed while being designed, published as the results come in, and the peer review is replaced by the number of views and comments plus the attention the research receives while being performed. It gives the opportunity for peers to give suggestions even during the data analysis phase. Data can be shared with others to allow for an even better quantification, or reveal additional hidden information. When such interaction takes place, there is also a reason to publish data yielding negative results, as these can be used then as references in other publications. All information and data flows would ideally be open and accessible.

To enable use of the links between scientists, research groups, topics, papers, meetings, protocols, data and equipment, a network storage model has to be put up in which the associated metadata can be stored in a natural and easy way. Links offer the possibility to order information based on multiple properties (metadata). It allows users to organize their data in a personal way without knowledge of the underlying storage model. Properties associated with files are called metadata. Metadata is already used in a filesystem. Properties such as ownership, date of modification, file type and size are used to order files. Programs can have and create their own specific metadata and access is available via a graphical user interface (gui). Sometimes, one wishes to have other (additional) metadata available, such as date of creation, picture width and height. When files are shared more metadata, like annotations, may become available for the users. For example the information 'made for project x', 'also used in project y' and 'therefore shared with user a, user b and user c'. As a conclusion we can say that metadata can add value to the data if easily accessible, properly used, and maintained and that we would like to use as much metadata as is available without having to fill in complete forms of properties. To allow better metadata use, the virtual layer describing the files should be extended. Social media have extended this virtual layer with websites, (phone) applications and search technologies. Most information is linked through the use of tags.

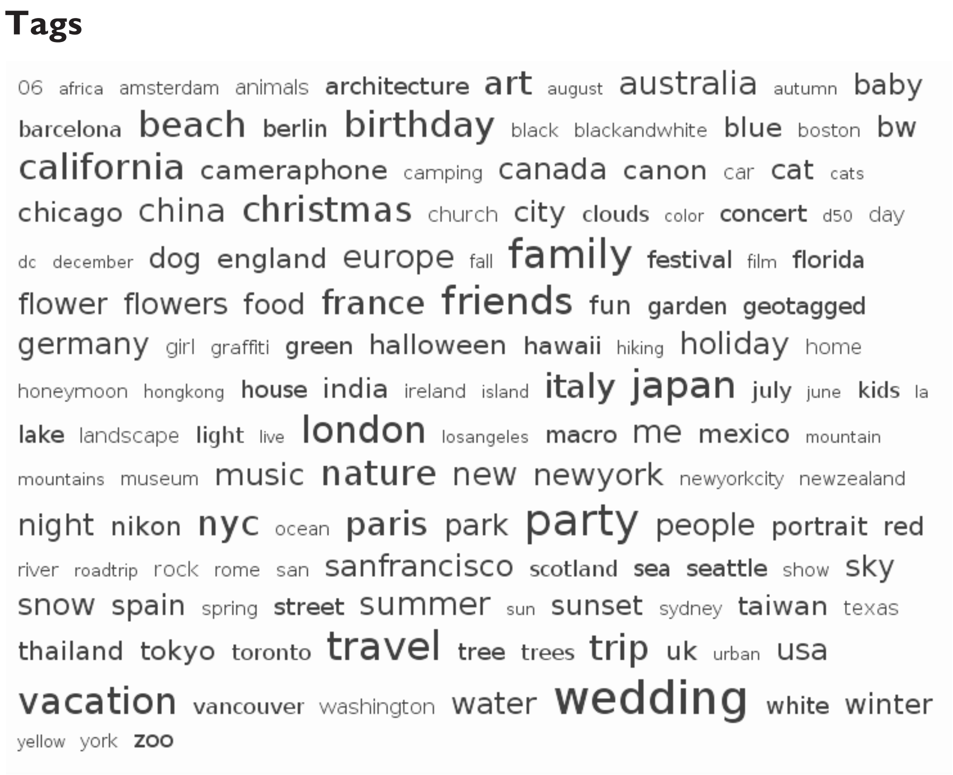

Figure 6.5 Tag cloud of most frequently used tags at flickr, source wikipedia

Tags are keywords associated with data, and are used online to share public information with a large amount of people. The popular site Flickr uses tags to sort and filter an enormous amount of photos. Users sharing data can choose their tags themselves, and other people can add tags resulting in a collaborative set of tags. Not all tags are used as much as others and the tags themselves are not stored in a predefined structure. To visualize the use of tags, tag-clouds can be used, as invented by Flickr co-founder and interaction designer Stewart Butterfield, see **Figure 6.5**. Within a tag cloud, tags are shown as floating entities, where tags which are used most often are sized in a larger font. Colors are sometimes used to make a clear distinction between tags.

Collaborative tagging has a large impact not only on the use of the stored data, but also on the use of the tags themselves[8]. Sites such as Flickr and Del.icio.us use tags without giving a structure to the tags, such as in annotation systems used in biology. As such the tag names are not controlled and the resulting tag set is often called a folksonomy[9]. Tags allow a user to index an item using

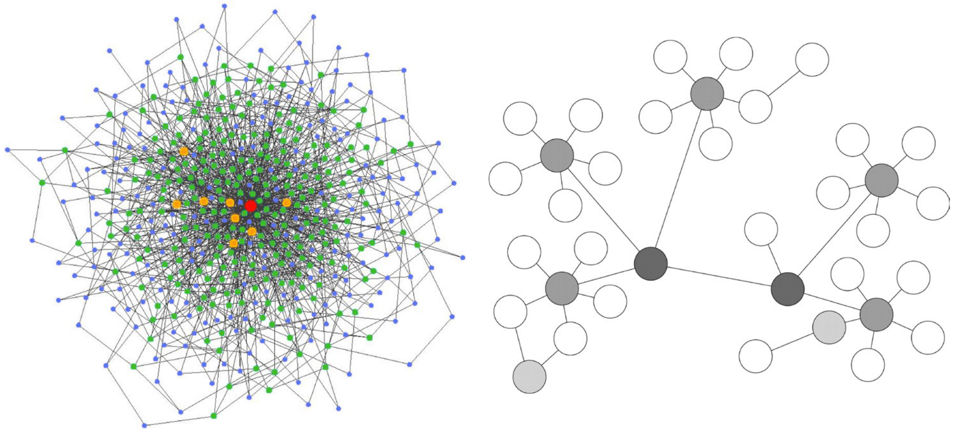

Figure 6.6 Two different visualizations of scale-free networks, source: www-news.uchicago.edu and pmj.bmj.com

multiple keywords. This is optimal when sharing items with a large number of people, as everyone can add keywords to index the particular item in his or her own index scheme. The advantage of tags with respect to folders is put forward by William Jones as follows:

> *"If folders become more "transparent" or more like tags, we might be more inclined to reference than to copy and more inclined to tag an item in several ways in order to represent different anticipated uses"* [4]

Document sharing can be seen as a certain type of relation in a network. For example, some nodes could be persons, and some documents, linked together by edges (tags). Sharing a document in a network visualization could then be explained as walking from node to node to a file, where different routes (tags) could lead towards the same object. In Wikipedia, one can "walk" from one document to the next by using WikiWords, special words used as tags to Wikipedia articles. Through the history section of an article, one can also jump to the wikipage of one of the authors, where links to other Wikipedia articles are present.

Using these networks as an interface could be done by creating a menu from the picture of a network as shown in **Figure 6.6**, for example like the Visual Thesaurus Online[10]. It allows easy viewing. But to use, say to select a couple of nodes, or to express more information than just words or colors makes this scheme quite difficult to use. Therefore another method of using information in networks should be invented. This chapter ends with one example which shows how tags can be used to share files in a file system.

Example: TagFS

One could translate the network of tags, as shown above to a tree-like structure by starting at a given node (root node) and walking the tags (lines), as if descending into deeper and deeper sub-directories. This is not always straightforward, connections forming rings, pose a problem of relation loops, as visible in the more complex network on the right side. Still, if we would allow reuse of the identical nodes in the same tree (but not in a single path), from any network topography, a tree structure of a network can be constructed. This can be seen as using the same image in multiple documents on your computer, or using the same documents in different folders without having to copy them (using links, also used in some backup/version systems to prevent the storage of multiple copies of the same data). Such a tree more closely suits the common use of files and other information in projects.

The tag translated tree differs from a common tree in the file browser, in the sense that is does not hide the enclosed information, but filters all information according to the enclosed folder names (hence, the transparency mentioned above). As such this browsing behavior is already used for public information on the internet, in the form of Tags. Selecting multiple tags fits the same behavior as to search for files, the autocompletion function in search engines basically show indexed tags. Note that a prototype tag based file system, containing some of the ideas presented in this chapter, was developed[11], but due to inefficiency of the code, the project has come to a standstill.

How can networks be used to define relations, data and metadata in a natural way?

When sharing is added, the network representation allows for a one to one visualization of relations between people and how documents in projects are used, see **Figure 6.7**.

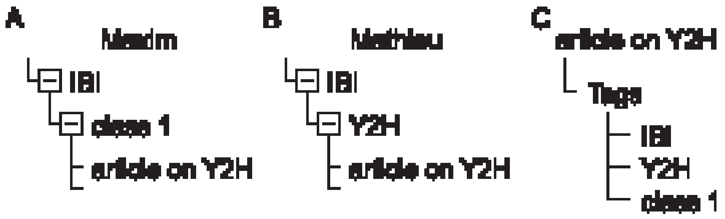

Figure 6.7 Tags vs Folders: A file "article on Y2H" is stored in a different (local) folder structure by Maxim(A) and Mathieu(B). When sharing this document, the local folder names could be translated to tags(C), giving both users the opportunity to find this document by selecting two of the three tags, instead of selecting two (sub)folders. This allows for a personal storage structure without the need to negotiate about the optimal (shared) storage tree.

A file "article on Y2H" is stored in a different (local) folder structure by Maxim (A) and Mathieu (B). When sharing this document, the local folder names could be translated to tags (C), giving both users the opportunity to find this document by selecting two of the three tags, instead of selecting two (sub)folders. This allows for a personal storage structure without the need to negotiate about the optimal (shared) storage tree.

Key point is that everyone is allowed to use their own preferred ordering of data, by walking the network of tags. While the starting position is different, when two people share a document, both can access it in exactly the same way, because the tags shared are identical as they are shared through the shared document.

Other advantages of a tag based file system

When working with files in a file system it is very inconvenient that files are only visible when a certain folder is visited. Often, especially during a search (query) operation one likes to view all files in all folders, and then sort them based on their content or properties. In an indexed tag system it is very easy to show all files including subfolders as this is only one query. This possibility enables a smarter use of folders not only for viewing but for applications as well, possibly eliminating information fragmentation as was mentioned earlier. Here, some examples are presented to show the advantages of such a system:

- What's new? Standing in the root folder of your personal tree, all data can be sorted on date, showing the newest item on top immediately, also if added and shared by a collaborator.
- Show all meetings - Agenda items could be indexed using the same tags, then all agenda items can be listed from the root folder to list all meetings of all projects.
- Email all users - Applications like an email application can use the same tree hierarchy. Email all users including users in subgroups allows for a natural way of creating a list of recipients without having to make a new mailing-list for each project.

Concluding remarks

There is currently no standard for complete data storage and retrieval in research. This not only leads to loss of valuable data and knowledge, it also does not prevent researchers from doing the same experiments. Research data is not easily contained and documented, as it is usually scattered and unorganized as projects grow and shrink, people join and leave, and (analysis)software is updated or replaced. Data and developed methods are considered as very personal properties, this may be used in future data sharing solutions, i.e. storing the link between data and people. Sharing data and methods in research will have many advantages, it allows for better reproduction, and saves time if protocols and comments are shared more openly. A simple sharing system is not easily developed, and much can be learned from current developments on the internet where more and more information is shared. Tag based sharing allows for freedom to order and retrieve information, while folders and hierarchy can be used to reduce the visible information. A combination of the two might be possible using a tag based file system.

As digital logbooks emerge and huge databases for data storage are set-up, social network sites grow, now seems the right time to find a better solution, such that future research is not lost, and a complete history of experimentation in the search of new knowledge is preserved and shared globally. This is not only a technical challenge, also users should be willing to share their methods. Then, a typical laboratories can form a community on the web, enabling other laboratory to follow the activities and comments on the results on a daily base like is done e.g. on Facebook when someone publishes a new picture and other people can say that they like it.

References

1. **SL Miller and HC Urey**, Organic Compound Synthesis on the Primitive Earth. *Science, 1959, 130: 245 - 251*.

2. **EC Childs**, The function of experiment. *Nature, 1937, 140: 852 - 853*.

3. **S Staab, T Franz, O Görlitz, C Saathoff, S Schenk and S Sizov**. Lifecycle knowledge management: Get the Semantics Across in X-Media. *Lecture Notes in Computer Science, Springer, 2006, 4203: 1 - 10*.

4. **W Jones**, Personal Information Management. *Ann. Rev. Information Science and Technology, 2007, 41: 453 - 504*.

5. http://www.earlyofficemuseum.com

6. **W Jones, AJ Phuwanartnurak, R Gill and H Bruce**, Don't take my folders away!: organizing personal information to get things done. *Human factors in computing systems, Proceedings CHI EA, ACM, 2005, 1505 - 1508*.

7. http://medical.nema.org

8. **SA Golder and BA Huberman**, Usage patterns of collaborative tagging systems. *Journal of Information Science, 2006, 32: 198 - 208*.

9. http://vanderwal.net/folksonomy.html

10. http://www.visualthesaurus.com

11. http://code.google.com/p/tagfs

Summary

Regulatory processes are responsible for the organization, division and death of cells in multicellular organisms such as humans. Additionally, cells are highly regulated internally, able to survive and respond in vastly different micro-environments. Many types of interactions of cells with their environment can be distinguished, and need to be controlled in experiments aimed at unravelling and predicting cellular behavior *in vivo*. The *in-vivo* microenvironment is mimicked by exposing cells to complex and changing environments. To describe the stochastic differences between cells and the local experimental conditions in sufficient detail and to obtain statistically relevant results, high-throughput experimentation is required. In this thesis four new research methods are developed, aimed at a deeper understanding of cellular regulation *in vivo*. The different aspects of cell biology are adressed and introduced in the first chapter.

A general interest in cell biology and interaction with many different people were the driving forces in this thesis work. In the Cell Observatory, different groups jointly focus on studying cellular processes down to molecular detail, share lab spaces, and stimulate interaction between scientists. The complexity of biological material requires open discussions between biologists, chemists, physicists and engineers to establish a high level of fundamental research and a shared experimental design of complex experiments. A common design methodology is proposed to lower language barriers between people from different fields, a short introduction is given in the appendix of chapter 1.

Reinventing microinjection

In this thesis, there is a technical overlap between the methods used. Microinjection is applied in different settings revealing new possibilities. An overview of these approaches is given in **Figure 7.1**. Taken from a tool off the shelf, microinjection is commonly perceived as difficult to use. Most applications such as cell or zebrafish injection require extensive training, and often obtained results differ from person to person. The integration of microinjection in the developed methods overcomes most of these difficulties, and demonstrates improved reproducibility, higher throughput and new research possibilities. For the innovations shown in the grey boxes, four patent applications have been written, which can be downloaded from Espacenet (EP1970121, EP2202522, UK1004629.0, UK1105226.3) after publication. The applications shown on the bottom row of **Figure 7.1** are described in chapters 2-5 and summarized below.

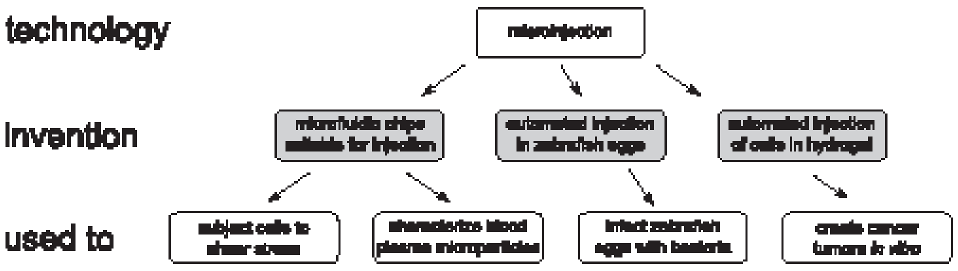
technology
microinjection
invention
microfluidic chips suitable for injection
automated injection in zebrafish eggs
automated injection of cells in hydrogel
used to
subject cells to shear stress
characterize blood plasma microparticles
infect zebrafish eggs with bacteria
create cancer tumors *in vitro*

Figure 7.1 Schematic overview of developed applications using microinjection

In organisms, tubular cells in the kidney are exposed to laminar flow, but are difficult to image and study. In standard cell culture there is no flow, and therefore the phenotype of these cells in culture is different. When cultured inside microfluidic channels, adherent cells can be subjected to a laminar flow which induces a physical shear stress in the cells. A microfluidic chip featuring multiple channels is used to study the effect of shear stress on the cell's phenotype, which is shown to change drastically upon shear stress stimulation, as compared to a no-flow control on the same chip. It is found, in chapter 2, that tubular cells do not align with the flow direction, as is the case with endothelial cells, but do show enhanced motility associated first lamellipodia formation and actin stress fibres formation together with a reinforcement of the cortical ring. The developed microfluidic chip does not need extensive support equipment, fits in a small confined climate chamber and is suitable for various light microscopy techniques in combination with high resolution imaging.

Microparticles are found in blood plasma, urine, and most other body fluids of organisms. These particles have been associated with various diseases as cardiovascular diseases, systemic inflammatory disease, thrombosis, and cancer. Detection and quantification of blood microparticles is difficult because of their small size and relatively low abundance in blood. Atomic Force Microscopy (AFM) can be used to characterize blood plasma microparticles captured on an antibody coated mica surface. In Chapter 3 a specific subset of microparticles is captured directly from blood plasma. The plasma is diluted, and subsequently rinsed over a small surface area using a microfluidic channel. After detachment of the microfluidic channel, "wet imaging" using AFM is used for high resolution imaging. It is demonstrated that high-speed centrifugation has no effect on the qualitative shape of the size distribution, and that AFM imaging allows for detailed quantification of both size and number of microparticles in a low throughput setup.

Bacterial infections of organisms can lead to life threatening diseases. *Mycobacterium tuberculosis* has infected about a third of the world population. Treatment is becoming more difficult as multi-drug-resistant strains are evolving. To study tuberculosis progression in organisms, a whole organism screening system is developed using the zebrafish *Mycobacterium marinum* infection model, which mimics many hallmarks of human tuberculosis pathology. A grid of hemispherical holes made in agarose gel is created to align the zebrafish eggs. This allowed for the automation of the injection of zebrafish eggs with bacteria up to a throughput of 2,000 eggs per hour with a 99 percent success rate.

In chapter 4, the whole embryo screening system is validated using reference compounds that prevent tuberculosis progression, making it highly suited for investigating novel antituberculosis compounds *in vivo*. The automation of the injection process allows usage in a BSL3 lab, where the human pathogen *M. tuberculosis* can be studied safely. For the first time, it is shown that zebrafish can be used to directly study infection and propagation of *M. tuberculosis*, where similar early disease symptoms were observed as found after *M. marinum* infection.

The extracellular matrix (ECM) forms the contact between cells in tissues. Hydrogel composed of the same or similar polymers are often used as ECM in cell-tissue studies. An aggregate of cancer cells embedded in a hydrogel is a well established *in vitro* cancer tumor model, mimicking *in-vivo* gradients of oxygen, nutrients, small molecules and drugs. In this method, first spheroids were created from cells that were stimulated to form cell-cell contacts, and subsequently the spheroids are embedded into hydrogel to study of cell migration and survival processes in different conditions. It is demonstrated in chapter 5 that microinjection of a cell-polymer suspension in collagen gel can be used to create similar spheroids immediately, reducing this spheroid formation time from days to minutes. Being dependent on physical rather than biological processes, this method of creating cellular spheroids is cell independent, and can be used for many cell types. The injected droplets of cells form ‘cellular spheroids’ in which cells form cell-cell contacts during the first day. After two days or more, cells start to migrate outwards, where the migration speed depends on the collagen density and cell-type. Using this method, reproducibly, spheroids are formed at predefined spots, enabling high-throughput 3D (optical) imaging and analysis. In addition, spheroids can be created from primary cells directly without intermediate culture steps, offering the ability to study responses to various drugs on patients own cells. In chapter 5 it is shown how such a screen can be performed and can possibly lead to targetted personalized drug medication within 10 days in future applications.

The above research projects were all performed in collaborative projects comprising eight groups in total, from four research institutes. Data and knowledge sharing was sometimes difficult and organized storage of the results, accessible for future use and sharing is not yet in place. In chapter 6 the needs and opportunities in data management are described in more detail. Hopefully this chapter may lead to better data management to make research more efficient and accessible for future scientists.

Samenvatting

Zorgvuldig gereguleerde processen zijn noodzakelijk om multicellulaire organismen zoals de mens te vormen. Deze processen zijn verantwoordelijk voor o.a. de structuur, celdeling en celdood van de tienduizenden miljarden cellen. Ook binnen de cellen zijn er veel regulerende processen verantwoordelijk voor overleving, stabiliteit, groei en respons in verschillende microscopische habitats. Interacties van cellen met hun directe omgeving kunnen worden bestudeerd in experimenten. Het voorspellende vermogen van deze experimenten, uitgevoerd *in vitro*, hangt af van het vermogen om de cellen bloot te stellen aan een omgeving die zo dicht mogelijk de *in-vivo* habitat benadert. Om het veranderende gedrag van cellen als gevolg van verschillende omgevingsfactoren te kunnen bestuderen zijn vele experimenten nodig om op basis van statistische argumenten conclusies te kunnen trekken. In dit proefschrift zijn vier nieuwe onderzoeksmethoden beschreven gericht op het beter begrijpen van celregulatie *in vivo*. De verschillende biologische onderzoeksgebieden waar deze methoden toegepast kunnen worden zijn kort beschreven in het inleidende hoofdstuk.

Interesse voor celbiologie en interactie met vele collega's vormden de drijvende kracht in het beschreven onderzoek. In het Cell Observatory werken verschillende groepen in gedeelde laboratoriaruimten samen om cellulaire processen tot in het moleculaire detail te doorgronden. De complexiteit van de biologie noopt tot open communicatie tussen biologen, chemici, natuurkundigen, technici en ingenieurs om fundamenteel onderzoek op hoog niveau mogelijk te maken. Om deze communicatie makkelijker te maken is een ontwerpmethode gebruikt, geïntroduceerd in het supplement van hoofdstuk één.

Reinventing microinjection

Er is een technologische overlap tussen de methoden die in dit proefschrift worden beschreven. Microinjectie is toegepast in verschillende onderzoeksgebieden om bestaande methoden te vereenvoudigen en/of om nieuwe toepassingen mogelijk te maken. Een overzicht van deze aanpak is schematisch weergegeven in **Figuur 8.1**. Microinjectie wordt ervaren als ingewikkeld in gebruik. Microinjectie toegepast in cellen of proefdieren vereist een gedegen training. Ook bij zorgvuldige training blijven de behaalde resultaten vaak verschillen van persoon tot persoon. Het is de integratie van microinjectie in de ontwikkelde methoden, die het gebruik makkelijker of zelfs mogelijk maken. De beschreven experimenten worden beter reproduceerbaar en kunnen bovendien sneller en betrouwbaarder uitgevoerd worden. De ontwikkelde methoden zijn beschreven in een aantal hoofdstukken en gedetailleerder beschreven in patentaanvragen die op het moment publiek beschikbaar zijn via espacenet (EP1970121, EP2202522) of beschikbaar zullen komen (UK1004629.0, UK1105226.3).

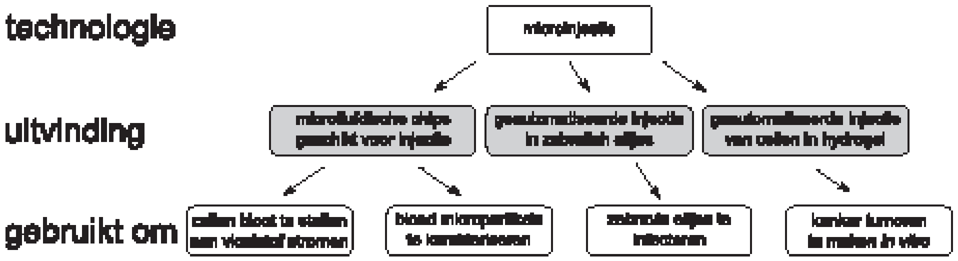
technologie
uitvinding
gebruikt om
microinjectie
microfluïdische chips geschikt voor injectie
geautomatiseerde injectie in zebravis eitjes
geautomatiseerde injectie van cellen in hydrogel
cellen bloot te stellen aan vloeistof stromen
bloed microparticles te karakteriseren
zebravis eitjes te infecteren
kanker tumoren te maken *in vivo*

Figuur 8.1 Schematisch overzicht van ontwikkelde op microinjectie gebaseerde toepassingen.

Vloeistofstroming

In organen, zoals de nier, worden bepaalde cellen (tubular cells) blootgesteld aan vloeistofstromen. In het levende organisme zijn deze cellen moeilijk in detail te bestuderen. In celkweek is stroming afwezig en daardoor wijkt het fenotype van deze cellen af. Niercellen zijn in speciale microkanalen blootgesteld aan een vloeistofstroom, waardoor zij in een natuurlijkere omgeving bestudeerd konden worden. In hoofdstuk 2 is het effect van stroming op het fenotype van deze cellen, in vergelijking met dezelfde situatie zonder stroming, bekeken. Het blijkt dat de cellen niet in de richting van de vloeistofstroom bewegen zoals sommige epitheelcellen dat doen. De cellen laten wel extra mobiliteit zien en vormen uitlopers (lamellipodia) en stressbundels in het actineskelet. Bundels in het actineskelet verstevigen de cel door vorming van een ringstructuur (cortical ring). De ontworpen celkweekchip kan gebruikt worden in combinatie met apparatuur die standaard aanwezig is de meeste celbiologielaboratoria en kan men een gecontroleerde omgeving voor de bestudeerde cellen realiseren. De chip is gebruikt in verschillende (hoge resolutie) optische microscopiemethoden en is eenvoudig te plaatsen in broedstoven.

Microdeeltjes

In bloed komen kleine deeltjes voor die worden gevormd door cellen en/of celresten. Deze deeltjes worden geassocieerd met verschillende ziekten zoals hart- en vaatziekten, diverse ontstekingsziekten, trombose en kanker. Detectie en kwantificatie van deze deeltjes in bloed wordt bemoeilijkt door de grootte en hun relatief lage concentratie. Atomaire kracht microscopie (AFM) kan worden gebruikt om deze deeltjes te kwantificeren na binding op een glad mica oppervlak. In hoofdstuk 3 worden microdeeltjes direct uit bloedplasma gevangen op een mica-oppervlak, dat gecoat is met een antilichaam. Dit gebonden antilichaam kan vervolgens specifieke deeltjes uit het bloedplasma invangen. Het na centrifugatie van bloed verkregen plasma wordt verdund en door een klein vloeistofkanaal over dit actieve oppervlak geleid. Vastgesteld is dat op deze wijze de lokale concentratie van de ingevangen deeltjes wordt verhoogd. Doordat het gebruikte systeem gedemonteerd kan worden is het mogelijk om het 'natte' oppervlak met AFM af te tasten. Geautomatiseerde data-analyse laat zien dat centrifugatie op hoge snelheid geen invloed heeft op de verdeling van de deeltjesgrootte, en dat AFM in combinatie met het vloeistofkanaal een geschikte methode vormt om gedetailleerd naar de deeltjesgrootte en deeltjesaantallen te kijken. Door het hoge aantal ingevangen deeltjes wordt een verbeterde statistiek verkregen.

Infecties

Bacteriële infecties kunnen levensbedreigende ziekten veroorzaken. Op het moment van schrijven heeft de bacterie *Mycobacterium tuberculosis* ongeveer een derde van de wereldbevolking besmet. Behandeling van deze infecties wordt steeds moeilijker door bacteriële evolutie, resulterend in antibiotica-resistente stammen. Om het ziekteproces van tuberculose te bestuderen in organismen is een onderzoeksmethode ontwikkeld, gebaseerd op het *Mycobacterium marinum* infectiemodel in zebravissen. Deze bacteriële infectie bij zebravissen laat overeenkomstige kenmerken zien ten opzichte van de menselijke tuberculose variant. Een belangrijk voordeel van het zebravismodel ten opzichte van andere diermodellen zoals muizen- of hamstermodellen is dat zebravis embryo's grotendeels optisch transparant zijn. Hierdoor kunnen ziekteprocessen tot in detail bekeken worden in levende organismen. De zebraviseitjes worden bacteriëel besmet door de eidooier te injecteren met bacteriën. Deze microinjectie is geautomatiseerd door de eitjes in een rooster van agarosegel met daarin halfronde kuiltjes te plaatsen. Hierdoor is de plaats van ieder embryo bijna perfect bekend. Zo kunnen 2000 eitjes per uur besmet worden met een succespercentage van 99 procent. In hoofdstuk 4 is deze besmettingsmethode beschreven en toegepast in een prototype onderzoek om nieuwe medicijnen te vinden. De automatisering van de microinjectie biedt tevens de mogelijkheid om in een BSL3 lab te werken, waar ook de humane vorm van tuberculose veilig bestudeerd kan worden. Voor de eerste keer is vastgesteld dat ook zebravisembryo's besmet kunnen worden met *Mycobacterium tuberculosis*. Na injectie van *Mycobacterium tuberculosis* en *Mycobacterium marinum* werden vergelijkbare ziekteverschijnselen gevonden in de zebravisembryo's.

Invasieve processen

De extracellulaire matrix (ECM) vormt het contact tussen cellen in weefsels. In weefselonderzoek wordt gebruik gemaakt van hydrogel, met dezelfde of vergelijkbare polymeren om de natuurlijke omgeving in weefsels na te bootsen. Zo wordt een klompje kankercellen in hydrogel geplaatst om de omgeving van tumorweefsel *in vitro* na te bootsen. Natuurlijke gradiënten van zuurstof, voedingsstoffen, kleine moleculen en eventueel medicijnen komen tot stand door een proces als gevolg van diffusie, opname en/of uitstoot van moleculen door cellen. Nu worden cellen eerst gestimuleerd om cel-cel contacten te vormen, vervolgens worden deze klompjes cellen ingegoten in een gel en tenslotte kunnen studies naar overleving en celmigratie uitgevoerd worden. In hoofdstuk 5 wordt aangetoond dat microinjectie van een mengsel van cellen en polymeren direct in een gel uitgevoerd kan worden om klompjes cellen in gel te verkrijgen. Hierdoor wordt de voorbereidingstijd verkort van dagen tot enkele minuten. Omdat dit proces niet van biologische eigenschappen van cellen afhankelijk is, kan het gebruikt worden voor vele celtypen. In het geïnjecteerde mengsel kunnen cellen gedurende de eerste dag aan elkaar en aan de gel hechten om zo een compact geheel te vormen. Na een dag of twee beginnen sommige typen cellen te migreren, op zoek naar voedsel en weg van de afvalstoffen van de naburige cellen. De migratiesnelheid hangt af van de gelstructuur en het type cel. Een bijkomend voordeel van deze methode is dat de celklompjes op gedefiniëerde posities gevormd worden, waardoor ze beter geautomatiseerd bekeken kunnen worden. Aangetoond wordt dat de methode toepasbaar is op cellen direct afkomstig van kankerweefsel van patiënten (biopten). In de toekomst kan de mogelijk voorspellende werking van deze methode op de medicijnrespons van individuele patiënten onderzocht worden. In hoofdstuk 5 is te lezen hoe zo'n onderzoek kan leiden tot persoonlijk medicijnadvies binnen tien dagen.

Kennisoverdracht

De projecten in dit proefschift werden uitgevoerd in samenwerking met acht onderzoeksgroepen, verdeeld over vier onderzoeksinstituten. Het delen van gegevens en kennis in deze projecten was soms moeilijk, en een systeem voor georganiseerde opslag van deze onderzoeksgegevens, toegankelijk voor toekomstig gebruik is nog niet beschikbaar. In hoofdstuk 6 wordt dit probleem nader bekeken. Hopelijk leidt deze analyse in de toekomst tot een toegankelijke opslag én efficiënter gebruik van kostbare onderzoeksinformatie.

Epiloog

In dit proefschrift zijn voor vier verschillende onderzoeksprojecten nieuwe methoden bedacht, ontwikkeld en gebruikt die hebben geleid tot het verkrijgen van nieuwe kennis op het gebied van celbiologie. Belangrijk voor dit onderzoek was de directe samenwerking tussen ingenieurs, natuurkundigen, chemici, biofarmaceuten, medici en biologen. Als ingenieur uit Delft was het een uitdaging om in een niet-technische omgeving te werken, de knelpunten te vinden en op te lossen zodat sneller, beter en nieuw biologisch / medisch onderzoek mogelijk werd.

Acknowledgements

Living as a child in an old farm house, constantly under construction, with lots of wood and tools lying around has been a great motivator to start creating. For this I'd like to thank my parents, Marja and Leo. Several of the fascinating projects were boats, the first ones being constructed from cardboard egg-containers. I was convinced it could support my weight. After I learned about the water adsorbing difference between cardboard and wood & styrofoam, my sister Daphne had enough faith to test one of my self-constructed boats. I'd like to thank my sister, my parents, my grandparents and the rest of my family for their love, continuous trust and support.

Dancing and studying in Delft brought a new episode in my life. My housemates at Villa67 (Krakeelhof) taught me many lifelong lessons. One being the most important is that most of the good things you do in life will always generate positive and negative responses. Positive thinking means to forget quickly about the negative, and to remember and cherish the positive responses.

The joy of dancing has been a great distraction during my study, shared with many friends. I'd like to thank those with whom I visited many salsa parties in my early salsa years: Olivier, Vivian, Andre, Perrie, Nalinie, Nooky, Aartie, Monique, Martha, Stuart and Wieske. Especially, I'd like to thank Vivian for the great salsa teaching experiences and I hope that we can continue for many years. I'd like to thank all of my salsa students for the great fun and enthusiasm, especially Melissa, Vicki, Kees-Jan, Maurice, Tal and Rabih for forming the first SoSalsa board, and starting a salsa student association in Delft, you made one of my dreams come true!

Learning more and more about biology I became amazed by the control and organisation in cells. It intrigued me that the cytoplasm of cells was more than just a soup of proteins, as Mathieu explained to me once during a Cyttron lecture. After, I truly loved the freedom to change course as given to me by Jan Pieter and Mathieu during my internship, and later again during my PhD project.

Hans, thank you for learning me the basics of moulding PDMS and polyurethane. Maxim, we truly enjoyed spending many years of research, Amsterdam humor and solving one problem after another. Without that we wouldn't have invented the microfluidic chip as described in this thesis.

My first invention, what would it be without the help of Johan and Mark from Vereenigde? You taught me not only how to write a patent text, but also how to claim the invention of a bicycle in case a motorcycle already exists.. I enjoyed learning about the ins and outs of patents and IP management, and used it over and over again.

Attracted by the academic freedom I was happy to continue as a PhD student, many thanks to Leiden University, Jan Pieter and Mathieu for giving me this opportunity. I'd like to thank all my colleagues of the Cell Observatory, especially Jasper, Dilyana, Ellen, Linhua, Henriette, Rhyenne, Wilbert, Backey, Hans (2x), Raj, Daniel, Patrick (2x), Rosalie, Igor, Helen, Françoise, Zunfeng, Elisabeth, Willem-Jan, RAG, Pavol, Irakli, Maarten and Marta for the very enjoyable time.

I owe a special thanks to Henk, Fred, Emiel, Ewie, Arjen, Tim, Rafael, Jeroen and Frits from the department of Fine Mechanics and Co from the department of Electronics, not only for their insight, time and effort, but also for their enthusiasm during all the different projects and challenges.

Many students were involved in my research. Jos, you were my first student, very enthusiastic, and I remember beautiful experiments you performed with the dictostelium cells we received from Freek. Esther, thank you for bringing the microfluidic cell culture several steps further. Rafael, you came all the way from France to work on the automation of the microfluidic connection technique, thank you for your patience, time and effort. Wendy, you worked on many different projects with the aim to get the first usable data from the prototype systems. You took it all with great care and proved to be very valuable as researcher and you knew exactly how to write it down, thank you for your work, you earned my highest mark with great pride. Kim, you came to me for an internship which could not be completed during my PhD, still we took the chance to create a novel zebrafish culture plate, thank you for your time and effort. Next to internships, many students visited for a short period of experimental work. I'd like to thank Jos, Stein, Dwight, Sander, Pieter, Daan, Frithjof, Bartjan, Thomas, Alexi, Teun, Jaap, Robbin, Eva, Silvia, Yingying and Yorrick for their enthusiastic work on PDMS, microfluidic chips and Zebrafish.

All the chapters in this thesis describe collaborative projects which were impossible without the many people from the research groups involved.

Sylvia, who would have guessed how much patience it required to study cells under flow conditions? I'd like to thank you and Hans for your continuous trust and support, and Bob for the opportunity to work on this joint project.

Brian, our experiments on blood plasma micro-particles were not perfect, as we were continuously searching for the right experimental conditions. I'd like to thank you for all the time and effort you put into AFM imaging, the data-analysis and the paper. Tjerk, thank you for bringing me and Maxim into this project, you had the perfect timing. Yuana, you have laid the groundwork on AFM imaging on micro-particles, thank you for helping us all along. Susanne and Rogier, thank you for your professional advice and experience, I hope the research on micro-particles will continue and that it will flourish in the future.

Herman, Ron, somehow I could convince you to invest in a new automated injection method for zebrafish eggs, which proved to require more innovations than we anticipated. Step by step with the help of students and Gabby, followed by Ralph, Oliver, Nigel and Wouter we could finally show that zebrafish can be infected with *Mycobacterium Tuberculosis*. Ralph, Oliver, Nigel, Wouter thank you for the joy and professionalism during experiments, together we made every experiment count and usable for the paper. Nigel, I'll remember to keep the beer close when you need it.

The automated injection system could also be used for cell injections in gel, and I'd like Ron and Herman for the opportunity to show this and use the injection system for that purpose. That the cell observatory principle works was proven by Sylvia, who pointed me to Erik and Hoa, who were microinjecting cells by hand, an application ideal for automation, and exactly what I was looking for. Erik, Hoa, thank you for the patience, during the setup of the automated injection system. Together we created a novel 3D culture method which opens a whole new world of possibilities.

Art, Sebastiaan and Laura, more ideas than could fit in this thesis were discussed with you. Thank you for the energy and enthusiasm, let's hope that many of the patents applications will lead to commercial success. David and Timothy from Potter Clarkson, thank you for translating most of my ideas into perfect English, it was always a thrill to read back the detailed descriptions of the inventions.

For the last chapter on data management I used many comments and tips from Albert, Henriette, Erica, Elisabeth, Willem-Jan, Maxim, Jouke, Tal, Kees-Jan, Joke, Nora, Zaid, Mathieu, Martine, Alfons and Wieske, thank you so much for contributing.

Working with so many people from so many groups, it is impossible to list everyone involved. Still I'd like to thank everyone who contributed to this work, even if your name is not listed above.

Curriculum Vitae

Jan de Sonneville

born in Amsterdam, the Netherlands,
14 september 1980
email: mail@jandesonneville.nl
mobile: +31 (0)6 - 55 700 794

Languages

English (fluent), Dutch (mother tongue), German (foundations), Spanish (foundations)

Software

Linux (Ubuntu, Debian), MacOSX, Python, C++, PHP, Javascript, HTML, CSS, serial interface programming, multithreaded programming for real-time applications

Education

Bachelor Electrical Engineering (1998-2004),
Delft University of Technology, the Netherlands

Master Nanoscience (physics) (2003-2006)
joint program of Delft University of Technology & Leiden University, the Netherlands

Major thesis project on microfluidic single cell analysis
Biophyscial structural chemistry, Leiden University (2006)

Internship

wrote a patent application for a novel connection technique for microfluidic chips, invented during my major thesis project (WO 2008072968)
Patent office Vereenigde, Amersfoort, the Netherlands (2006)

PhD

on novel microfluidic methods for cell biology, this thesis
Leiden Institute of Chemistry (LIC), Cell observatory, Leiden University (2007-2011)

Work

Salsa dance teacher and initiator of student dance society SoSalsa
(http://www.sosalsa.nl)
Cultural Center of Delft University of Technology (2005 - current)

Publications

Journal articles

J de Sonneville, ME Kuil, E van Stapele, H. de Bont, H. Verpoorten, MHM Noteborn, JP Abrahams, B van de Water, SE Le Dévédec
A versatile microfluidic device for studying the dynamics of shear-stress induced actin reorganization in renal cells
(submitted for publication)

B.A. Ashcroft*, J. de Sonneville*, Y. Yuana*, S. Osanto, R. Bertina, M.E. Kuil, T.H. Oosterkamp
Determination of the size distribution of blood microparticles directly in plasma using atomic force microscopy and microfluidics
(submitted for publication)

Carvalho R*, de Sonneville J*, Stockhammer OW, Savage NDL, Veneman WJ, et al.
A High-Throughput Screen for Tuberculosis Progression
PLoS ONE, 2011, 6: e16779

HH Truong*, J de Sonneville*, VPS Ghotra, J Xiong, L Price, P Hogendoorn, HP Spaink, B van de Water, EHJ Danen
Automated microinjection of cell-polymer suspensions in 3D ECM scaffolds for high throughput quantitative cancer invasion screens
(Biomaterials, in press)

Patent applications

J de Sonneville, JP Abrahams, MHM Noteborn, ME Kuil, H Verpoorten
Microfluidic chip comprising capillaries – *WO 2008072968*

S Osanto, RM Bertina, Y Yuana, TH Oosterkamp, BA Ashcroft, ME Kuil, J de Sonneville
Methods for immobilizing microvesicles, means and methods for detecting them and uses thereof - *WO 2010072410*

J de Sonneville, ME Kuil
A cell cultivation receptacle and related apparatuses
WO 2010105845

J de Sonneville
Array microinjection apparatusses and methods**
GB 1004629.0

EHJ Danen, J de Sonneville, HH Truong
Multicellular spheroid production by injection of a cell suspension into a gel**
GB 1105226.3

*equal contribution

**patent application is not yet published, name may be subject to change

Regulatory processes are responsible for the organization, division and death of cells in multicellular organisms such as humans. Additionally, cells are highly regulated internally, able to survive and respond in vastly different micro-environments. Many types of interactions of cells with their environment can be distinguished, and need to be controlled in experiments aimed at unravelling and predicting cellular behavior *in vivo*. The *in-vivo* microenvironment is mimicked by exposing cells to complex and changing environments. To describe the stochastic differences between cells and the local experimental conditions in sufficient detail and to obtain statistically relevant results, high-throughput experimentation is required. In this thesis four new research methods are developed, aimed at a deeper understanding of cellular regulation *in vivo*.